NASA TECHNICAL NOTE

NASA TN D-5419

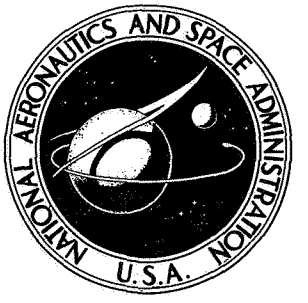

NASA TN D-5419

DEVELOPMENT OF THREE-DIMENSIONAL PRESSURE-DISTRIBUTION FUNCTIONS FOR LIFTING SURFACES WITH TRAILING-EDGE CONTROLS BASED ON THE INTEGRAL EQUATION FOR SUBSONIC FLOW

by Alfredo Navarro Crespo and Herbert J. Cunningham

Langley Research Center

Langley Station, Hampton, Va.

NATIONAL AERONAUTICS AND SPACE ADMINISTRATION • WASHINGTON, D. C. • OCTOBER 1969

1. Report No. NASA TN D-5419	2. Government Accession No.	3. Recipient's Catalog No.
4. Title and Subtitle DEVELOPMENT OF THREE-DIMENSIONAL PRESSURE-DISTRIBUTION FUNCTIONS FOR LIFTING SURFACES WITH TRAILING-EDGE CONTROLS BASED ON THE INTEGRAL EQUATION FOR SUBSONIC FLOW		5. Report Date October 1969 6. Performing Organization Code
7. Author(s) Navarro Crespo, Alfredo (NRC-NASA Resident Research Post-doctoral Associate) and Cunningham, Herbert J.		8. Performing Organization Report No. L-6305
9. Performing Organization Name and Address NASA Langley Research Center Hampton, Va. 23365		10. Work Unit No. 126-14-14-08-23 11. Contract or Grant No.
12. Sponsoring Agency Name and Address National Aeronautics and Space Administration Washington, D.C. 20546		13. Type of Report and Period Covered Technical Note 14. Sponsoring Agency Code

15. Supplementary Notes

16. Abstract

For partial-span control surfaces of the trailing-edge-flap type with leading-edge hinge and sealed gaps, a series of lifting pressure distributions are developed for deflected and deformed flaps on thin, swept, tapered wings for use in aeroelastic analysis. Solutions for the steady case are presented that overcome the fundamental problem of determining the nature and distribution of the pressure singularity along the flap leading edge and provide an advanced basis for extension to the oscillating case of flutter.

17. Key Words Suggested by Author(s)	18. Distribution Statement
Aerodynamic force distribution – wings and control surface Aeroelasticity Flutter	Unclassified – Unlimited

19. Security Classif. (of this report)	20. Security Classif. (of this page)	21. No. of Pages	22. Price*
Unclassified	Unclassified	73	$3.00

*For sale by the Clearinghouse for Federal Scientific and Technical Information Springfield, Virginia 22151

DEVELOPMENT OF THREE-DIMENSIONAL PRESSURE-DISTRIBUTION FUNCTIONS FOR LIFTING SURFACES WITH TRAILING-EDGE CONTROLS BASED ON THE INTEGRAL EQUATION FOR SUBSONIC FLOW

By Alfredo Navarro Crespo* and Herbert J. Cunningham
Langley Research Center

SUMMARY

The problem of calculating subsonic pressure distributions on thin lifting surfaces with slightly deflected or deformed control surfaces is studied by the approach of the linear-integral-equation procedure. The results are expected to find application to the oscillating case. The singularities introduced in the pressure distribution by the deflection of a control surface are studied by an analogy between the fluid flow suddenly deflected when passing over the hinge of a control surface and the flow also suddenly deflected at the sharp (zero-radius) leading edge of a wing with symmetric thickness, flying with zero angle of attack at subsonic speed.

As a result of this study, a suitable set of loading functions (or modes of pressure) has been generated to represent the influence of the control surfaces on the pressure distribution on the wing. These loading functions can be applied to any wing planform, and once they have been integrated through the mentioned integral equation, they produce a set of modes of downwash which has a fairly good capability to represent the first-order discontinuity that the actual downwash distribution displays along the contours of the control surfaces. These resulting modes of downwash should improve the conditioning of the matrix equation to which the associated collocation procedure leads, in comparison with previously used pressure modes. This effect is very important in the numerical calculations.

INTRODUCTION

A great deal of work has already been done on the problem of calculating steady or unsteady aerodynamic pressure distributions on lifting surfaces in subsonic flow. (See, for example, refs. 1 to 20.) As a result of this work, it is possible at present to predict with fairly good accuracy the subsonic aerodynamic loads on a thin wing of any planform, if the frequency of oscillation of the wing is not too high and the Mach number is not too

---

*NRC-NASA Resident Research Postdoctoral Associate.

close to unity. Different improvements of the already well-established calculation procedures have been proposed (refs. 12 to 16) and useful work has also been done on the case of nonplanar lifting surfaces (e.g., refs. 19 and 20.)

But there are problems associated with the lifting-surface theory which still remain unsolved or are in an early stage for their practical solution. Such is the case of the problem of determining pressure distributions on thin wings of arbitrary planform with slightly deflected or oscillating control surfaces. An important problem of the latter type is the flutter of thin wings with control surfaces. This problem should be amenable to linear-theory analysis because just when this instability appears, it is very possible that the flow can still be considered as a potential flow and the perturbations as small.

For many years, methods of calculation based on the lifting-line theory (or the strip theory) have been used to determine the aerodynamic loading that the control surfaces produce (refs. 21 and 22). Those procedures, however, have proven to be inadequate for low-aspect-ratio wings and partial-span flaps in common use.

The reverse-flow theorem (ref. 7) has provided a useful tool for determining generalized aerodynamic forces on wings of any planform with control surfaces. (See section 11 of ref. 4.) But its use does not make possible the calculation of the pressure distribution itself.

Many attempts have been made to solve the wing—control-surface problem by employing the approach successfully used to solve the lifting-surface problem for the wing alone. (For the latter, see refs. 1 to 6, for example.) Briefly, the procedure is as follows: In the integral equation that relates the usually unknown aerodynamic lifting pressure and the usually known downwash distribution, the pressure distribution is represented by a truncated series expansion of loading terms (or pressure modes) with the terms multiplied by their respective weighting factors, which become the unknowns of the problem. Then, the weighting factors are determined by a collocation or a least-squares-error procedure.

In applying this approach to wings with controls the logarithmic pressure singularity at the hinge line indicated by two-dimensional theory (e.g., ref. 23) has usually been accounted for as in reference 24, for example. For partial-span controls, difficulties have been encountered in accounting for the ends of the controls and most results have not been satisfactory enough to be published. The reason for much of these poor results, as experience from the present investigation has shown, is that multiplication of the two-dimensional chordwise pressure distribution by separated-variable functions of chord and span variables (notably power series) produces individual downwash modes that in linear combination have little capability of representing even the statically deflected control. Furthermore, the individual higher-order downwash modes tend to be too similar in shape and thus contribute to a poor conditioning of the downwash matrix in the collocation

process. A recent report (ref. 25) describes results of an effort of this general type. Fairly good success was achieved, but some results displayed a noticeably erratic behavior as the number of pressure modes was increased.

The conclusion is reached herein that, in general, the two-dimensional chordwise distribution of pressure does not reliably represent the pressure distribution for a finite-span control. New pressure-distribution functions, developed from three-dimensional theory, are needed.

A new insight to the problem has been given by Landahl in reference 26. The local flow at points located near the control surface hinge, side edges, and corners was studied by use of the method of matched asymptotic expansions. That study provides very useful information which can be applied to originate the first-order mode of pressure associated with the control-surface deflection.

The control surface treated herein is the trailing-edge, flap type with sealed leading-edge hinge and no gap at inboard and outboard edges. The terms "control surface" and "flap" are used interchangeably. Adaptation could be readily made to the geometry of leading-edge controls, but the present report treats only trailing-edge controls.

The aim of the present paper has been to originate a set of pressure modes which can be applied to any planform with statically deflected and deformed control surfaces and, which when transformed through the integral equation previously mentioned, can produce a set of downwash modes able to represent adequately, with only a few terms, actual downwash distributions and, at the same time, feature strong linear independence of the downwash equations. The results are expected to find application to oscillating as well as to steady-state problems.

The way to originate these modes of pressure has been by the use of an analogy between the fluid flow suddenly deflected at a control-surface hinge on the upper or lower side of a lifting surface and the flow also suddenly deflected by the sharp (zero-radius) leading edge of a wing of symmetric thickness flying at zero angle of attack. The downwash distribution on this wing of symmetric thickness is expanded in a series of orthogonal terms. This originates a resulting pressure distribution also expanded in a set of terms which can be used to define appropriate modes of pressure needed in the lifting-surface case.

The fundamental or first-order term obtained in this way displays a logarithmic singularity which is identical with that found in reference 26. Appropriate modifications have been introduced to account for the wing-edge effects as well as the effect of a swept-back control-surface hinge, which appears to be very appreciable. The higher order modes of pressure have been generated by following a systematic procedure of modifying

the first-order term. A parameter E_S has been introduced that, if given a suitable value, has the effect of improving the downwash distribution produced by the first mode of pressure. The suitability of the pressure-mode functions is assessed by plotting their associated downwashes and making a visual comparison of these downwashes with desired downwashes and with each other.

Certain auxiliary functions are given in appendixes A and B, and appendix C describes the numerical integrations employed.

SYMBOLS

A bar over a coordinate variable indicates that it is dimensional.

a_{nm} weighting factors for wing modes of lifting pressure

$\begin{Bmatrix} a \\ b \end{Bmatrix}$ column matrix of subcolumns a_{nm} and b_{nm}

$A_{nm}(\theta,\eta)$ wing modes (distributions) of lifting pressure (see eqs. (3) and (5))

$b(\eta)$ local wing semichord

b_{nm} weighting factors for control-surface, or flap, modes of lifting pressure

$B_{nm}(\theta,\eta)$ flap modes (distributions) of lifting pressure (see eq. (3))

$B_{nm}^{(1)}(\theta,\eta)$ preliminary exploratory choice for B_{nm} (see eq. (6)) based on two-dimensional flow

$B_{00}^{(2)}(\theta,\eta)$ second exploratory choice for $B_{00}(\theta,\eta)$ (eq. (21b)) without the empirical modifications that lead to equation (24)

$B_{00}^{(3)}(\theta,\eta)$ designation for $B_{00}(\theta,\eta)$ of equation (24) when applied to a swept flap, but without the sweep effect included in equations (28)

$B'_{10}(\theta,\eta)$, $B'_{20}(\theta,\eta)$ incomplete exploratory flap modes of pressure (see eq. (36))

c_c control-surface chord length

$C_{nr}(\theta,\eta)$ spanwise symmetric lift distribution functions contained in $B_{nm}(\theta,\eta)$ (see eqs. (30) to (35))

$C_{H_{nr}}(\bar{x},\bar{y},\bar{z})$, $C_{T_{nr}}(\bar{x},\bar{y},\bar{z})$ perturbation-pressure distribution functions that contain and account for leading-edge and trailing-edge singularities, respectively, of the thick-wing analogy (see eq. (14) and appendix B)

d_{nr} constant coefficients (see eq. (11))

E_s span expansion-contraction factor (see eq. (23d))

$F_{nr}(\eta;x,y)$ chordwise integral (eq. (C2))

$F^*_{nr}(\eta;x,y)$ chordwise integral (see eq. (C8))

$H_{nr}(\theta,\eta)$ defined with equation (C10)

k reduced frequency, referred to b_0, $k = \frac{b_0\omega}{U}$

K kernel function of the integral equation (1), $K \equiv K\left[M,x-\xi,s(y-\eta)\right]$

$\overline{K}$ dimensionless part of $K = \frac{\overline{K}}{b_0^2 s^2 (y-\eta)^2}$ as applied to equation (C1),

$\overline{K} \equiv \overline{K}\left[M,x-\xi(\theta),s(y-\eta)\right]$

l wing semispan (see sketch 2)

$L_{A_n}(\theta)$, $L_{B_n}(\theta)$ chordwise distributions of lifting pressure for wing modes $A_{nm}(\theta,\eta)$ (see eq. (5)) and flap modes $B_{nm}(\theta,\eta)$ (see eq. (7)), respectively

m_c slope of parallel leading and trailing edges of swept control surface whether part of a wing or not (see sketch 6 and eqs. (25) and (29))

M Mach number of unperturbed air stream

$N_{nr}(\theta,\theta_c,\eta)$ distribution functions in the lift (see eqs. (C5) to (C7))

$N_0(\theta,\theta_c,\eta)$ distribution function in the lift (see eqs. (C4))

$\Delta p(\xi,\eta)$ lifting pressure distribution (eqs. (1) and (3)), positive up, $\Delta p(\xi,\eta) = p_l(\xi,\eta) - p_u(\xi,\eta)$

$p_l(\xi,\eta)$, $p_u(\xi,\eta)$ pressure perturbation on lower and upper sides, respectively, of wing surface

$p_s(\bar{x},\bar{y},\bar{z})$ pressure perturbation upon and originated by wing of z-symmetrical thickness

$p_{H_s}(\bar{x},\bar{y},\bar{z})$ local distribution of $p_s(\bar{x},\bar{y},\bar{z})$ in vicinity of wing leading edge (see eq. (20))

$P_n[\ ]$, $P_r[\ ]$ Legendre polynomial of first kind of degree n and r, respectively, and argument $[\ ]$ (see eq. (11))

$Q_{r-1}(\ )$ polynomial of degree $r - 1$ and argument $(\ )$ introduced in equation (17) and listed in appendix A

$s = l/b_0$

s_e effective value of s (see eq. (23d)), $s_e = sE_s$

S_w planform area of full-span wing

U speed of unperturbed air stream

$w(x,y)$ downwash distribution at wing surface, positive up (see eq. (1))

$w_0(x)$, $w_1(x)$, $w_2(x)$, $w_3(x)$, $w_{23}(x)$ illustrative downwash distributions (see sketches 3 and 4)

$w_s(x,y,0)$ downwash distribution on upper side of wing of z-symmetrical thickness

$\{w\}$ matrix column of downwash ratios w/U at control points (eqs. (8))

$W_{A_{nm}}(x,y)$, $W_{B_{nm}}(x,y)$ distribution of downwash ratio w/U at wing surface originated by wing modes and flap modes of pressure, respectively

$W_{nm}(x,y)$ includes both $W_{A_{nm}}(x,y)$ and $W_{B_{nm}}(x,y)$

$[W]$ matrix of values of $W_{A_{nm}}(x,y)$ and $W_{B_{nm}}(x,y)$ at control points (see eqs. (8))

$W^{(1)}_{B_{n0}}(x,y)$, $W^{(2)}_{B_{00}}(x,y)$, $W^{(3)}_{B_{00}}(x,y)$, $W'_{B_{10}}(x,y)$, $W'_{B_{20}}(x,y)$ } downwash distributions originated by flap modes of pressure $B^{(1)}_{n0}(\theta,\eta)$, $B^{(2)}_{00}(\theta,\eta)$, $B^{(3)}_{00}(\theta,\eta)$, $B'_{10}(\theta,\eta)$, and $B'_{20}(\theta,\eta)$, respectively

$\bar{x},\bar{y},\bar{z}$ dimensional rectangular coordinates (see sketch 1)

x,y,z dimensionless coordinates, $x = \bar{x}/b_0$, $y = \bar{y}/l$, $z = \bar{z}/b_0$

$\bar{x}_c(\bar{y})$, $x_c(y)$ chordwise coordinate of control-surface hinge line

$\bar{x}_m(\bar{y})$, $x_m(y)$ chordwise coordinate of wing midchord line

X distribution function introduced into flap lifting-pressure modes (see eqs. (23) and (29)), $X \equiv X(\theta,\theta_c,\eta)$

X_T see equation (23c), $X_T = X(\pi,\theta_c,\eta)$

$\bar{y}_{c1}$, y_{c1} spanwise coordinate of inboard end of partial-span flap (see sketches 2 and 6) and of left end of full-span flap

$\bar{y}_{c2}$, y_{c2} spanwise coordinate of outboard end of partial-span flap (see sketches 2 and 6) and of right end of full-span flap

y_{c0} spanwise midpoint coordinate of flap, $y_{c0} = \dfrac{y_{c1} + y_{c2}}{2}$

$\beta = \sqrt{1 - M^2}$

$\Gamma_r(\bar{x}-\bar{\xi},\bar{y},\bar{z})$ distribution function in perturbation pressure (see eqs. (15) and (16))

$\bar{\delta}_c = \dfrac{2}{\bar{y}_{c2} - \bar{y}_{c1}}$

$\delta_c = \dfrac{2}{y_{c2} - y_{c1}} = \bar{\delta}_c l$

ϵ infinitesimal computational quantity (see eq. (C16))

Λ sweep angle of wing quarter-chord line, positive for sweepback

λ taper ratio, b_t/b_0

$\lambda(\theta_c,\eta)$ see equations (C12) and (C13)

$\bar{\mu} = \bar{x}_T - \bar{x}_c$

$\mu = c_c/b_0 = \bar{\mu}/b_0$

$\nu_r(\bar{\xi})$ distribution function (see eq. (17) and appendix A)

$\Pi_0(\eta)$, $\Pi(\theta,\theta_c,\eta)$ distribution functions (see eqs. (28))

ρ mass density of unperturbed air stream

θ angular chordwise coordinate (see eq. (4))

$\theta_c(\eta)$ value of θ at flap hinge line

$\theta_{c0}(\eta)$ value of θ at flap midchord point $\left(\text{i.e., at } \xi_{c0}\right)$

$\theta_x(\eta)$ as in reference 1, the value of θ on span station η at its intersection with the line that passes through the control point (x,y) and is parallel to the y-axis

$\bar{\xi},\xi,\xi(\theta)$ dimensional and dimensionless $\left(\xi = \bar{\xi}/b_0\right)$ dummy variables for $\bar{x}$ and x, respectively, and with same system of subscripts (see eq. (4))

$\bar{\eta},\eta$ dimensional and dimensionless $(\eta = \bar{\eta}/l)$ dummy variables for $\bar{y}$ and y, respectively, and with same system of subscripts

$\phi(\theta,\eta)$ see equation (C11)

ω circular frequency of oscillation

Subscripts:

c flap leading edge (hinge line)

c_1 inboard end of partial-span flap and left end of full-span flap

c_2 outboard or right end of flap

c_0 midpoint or midstation on flap

m wing midchord line

t wing tip

T trailing edge

0 wing root or plane of symmetry

ANALYTICAL DEVELOPMENT

Formulation of the Problem

The purpose of this investigation has been to arrive at some practical method of calculating the steady pressure distribution on elastic wings with slightly deflected or deformed control surfaces in subsonic flow. For this research, the following linearizing assumptions were made: a potential flow, an ideal fluid, and small perturbations from the main stream.

These assumptions could seem unrealistic under actual conditions where deflected or deformed control surfaces are involved. However, accurate solutions of the three-dimensional flow equations, under the mentioned idealized conditions, should be useful for the theoretical study and calculation of many aerodynamic and aeroelastic phenomena, such as rolling effectiveness, loss of control effectiveness, hinge moments, and so forth, where small deflections of the control surfaces can play an important role.

In the present approach to the problem, a generalization has been made from the common procedure of calculating pressure distributions on lifting surfaces without controls to the case of control surfaces of immediate interest. That means that deformations of the idealized wing surface have been considered, and the development is based on the well-known integral equation:

$$\frac{w(x,y)}{U} = \frac{b_0 l}{4\pi\rho U^2} \iint_{S_W} \Delta p(\xi,\eta)\, K\left[M, x-\xi, s(y-\eta)\right] d\xi\, d\eta \tag{1}$$

where S_W is the wing surface. Equation (1) is the steady-state equivalent of equation (1) of reference 1. A collocation procedure is used in order to get its numerical inversion.

The surface integrations have been performed following the technique exposed in reference 1, with proper modifications which take care of the singularities that the control surfaces introduce in the function $\Delta p(\xi,\eta)$. The notations are also analogous to those used in reference 1.

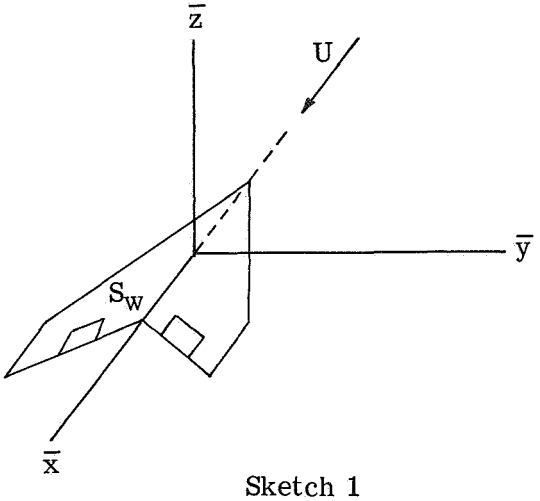

Sketch 1

The adopted coordinate system is represented in sketch 1, where S_W represents the idealized wing surface, which lies very close to the xy-plane. The function $\Delta p(\xi,\eta)$ is defined as $\Delta p(\xi,\eta) = p_l(\xi,\eta) - p_u(\xi,\eta)$, that is, the local pressure difference between the lower and upper surfaces of the wing. By definition, the function is positive when it produces a local lifting force directed towards the positive sense of the z-axis. Consistent with the adopted coordinate system, $w(x,y)$ is also positive upwards. The kernel function K is defined as in reference 1.

The planform of the wing and control surface considered is represented in sketch 2, its geometry being fixed by Λ and the parameters

$$s = \frac{l}{b_0} \qquad \lambda = \frac{b_t}{b_0} \qquad \mu = \frac{c_c}{b_0} \qquad y_{c1} = \frac{\bar{y}_{c1}}{l} \qquad y_{c2} = \frac{\bar{y}_{c2}}{l} \tag{2}$$

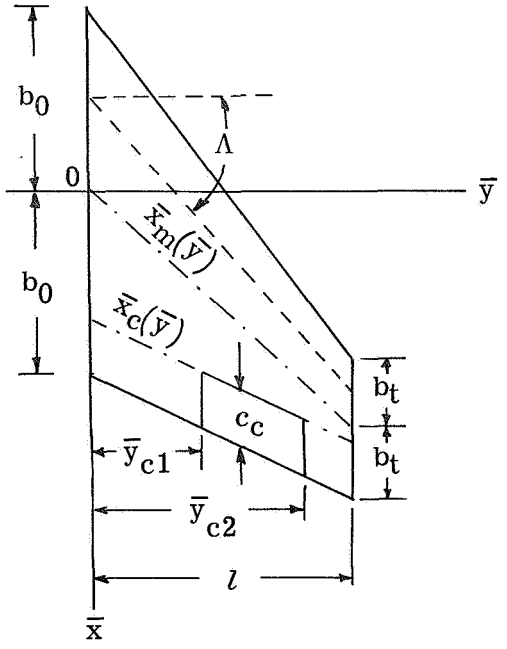

Sketch 2

The formulation and the computing program could be adapted to a more general planform, in particular to tapered controls, but the one programed is general enough for the present purpose.

The main feature that a control surface introduces in the problem of calculating pressure distributions on a wing, under the hypothesis of a linearized flow ($M < 1$) and idealized conditions of a sealed hinge and side edges, is a distribution of logarithmic singularity on such a hinge. If this singularity is approximated by the usual pressure mode series associated with a wing without controls, slow convergence may result as the number of modes is increased, or the series may be found to be inapplicable. This circumstance, together with other possible problems associated with gaps

and possible flow separations, makes it necessary to treat the case of control surfaces with special care.

Following formulation of the idealized problem through integral equation (1), attention focuses on a search for a suitable analytical representation of the function $\Delta p(\xi,\eta)$ and on accurate numerical integration over the wing surface S_w. For a given downwash distribution $w(x,y)$ over the wing, the function $\Delta p(\xi,\eta)$ should be represented by a suitable series expansion which converges as quickly as possible toward the exact solution of the integral equation and produces at the same time a good conditioning of the matrix of the set of linear algebraic equations to which the collocation procedure leads. Achievement of these two properties would mean that the kernel transforms of the pressure modes would yield a series of downwash modes which should combine to give rapid convergence toward a prescribed downwash $w(x,y)$. In order to determine how accurate this approximate solution is, the resulting downwash distribution is calculated and visually compared with the desired downwash $w(x,y)$.

In order to represent conveniently the loading due to both wing modes and flap modes of pressure, a pressure expansion is chosen of the form

$$\Delta p\left[\xi(\theta),\eta\right] = 4\pi\rho U^2 \frac{l}{b_0}\frac{b_0}{b}\sqrt{1-\eta^2}\left[\sum_{n,m} a_{nm}A_{nm}(\theta,\eta) + \sum_{n,m} b_{nm}B_{nm}(\theta,\eta)\right] \tag{3}$$

where the transformation

$$\xi = \xi(\theta) = \xi_m(\eta) - \frac{b}{b_0}\cos\theta \tag{4}$$

has been introduced as in reference 1. Although the pressure modes are the products of $\frac{b_0}{b}\sqrt{1-\eta^2}$ times $A_{nm}(\theta,\eta)$ and times $B_{nm}(\theta,\eta)$, for convenience in the rest of the report they are referred to simply as $A_{nm}(\theta,\eta)$ for wing modes and $B_{nm}(\theta,\eta)$ for flap modes and they can be combined additively because the governing equation has been linearized. The second subscript m is even for spanwise symmetry and odd for spanwise antisymmetry of the functions.

The wing modes can be defined in any conventional form. (See refs. 1 to 5.) As in reference 1, the following form was chosen:

$$\left.\begin{aligned} A_{nm}(\theta,\eta) &= \eta^m L_{A_n}(\theta) \\ L_{A_0}(\theta) &= \cot\frac{\theta}{2} \\ L_{A_n}(\theta) &= \frac{1}{2^{2n-1}}\sin n\theta \qquad (n = 1, 2, \ldots) \end{aligned}\right\} \tag{5}$$

where

and even and odd m apply to spanwise symmetry and antisymmetry, respectively.

Equations (5) represent the pressure distributions over the complete lifting surface without the influence of flap deflection. Since the highest order singularity in the kernel function is the same for both steady and unsteady flow, the singularities in the pressure distributions can be expected to be the same for both steady and unsteady flow. Hence, the pressure modes appropriate to steady flow are expected to be applicable to unsteady flow as well.

The flap modes are developed in the rest of the present report. The coefficients a_{nm} and b_{nm} are the initially unknown weighting factors in the pressure distribution.

Preliminary Investigation Based on Separation of Variables

In preliminary calculations the special case was studied of $M = 0$ and a flat wing of rectangular planform with an aspect ratio of 4 ($s = 4$, $\lambda = 1$, and $\Lambda = 0$) and a deflected full-span flap hinged at 75 percent of the wing chord. Subsequent discussion in this section related to the inadequacy of the two-dimensional type of loading function is based on these calculations.

In order to gain insight into the problem, begin by assuming the following form for the flap loading functions:

$$B_{nm}^{(1)}(\theta,\eta) = \eta^m L_{B_n}(\theta) \tag{6}$$

(the notation $B_{nm}^{(1)}(\theta,\eta)$ is used to distinguish these as exploratory modes)

$$L_{B_n}(\theta) = \frac{1}{2^{2n-1}}(\cos\theta - \cos\theta_c)^n \ln\frac{1 - \cos(\theta - \theta_c)}{|\cos\theta - \cos\theta_c|} \tag{7}$$

where θ_c is the coordinate of the flap hinge. For $n = 0$, 1, and 2, these modes conform to the velocity potentials in reference 23.

The downwash input $w(x,y)$ considered in the calculations is 0 over the wing and 1 over the flap. Eighteen modes of pressure were used to represent the pressure distribution: All combinations of $n = 0, 1, 2$ and $m = 0, 2, 4$ for both kinds of pressure modes $A_{nm}(\theta,\eta)$ and $B_{nm}(\theta,\eta)$.

The numerical inversion of the integral equation (eq. (1)) relating $w(x,y)$ with $\Delta p(\xi,\eta)$ was programed on a computer, and the resulting pressure distribution with the weighting factors now known was the new input required to recalculate, through equation (1), the corresponding downwash distribution. Although this recalculated downwash and the initial input $w(x,y)$ coincided at the collocation points as required, the agreement elsewhere was poor and remained poor through various modifications of the numerical chordwise integration procedure used for the modes $B_{nm}^{(1)}(\theta,\eta)$.

This result is mentioned because this kind of representation, inspired like $B_{nm}^{(1)}(\theta,\eta)$ by the two-dimensional theory, has been for years a common approach that has been tried, often without satisfactory results, to analyze the aerodynamic forces on three-dimensional (finite-span) control surfaces.

Neither the use of new flap modes, made with combinations of modes $B_{nm}^{(1)}(\theta,\eta)$, nor the use of a least-squares procedure (with 32 control points) for calculating the coefficients a_{nm} and b_{nm} had an appreciable effect of improving the solution. With the least-squares procedure, better shapes of the recalculated downwash distribution were obtained in the regions where some number of control points were concentrated, but the results remained poor in other regions of the wing. With a limited number of pressure modes, a more dense distribution of control points can average on the wing surface the good or poor quality of the results but not make them substantially better. Alternatively, increasing the number of modes of pressure does not always improve these results but can even make them worse if the solution does not converge.

In the calculations for which the same number of control points and unknown coefficients a_{nm} and b_{nm} were used, the location of the control points over the wing also showed a great influence on the results. An apparently insignificant change in the control-point locations can produce a drastic change in the shape of the recalculated downwash but, in general, without introducing any significant improvement in the total result.

From these results, equation (7) is concluded to be an unsatisfactory representation of the pressure distribution.

Another possible source of trouble which can considerably influence the results is inaccuracy in the numerical integrations. Accurate techniques can be used to perform the numerical integration of functions which contain a logarithmic singularity, such as the Berthod-Zaborowski quadrature (a weighted Gaussian type of quadrature, see, e.g., table 9 in ref. 27). But in the present case, the kernel function introduces an additional problem (it approaches a chordwise step function in the vicinity of the collocation point; i.e., as $y - \eta \to 0$) which is difficult to treat and can be a source of important errors, mainly when the control point is located very near the control-surface hinge. The numerical surface integration of a logarithmic singularity which terminates within the region of integration (such as that at the hinge of the usual control surface with a span smaller than the wing span) also presents some special difficulties. This is the kind of logarithmic singularity that the functions $B_{nm}(\theta,\eta)$ possess, as will be shown in a subsequent section herein. Nevertheless, experience gained during the preliminary calculations has given confidence in the accuracy of the integration procedure adopted (also described below) even though the quality of the pressure representation was not satisfactory.

With the purpose of gaining better insight into the reasons why this representation of the pressure distribution was so poor, the downwash distribution which corresponds to

each mode of pressure used in equation (6) was studied. These distributions are called wing modes of downwash $W_{A_{nm}}(x,y)$ and flap modes of downwash $W_{B_{nm}}(x,y)$.

Each downwash mode $W_{A_{nm}}(x,y)$ or $W_{B_{nm}}(x,y)$ comes from its related pressure mode $A_{nm}(\theta,\eta)$ or $B_{nm}(\theta,\eta)$, respectively, through the basic integral equation.

The function $\frac{w(x,y)}{U}$ becomes represented by the expansion

$$\frac{w(x,y)}{U} = \sum_{n,m} a_{nm} W_{A_{nm}}(x,y) + \sum_{n,m} b_{nm} W_{B_{nm}}(x,y) \tag{8a}$$

where $n = 0, 1, \ldots n_{max}$ and $m = 0, 1, \ldots m_{max}$. (The maximum values n_{max} and m_{max} can be different in each summation.)

The evaluation of this truncated expansion at some particular points (control points) on the wing surface gives the matrix expression

$$\{w\} = [W]\begin{Bmatrix} a \\ b \end{Bmatrix} \tag{8b}$$

from which it is possible to calculate the values of the weighting factors a_{nm} and b_{nm}. Good convergence of this downwash expansion and good conditioning of the matrix $[W]$ are qualities which are sought when a collocation procedure is adopted.

A convenient and possibly ideal choice of pressure modes $A_{nm}(\theta,\eta)$ and $B_{nm}(\theta,\eta)$ to be used in the pressure expansion would be that which originates a set of downwash modes $W_{nm}(x,y)$ that not only is orthogonal but also converges rapidly (with a few of the lowest order modes) to a good approximation of the downwash for actual deflecting and deforming controls. Furthermore, the higher order terms should produce small and decreasing corrections to adjust closer to the desired downwash the approximation that results from the truncated expansion.

These qualities are particularly important in cases where control surfaces are involved. The deflection of a control surface introduces a first-order discontinuity in the function $w(x,y)$; that is, the downwash is a nonzero constant on the control surface and zero on the rest of the wing. This elementary mode of downwash accounts for the deflection of a control surface in the function $w(x,y)$. Furthermore, for the case in which the control surface behaves as a rigid structure, this downwash mode is the only one which introduces the logarithmic singularities in the pressure distribution. Sketch 3 illustrates this first flap mode of downwash.

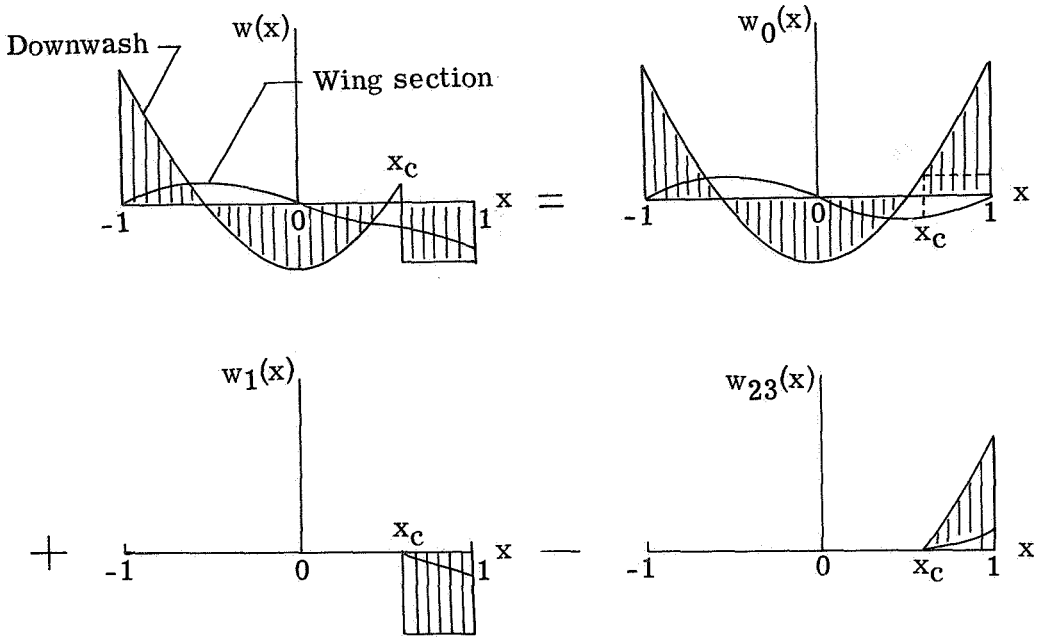

$$w(x) = w_0(x) + w_1(x) - w_{23}(x)$$

Sketch 3

The sketch represents a cambered wing section, taken in a region where a control surface has been deflected, and the chordwise downwash distribution which corresponds to this section. Also shown is the separation of the actual downwash $w(x)$ into three modes of downwash: $w_0(x)$, $w_1(x)$, and $w_{23}(x)$.

The mode $w_1(x)$ is the first flap mode of downwash. The mode $w_{23}(x)$ can be further separated into two more elementary modes, as is illustrated in sketch 4.

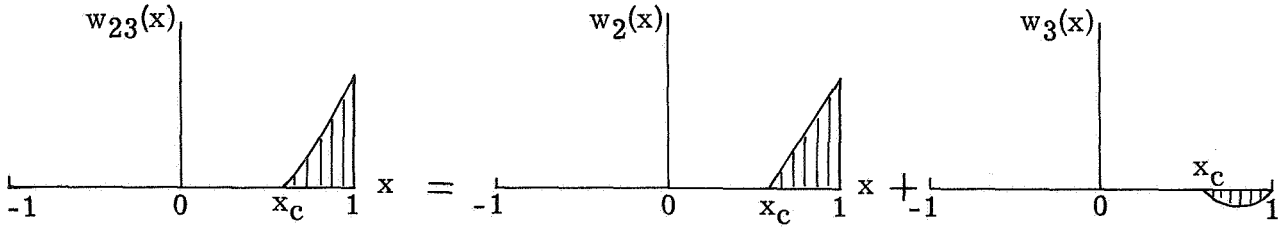

$$w_{23}(x) = w_2(x) + w_3(x)$$

Sketch 4

Thus, the downwash $w(x)$ can be separated into the four elementary modes

$$w(x) = w_0(x) + w_1(x) - w_2(x) - w_3(x) \tag{9}$$

The mode $w_0(x)$ is one of the kind called wing modes of downwash $W_{A_{nm}}(x,y)$. (It could be any chordwise third-order mode, represented by the general expression $W_{A_{3m}}(x,y)$.) The modes $w_1(x)$, $w_2(x)$, and $w_3(x)$ are flap modes of downwash, which are defined by $W_{B_{nm}}(x,y)$. (They could be any one of $W_{B_{0m}}(x,y)$, $W_{B_{1m}}(x,y)$, or $W_{B_{2m}}(x,y)$, respectively.) The mode $w_1(x)$ represents the first mode $W_{B_{00}}(x,y)$, when the downwash distribution on the control surface is a constant in the spanwise sense. This mode, together with a smaller contribution of the mode $W_{B_{01}}(x,y)$, which becomes important in cases where the control surface can experience an appreciable torsion, may be the only component of the downwash distribution $w(x,y)$ responsible for the logarithmic singularity of the pressure function in many practical calculations.

Clearly, it would be useful to develop in the pressure expansion a term $B_{00}(\theta,\eta)$ able to originate a downwash distribution $W_{B_{00}}(x,y)$ as close as possible to this ideal mode $w_1(x)$. If none of the modes $W_{B_{nm}}(x,y)$ appear to be a good approximation to this ideal shape, a high number of modes may be required to represent adequately the actual downwash and, consequently, the corresponding pressure distribution. This characteristic will also aggravate the additional problems of convergence and good conditioning of the martix $[W]$.

The "optimal location" of control points actually in use (see refs. 2 to 6) is based on a separation of variables which does not always yield significant improvements in practice in comparison with arbitrary location, at least for low frequencies and simple downwash modes (see refs. 17 and 18, for example), and which does not apply to the case of control surfaces. Anyway, the results of lifting-surface calculations depend more directly on the capability of the downwash truncated expansion to approximate the function $w(x,y)$ than on the optimizing of the control-point locations. That does not necessarily mean that the search for a realistic optimal conditioning of the matrix $[W]$ is unimportant for improving the results in calculations of wings with or without control surfaces. But it must be kept in mind that this optimal location depends essentially on the actual shapes of the modes $W_{nm}(x,y)$, its validity being dependent on the capability of these modes to represent the actual downwash distribution on the wing. Furthermore, for the analytic expressions and integration procedures used herewith, control-point locations must be selected that are not too close to regions where the modes $W_{nm}(x,y)$ can suffer appreciable distortions due to numerical errors; such regions are wing leading and trailing edges and control-surface boundaries. It is also recommended to avoid, as much as possible, the nodal lines of the modes $W_{nm}(x,y)$ and to spread the control points on the regions where these downwash modes are widely different among themselves.

In figure 1(a) is plotted the first downwash mode $W^{(1)}_{B_{00}}(x,y)$ obtained by the early calculations mentioned for a full-span flap on the wing with the parameters listed. (The superscript (1) is used to distinguish these modes as exploratory.) Figures 1(b) and 1(c) show two higher order modes $W^{(1)}_{B_{20}}(x,y)$ and $W^{(1)}_{B_{30}}(x,y)$. The mode $W^{(1)}_{B_{00}}(x,y)$ appears to be an unsatisfactory approximation to the ideal shape $w_1(x)$ in sketch 3, and the higher modes can do very little to improve this approximation. The modes $W^{(1)}_{B_{20}}(x,y)$ and $W^{(1)}_{B_{30}}(x,y)$ are too much alike for numerical purposes, and this is a circumstance which affects adversely the conditioning of the matrix $[W]$.

Figures 1(a), 1(b), and 1(c) also show for comparison the wing downwash modes $W_{A_{00}}(x,y)$, $W_{A_{20}}(x,y)$, and $W_{A_{30}}(x,y)$. The contrast between the good conditioning of these wing modes and the poor conditioning of the flap modes is evident. This is the reason why the results of calculations of pressure distributions on wings without control surfaces are much better than those on wings with control surface.

These particular results show that any combination of wing and flap modes shown would have a poor capability for representing the desired downwash $w(x,y)$ for a deflected flap and would cause a worsening condition of the matrix $[W]$ if an attempt were made to improve the results with additional higher modes from equation (7).

In contrast, the two-dimensional wing theory from which the pressure modes $A_{nm}(\theta,\eta)$ and $B^{(1)}_{nm}(\theta,\eta)$ are selected provides a good basis for comparison of these results. It is known from the existing literature (see, e.g., ref. 23) that for the analogous case of a thin planar airfoil with a deflected flap, a combination of only the two first modes $L_{A_0}(\theta)$ and $L_{B_0}(\theta)$ is enough to represent the exact solution of the lifting pressure in steady flow. The term $L_{A_0}(\theta)$ originates a downwash mode which is a constant on the total airfoil, and the term $L_{B_0}(\theta)$ originates a downwash which takes a constant value on the flap region and another substantially different constant value on the rest of the airfoil. That should be an ideal goal for the three-dimensional case too. But figure 1 shows that this goal has not been achieved in the early calculations based on equation (7).

These results make evident the need for new pressure modes $B_{nm}(\theta,\eta)$ able to originate a set of better conditioned downwash modes $W_{B_{nm}}(x,y)$.

Search for Surface Loading Functions

Because of the desired nature of the downwash mode $W_{B_{00}}(x,y)$ (as close as possible to a constant value on the control surface and a different constant value on the rest of the wing), one cannot expect to get a general orthogonal set of modes $W_{nm}(x,y)$ that includes both wing and flap downwash modes. But it appears to be possible to get wing modes which are already fairly close to a set of orthogonal functions (by combining the

chordwise pressure distributions $L_{A_n}(\theta)$ with proper spanwise distributions), then to find flap modes $W_{B_{nm}}(x,y)$ which also are nearly an orthogonal set. The problem is how to find a set of pressure modes able to originate these downwash modes.

The following section presents the development of pressure modes based on an analogy between (1) the flow perturbations over a nonlifting wedge-shaped wing with symmetric thickness distribution and (2) the perturbations over a lifting deflected flap.

Analogy of nonlifting wing with thickness.- It is hypothesized here that for a nonlifting finite-planform wing with symmetric (with respect to the xy-plane) nonzero thickness distribution and a sharp leading edge, those fluid particles traveling infinitesimally close to the xy-plane and suddenly deflected in their trajectories when passing by the leading edge are subjected to physical conditions very similar to those particles traveling close to the upper side of a lifting surface and being suddenly deflected in passing the concave corner at the hinge of an upward deflected control surface. From linear theory, the effect of a convex corner would be equal and opposite in sign. Such a nonlifting wing with symmetric thickness and sharp leading edge is illustrated in sketch 5. On the basis of this hypothesis, it is expected that the solution for the flow past the leading edge, including the corners, of the wing of sketch 5 can provide useful information on the analytical form of the local pressure distribution in the neighborhood of a control-surface hinge and edges.

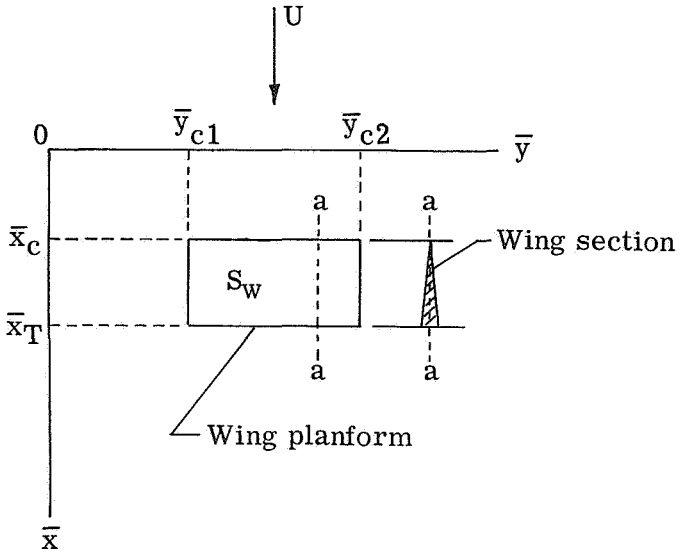

Sketch 5

If $w_s(\bar{x},\bar{y},0)$ is the distribution of simple sources that matches the downwash distribution on the upper surface of this wing (sketch 5) and $p_s(\bar{x},\bar{y},\bar{z})$ is the associated pressure perturbation, then for the steady wing they are related, according to linear theory, by the expression

$$p_s(\bar{x},\bar{y},\bar{z}) = -\frac{\rho U}{2\pi}\frac{\partial}{\partial \bar{x}}\iint_{S_w}\frac{w_s(\bar{\xi},\bar{\eta},0)}{\sqrt{(\bar{x}-\bar{\xi})^2+\beta^2\left[(\bar{y}-\bar{\eta})^2+\bar{z}^2\right]}}\,d\bar{\xi}\,d\bar{\eta} \tag{10}$$

The advantage of this approach becomes apparent. Only simple sources need be considered, and the desired pressure is directly obtainable rather than being contained within an integral of an integral equation.

Consider a function $w_s(\bar{\xi},\bar{\eta},0)$ defined on the wing surface by the series expansion of orthogonal terms

$$w_s(\bar{\xi},\bar{\eta},0) = U \sum_{n,r} d_{nr} P_n\left[\frac{2}{\bar{\mu}}\left(\bar{x}_{c0}-\bar{\xi}\right)\right] P_r\left[\bar{\delta}_c\left(\bar{y}_{c0}-\bar{\eta}\right)\right] \tag{11}$$

where the quantities d_{nr} are constant factors whose numerical determination is of no concern here, and

$$\bar{\mu} = \bar{x}_T - \bar{x}_c$$

$$\bar{\delta}_c = \frac{2}{\bar{y}_{c2} - \bar{y}_{c1}} \qquad \left(\bar{y}_{c2} > \bar{y}_{c1}\right)$$

$$\bar{x}_{c0} = \frac{\bar{x}_T + \bar{x}_c}{2}$$

$$\bar{y}_{c0} = \frac{\bar{y}_{c2} + \bar{y}_{c1}}{2}$$

The functions P_n and P_r are Legendre polynomials of arguments $\frac{2}{\bar{\mu}}\left(\bar{x}_{c0}-\bar{\xi}\right)$ and $\bar{\delta}_c\left(\bar{y}_{c0}-\eta\right)$, respectively, and can be defined by

$$P_r[f] = \frac{1}{2^r} \sum_{j=0}^{[r/2]} (-1)^j \binom{r}{j} \binom{2r-2j}{r} f^{r-2j} \tag{12a}$$

(where $[r/2]$ indicates the integer part of $r/2$ and f is a dummy argument), or alternatively by Rodrigues' form

$$P_r[f] = \frac{1}{2^r r!} \frac{d^r}{df^r}\left[\left(f^2 - 1\right)^r\right] \tag{12b}$$

This downwash (eq. (11)) originates a pressure

$$p_s(\bar{x},\bar{y},\bar{z}) = -\frac{\rho U^2}{2\pi} \sum_{n,m} d_{nr} \int_{\bar{x}_c}^{\bar{x}_T} P_n\left[\frac{2}{\bar{\mu}}\left(\bar{x}_{c0}-\bar{\xi}\right)\right] d\bar{\xi} \frac{\partial}{\partial \bar{x}} \int_{\bar{y}_{c1}}^{\bar{y}_{c2}} \frac{P_r\left[\bar{\delta}_c\left(\bar{y}_{c0}-\bar{\eta}\right)\right]}{\sqrt{(\bar{x}-\bar{\xi})^2 + \beta^2\left[(\bar{y}-\bar{\eta})^2 + \bar{z}^2\right]}} d\bar{\eta} \tag{13}$$

The integration with respect to $\bar{\eta}$ can be carried out in closed form so that the pressure is then represented by the expansion

$$p_s(\bar{x},\bar{y},\bar{z}) = -\frac{\rho U^2}{2\pi} \sum_{n,m} d_{nr}\left[C_{T_{nr}}(\bar{x},\bar{y},\bar{z}) - C_{H_{nr}}(\bar{x},\bar{y},\bar{z})\right] \tag{14}$$

where $C_{T_{nr}}$ and $C_{H_{nr}}$ are the values that the indefinite integral

$$C_{\xi_{nr}}(\bar{x},\bar{y},\bar{z}) = \int^{\bar{\xi}} P_n\left[\frac{2}{\bar{\mu}}\left(\bar{x}_{c0}-\bar{\xi}\right)\right]\frac{\partial}{\partial\bar{x}}\,\Gamma_r(\bar{x}-\bar{\xi},\bar{y},\bar{z})d\bar{\xi} \tag{15}$$

takes at the trailing edge $\bar{\xi} = \bar{x}_T$ and leading edge $\bar{\xi} = \bar{x}_c$, respectively.

The function $\Gamma_r(\bar{x}-\bar{\xi},\bar{y},\bar{z})$ is defined as

$$\Gamma_0(\bar{x}-\bar{\xi},\bar{y},\bar{z}) = \frac{-1}{\beta}\ln\frac{\sqrt{(\bar{x}-\bar{\xi})^2+\beta^2\left[\left(\bar{y}-\bar{y}_{c1}\right)^2+\bar{z}^2\right]}-\beta\left(\bar{y}-\bar{y}_{c1}\right)}{\sqrt{(\bar{x}-\bar{\xi})^2+\beta^2\left[\left(\bar{y}-\bar{y}_{c2}\right)^2+\bar{z}^2\right]}-\beta\left(\bar{y}-\bar{y}_{c2}\right)} \tag{16}$$

When $r \geq 1$,

$$\Gamma_r(\bar{x}-\bar{\xi},\bar{y},\bar{z}) = \sqrt{(\bar{x}-\bar{\xi})^2+\beta^2\left[\left(\bar{y}-\bar{y}_{c1}\right)^2+\bar{z}^2\right]}\,Q_{r-1}\left(\bar{y}-\bar{y}_{c1}\right)$$

$$-\sqrt{(\bar{x}-\bar{\xi})^2+\beta^2\left[\left(\bar{y}-\bar{y}_{c2}\right)^2+\bar{z}^2\right]}\,Q_{r-1}\left(\bar{y}-\bar{y}_{c2}\right)+\nu_r(\bar{\xi})\Gamma_0(\bar{x}-\bar{\xi},\bar{y},\bar{z}) \tag{17}$$

where Q_{r-1} is a polynomial (not Legendre's second kind) of degree $r-1$ and argument $\bar{y}-\bar{y}_{c1}$ or $\bar{y}-\bar{y}_{c2}$, and $\nu_r(\bar{\xi})$ is a function of $\bar{\xi}$ (also of $\bar{x}$, $\bar{y}$, and $\bar{z}$) and does not depend on $\bar{\eta}$. Both can be calculated by the method of undetermined coefficients through the identity

$$P_r\left[\bar{\delta}_c\left(\bar{y}_{c0}-\eta\right)\right] \equiv -\left\{(\bar{x}-\bar{\xi})^2+\beta^2\left[\left(\bar{y}-\bar{\eta}\right)^2+\bar{z}^2\right]\right\}Q'_{r-1}(\bar{y}-\bar{\eta})+\beta^2(\bar{y}-\bar{\eta})Q_{r-1}(\bar{y}-\bar{\eta})+\nu_r(\bar{\xi}) \tag{18}$$

by matching on left and right sides the coefficients of each power of $\bar{\eta}$, the coefficients themselves being functions of $\bar{\xi}$, $\bar{x}$, $\bar{y}$, and $\bar{z}$. In equation (18),

$$Q'_{r-1}(\bar{y}-\bar{\eta}) \equiv \frac{\partial}{\partial\bar{\eta}}\,Q_{r-1}(\bar{y}-\bar{\eta}) \tag{19}$$

Expressions for $Q_{r-1}(\bar{y}-\bar{\eta})$ and $\nu_r(\bar{\xi})$ for r up to 5 are given in appendix A.

The local distribution in the neighborhood of the wing leading edge (which simulates a control-surface hinge) is given by the expression

$$p_{H_S}(\bar{x},\bar{y},\bar{z}) = \frac{\rho U^2}{2\pi}\sum_{n,r} d_{nr}C_{H_{nr}}(\bar{x},\bar{y},\bar{z}) \tag{20}$$

By taking the limit $\bar{z} \to 0$, the local pressure distribution $p_{H_S}(\bar{x},\bar{y},0)$ in the $\bar{x}\bar{y}$-plane is obtained. This function also represents the local pressure distribution which appears on the upper side of a flat lifting surface in the neighborhood of the hinge of an upward deflected control surface, when the downwash is zero on the wing and $w_S(\bar{x},\bar{y},0)$ on the

control-surface region. The terms $C_{H_{nr}}(\bar{x},\bar{y},0)$ of the resulting expansion are then pressure distributions associated with an orthogonal set of downwash modes. They contain the appropriate singularities that the hinge of a control surface introduces in the pressure distribution, and with the usual corrections to account for the effect of wing tips and leading and trailing edges (as in ref. 1), they can serve to originate the flap modes of pressure $B_{nm}(\theta,\eta)$ that are sought for the lifting-surface case.

The terms $C_{H_{00}}(\bar{x},\bar{y},0)$, $C_{H_{10}}(\bar{x},\bar{y},0)$, $C_{H_{20}}(\bar{x},\bar{y},0)$, $C_{H_{01}}(\bar{x},\bar{y},0)$, and $C_{H_{02}}(\bar{x},\bar{y},0)$ are given in appendix B. Since the main effect of deflection of the control surface is given by the mode $B_{00}(\theta,\eta)$ and since the higher order modes $B_{nm}(\theta,\eta)$ serve mainly as corrections of the distortion that the wing modes $A_{nm}(\theta,\eta)$ introduce in the downwash distribution on the control-surface region, only a few flap modes of pressure $B_{nm}(\theta,\eta)$ are expected to be needed in most of the practical calculations. The relationship between the indices m and r is given subsequently in the development of higher order pressure modes, where it becomes necessary for $m > 0$.

The term $C_{H_{00}}(\bar{x},\bar{y},0)$ has the expression (in dimensional coordinates)

$$C_{H_{00}}(\bar{x},\bar{y},0) = \frac{1}{\beta} \ln \frac{\sqrt{(\bar{x} - \bar{x}_c)^2 + \beta^2(\bar{y} - \bar{y}_{c1})^2} - \beta(\bar{y} - \bar{y}_{c1})}{\sqrt{(\bar{x} - \bar{x}_c)^2 + \beta^2(\bar{y} - \bar{y}_{c2})^2} - \beta(\bar{y} - \bar{y}_{c2})} \tag{21a}$$

which except for notation is the same as the local solution found by Landahl (eqs. (33) to (35) of ref. 26, with reduced frequency set equal to zero). In reference 26, the pressure distribution for an oscillating planar rectangular control surface was developed by the method of matched asymptotic expansions.

One way of introducing the correct wing-edge behavior is by multiplying $C_{H_{00}}(\bar{x},\bar{y},0)$ by the factor

$$\sqrt{\frac{(\bar{x} - \bar{x}_L)(\bar{x}_T - \bar{x})}{(\bar{x}_c - \bar{x}_L)(\bar{x}_T - \bar{x}_c)}}$$

as in reference 26. The resulting flap pressure mode is denoted for a wing with partial-span flaps (as in fig. 6) by

$$B_{00}^{(2)}(\theta,\eta) = \frac{1}{\beta} \frac{\sin\theta}{\sin\theta_c} \ln \frac{\sqrt{(\cos\theta - \cos\theta_c)^2 + \beta^2 s^2(|\eta| - y_{c1})^2} - \beta s(|\eta| - y_{c1})}{\sqrt{(\cos\theta - \cos\theta_c)^2 + \beta^2 s^2(|\eta| - y_{c2})^2} - \beta s(|\eta| - y_{c2})} \tag{21b}$$

where the variables $\bar{x}$ and $\bar{y}$ have been changed into θ and η, respectively, and a superscript (2) is used to differentiate this mode from the finally adopted $B_{00}(\theta,\eta)$. For a full-span flap (as in fig. 2), $y_{c1} = -1$, $y_{c2} = 1$, and $|\eta|$ is replaced by η.

In figure 2, is shown the downwash distribution $W^{(2)}_{B_{00}}(x,y)$ that the mode $B^{(2)}_{00}(\theta,\eta)$ originates when applied to a square planform wing with a full-span flap $\eta_{c2} = -\eta_{c1} = 1.0$. A good characteristic of this downwash distribution is that it has at the hinge nearly a first-order discontinuity in the chordwise sense, and this discontinuity has a nearly constant magnitude along the span. This quality is found in all the numerical calculations performed with the mode $B^{(2)}_{00}(\theta,\eta)$. That means a good approximation to the ideal first-order discontinuity which is sought in the mode $W_{B_{00}}(x,y)$. But the mode $W^{(2)}_{B_{00}}(x,y)$ also presents, for a reasonable amplitude of the discontinuity, the undesirable qualities of a high slope chordwise and a too high curvature in the spanwise sense. These qualities produce a general shape which is not close to the flat distribution (with a first-order discontinuity on the control-surface contour) desired for the mode $W_{B_{00}}(x,y)$.

There is another difficulty involved in the mode $B^{(2)}_{00}(\theta,\eta)$: If s increases in such a way that the wing planform tends to become a two-dimensional wing with a deflected flap, the values of the pressure distribution on the wing also increase and tend to infinity in the limit. This result does not make physical sense and indicates that the analytical expression of the mode must be corrected.

This difficulty would not be present if, together with each term $C_{H_{nr}}(\bar{x},\bar{y},0)$ in the expansion of the local pressure distribution $p_{H_s}(\bar{x},\bar{y},0)$, there had been included the effect that the corresponding term $C_{T_{nr}}(\bar{x},\bar{y},0)$, which also appears in the total solution $p_s(\bar{x},\bar{y},0)$, introduces in the limit when the magnitudes $\bar{y}_{c1}$ and $\bar{y}_{c2}$ increase in the mentioned way.

Empirical modifications of pressure modes.- An attempt was made to improve the mode $B^{(2)}_{00}(\theta,\eta)$, and all the following higher order modes, by introducing the following empirical modifications to equations (21):

(1) For use on the lifting case, each term $C_{H_{nr}}(\bar{x},\bar{y},0)$ has been "corrected" with a function which behaves as $C_{T_{nr}}(\bar{x},\bar{y},0)$ (from eq. (15)) when $\bar{y}_{c1} \to -\infty$ and $\bar{y}_{c2} \to \infty$ but which obeys the trailing-edge Kutta condition rather than having the logarithmic singularity that each term $C_{T_{nr}}(\bar{x},\bar{y},0)$ has on the trailing edge for the nonlifting wing of symmetrical thickness.

(2) The variable $\bar{x}$ always appears in the combination $\bar{x} - \bar{x}_c$ in each term $C_{H_{nr}}(\bar{x},\bar{y},0)$.

Introduction of the same transformation as in equation (4) leads to

$$\xi - \xi_c(\eta) = -\frac{b}{b_0}(\cos\theta - \cos\theta_c) \tag{22a}$$

where

$$\theta_c = \arccos\left\{\frac{b_0}{b}\left[\xi_m(\eta) - \xi_c(\eta)\right]\right\}$$

Note that in the vicinity $\theta \approx \theta_c$ the quantity

$$\left|\cos\theta - \cos\theta_c\right| \sim \left|\theta - \theta_c\right|\sin\theta_c \tag{22b}$$

In order to cause the functions $B_{nm}(\theta,\eta)$ to approach the two-dimensional pressure distribution of equation (7) (for $nm = 00$) as the wing planform tends toward a two-dimensional wing plus flap, wherever $\xi - \xi_c(\eta)$ appears, it is replaced by

$$-X(\theta,\theta_c,\eta) = -\frac{b}{b_0}\frac{1 - \cos(\theta - \theta_c)}{\left|\cos\theta - \cos\theta_c\right|}\,2\sin^2\theta_c \tag{23a}$$

which is asymptotic to $\xi - \xi_c(\eta)$ as $\xi \to \xi_c(\eta)$; that is, in the vicinity $\theta \approx \theta_c$

$$-\frac{1 - \cos(\theta - \theta_c)}{\left|\cos\theta - \cos\theta_c\right|}\,2\sin^2\theta_c \sim \left|\theta - \theta_c\right|\sin\theta_c \tag{23b}$$

which is the same asymptotic behavior as that expressed by equation (22b). In addition the following definition is introduced:

$$X_T \equiv X(\pi,\theta_c,\eta) = -\frac{b}{b_0}\,2\sin^2\theta_c \tag{23c}$$

(3) The semispan-semichord ratio s is replaced by an effective value

$$s_e = sE_S \tag{23d}$$

where E_S is a span expansion-contraction factor that can be a constant or a span variable. The function of E_S is to make relatively stronger ($E_S < 1.0$) or weaker ($E_S > 1.0$) the induced effect of the control-surface tips. A value of E_S greater than 1.0 has the effect of putting the control tips farther away from the rest of the control surface and wing. The effect of the control tip is thus attenuated and the pressure distribution in the central region of the control surface is closer to the two-dimensional distribution. When E_S is given an appropriate value, it has a very noticeable effect of improving the downwash distribution $W_{B_{00}}(x,y)$. This value depends mainly on the wing and control-surface configuration, but it is also affected by the Mach number and possibly by the reduced frequency considered in the analysis of any unsteady case. The influence of this parameter and its order of magnitude for several configurations, as well as the influence of the Mach number, will be discussed further in the section entitled "Results and Discussion." Since no practical relation for predetermining the appropriate value of E_S is yet known, some numerical exploration in each particular case is recommended. The first mode $B_{00}(\theta,\eta)$ can be programed with E_S as an input parameter, and then several values of E_S can be tested to pick the one which gives the best downwash mode $W_{B_{00}}(x,y)$.

With these three empirical modifications to equation (21b), the first flap mode of lifting pressure for an unswept flap becomes

$$B_{00}(\theta,\eta) = \frac{1}{\beta} \ln \left[\frac{\sqrt{X_T^2 + \beta^2 s_e^2 \left(y_{c2} - |\eta|\right)^2} + \beta s_e \left(y_{c2} - |\eta|\right)}{\sqrt{X_T^2 + \beta^2 s_e^2 \left(y_{c1} - |\eta|\right)^2} + \beta s_e \left(y_{c1} - |\eta|\right)} \right.$$

$$\left. \cdot \frac{\sqrt{X^2\left(\theta,\theta_c,\eta\right) + \beta^2 s_e^2 \left(y_{c1} - |\eta|\right)^2} + \beta s_e \left(y_{c1} - |\eta|\right)}{\sqrt{X^2\left(\theta,\theta_c,\eta\right) + \beta^2 s_e^2 \left(y_{c2} - |\eta|\right)^2} + \beta s_e \left(y_{c2} - |\eta|\right)} \right] \tag{24}$$

where the absolute value $|\eta|$ is taken in order to make the expression applicable to both right- and left-wing semispans, and where the first factor in the argument of the log function (the one containing X_T) is the correction factor resulting from modification (1) above. The multiplication of the log function by $\sin\theta/\sin\theta_c$ as in equation (21b) is not needed because with the given modifications the function B_{00} of equation (24) has the desired zero lift at wing leading and trailing edges. Also note that

$$\lim_{\substack{s_e y_{c1} \to -\infty \\ s_e y_{c2} \to \infty}} B_{00}(\theta,\eta) = \frac{1}{\beta} \ln X\left(\theta,\theta_c,\eta\right)$$

which represents the two-dimensional pressure distribution. (See eqs. (6) and (7).)

Pressure modes for swept controls.- As will be described in the section "Results and Discussion," the function $B_{00}(\theta,\eta)$ has produced a downwash mode $W_{B00}(x,y)$ fairly close to the ideal function that is desired. But this pressure mode has been deduced under the assumption of a control-surface hinge placed perpendicular to the direction of the main flow. The numerical calculations have shown that when the hinge sweepback angle is large, the downwash distribution $W_{B00}(x,y)$ becomes very distorted if the sweep is not accounted for, and a more general mode of pressure is needed that does account for the sweep.

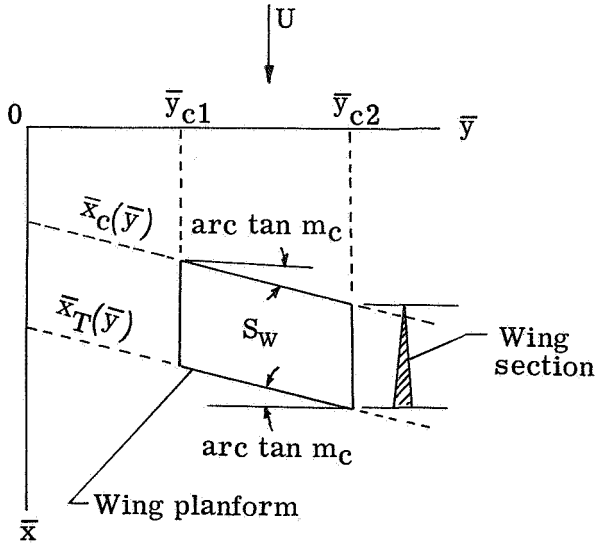

Sketch 6

This more general expression has been obtained by returning to the analysis of a thin wing of symmetrical thickness and a sweptback

leading edge, as represented in sketch 6. The leading edge is represented by the straight line

$$\bar{x}_c(\bar{y}) = \bar{x}_c(0) + m_c\bar{y} \tag{25}$$

of slope m_c.

A constant downwash distribution has been considered, and the more general function $C_{H_{00}}(\bar{x},\bar{y},0)$ takes the form analogous to that for the unswept surface (eq. (21a)):

$$C_{H_{00}}(\bar{x},\bar{y},0) = \frac{1}{\sqrt{\beta^2 + m_c^2}} \cdot \ln \frac{\sqrt{\beta^2 + m_c^2}\sqrt{\left[\bar{x} - \bar{x}_c(\bar{y}_{c1})\right]^2 + \beta^2(\bar{y} - \bar{y}_{c1})^2} - (\beta^2 + m_c^2)(\bar{y} - \bar{y}_{c1}) - m_c\left[\bar{x} - \bar{x}_c(\bar{y})\right]}{\sqrt{\beta^2 + m_c^2}\sqrt{\left[\bar{x} - \bar{x}_c(\bar{y}_{c2})\right]^2 + \beta^2(\bar{y} - \bar{y}_{c2})^2} - (\beta^2 + m_c^2)(\bar{y} - \bar{y}_{c2}) - m_c\left[\bar{x} - \bar{x}_c(\bar{y})\right]} \tag{26}$$

From the relations

$$\left.\begin{aligned} \bar{x} - \bar{x}_c(\bar{y}_{c1}) &= \left[\bar{x} - \bar{x}_c(\bar{y})\right] + \left[\bar{x}_c(\bar{y}) - \bar{x}_c(\bar{y}_{c1})\right] \\ \bar{x} - \bar{x}_c(\bar{y}_{c2}) &= \left[\bar{x} - \bar{x}_c(\bar{y})\right] + \left[\bar{x}_c(\bar{y}) - \bar{x}_c(\bar{y}_{c2})\right] \\ \bar{x}_c(\bar{y}) - \bar{x}_c(\bar{y}_{c1}) &= m_c(\bar{y} - \bar{y}_{c1}) \\ \bar{x}_c(\bar{y}) - \bar{x}_c(\bar{y}_{c2}) &= m_c(\bar{y} - \bar{y}_{c2}) \end{aligned}\right\} \tag{27}$$

and the use of the same modifications that were made to equation (21a) the definitive function $B_{00}(\theta,\eta)$ to be used in the definition of the flap modes of lifting pressure is obtained:

$$B_{00}(\theta,\eta) = \frac{1}{\sqrt{\beta^2 + m_c^2}} \ln\left[\Pi_0(\eta)\Pi(\theta,\theta_c,\eta)\right] \tag{28a}$$

where

$$\Pi_0(\eta) = \frac{\sqrt{\left[X_T + m_c s_e(y_{c2} - |\eta|)\right]^2 + \beta^2 s_e^2(y_{c2} - |\eta|)^2} + s_e\sqrt{\beta^2 + m_c^2}(y_{c2} - |\eta|) + \frac{m_c}{\sqrt{\beta^2 + m_c^2}}X_T}{\sqrt{\left[X_T + m_c s_e(y_{c1} - |\eta|)\right]^2 + \beta^2 s_e^2(y_{c1} - |\eta|)^2} + s_e\sqrt{\beta^2 + m_c^2}(y_{c1} - |\eta|) + \frac{m_c}{\sqrt{\beta^2 + m_c^2}}X_T} \tag{28b}$$

$$\Pi(\theta,\theta_c,\eta) = \frac{\sqrt{\left[X(\theta,\theta_c,\eta) + m_c s_e (y_{c1} - |\eta|)\right]^2 + \beta^2 s_e^2 (y_{c1} - |\eta|)^2} + s_e\sqrt{\beta^2 + m_c^2}(y_{c1} - |\eta|) + \left(\frac{m_c}{\sqrt{\beta^2 + m_c^2}}\right) X(\theta,\theta_c,\eta)}{\sqrt{\left[X(\theta,\theta_c,\eta) + m_c s_e (y_{c2} - |\eta|)\right]^2 + \beta^2 s_e^2 (y_{c2} - |\eta|)^2} + s_e\sqrt{\beta^2 + m_c^2}(y_{c2} - |\eta|) + \left(\frac{m_c}{\sqrt{\beta^2 + m_c^2}}\right) X(\theta,\theta_c,\eta)} \tag{28c}$$

and the log function approaches zero as $\theta \to 0$ or π at wing leading and trailing edges. As s_e becomes indefinitely large, $B_{00}(\theta,\eta)$ approaches the two-dimensional distribution.

For the particular kind of planform that is considered, that is, with the flap hinge line parallel to the trailing edge,

$$\left.\begin{aligned} X(\theta,\theta_c,\eta) &= \left[1 - |\eta|(1 - \lambda)\right]\frac{1 - \cos(\theta - \theta_c)}{|\cos\theta - \cos\theta_c|}\, 2\sin^2\theta_c \\ \theta_c &= \pi - \arccos\left[1 - \frac{\mu}{1 - |\eta|(1 - \lambda)}\right] \\ \text{and} \qquad m_c &= \tan\Lambda - \frac{3}{2s}(1 - \lambda) \end{aligned}\right\} \tag{29}$$

When the slope $m_c = 0$, equation (28a) reduces to equation (24) for the unswept wing.

On the control-surface hinge, the function $B_{00}(\theta,\eta)$ has a logarithmic singularity which disappears beyond the tips of such a hinge. It also has the proper leading- and trailing-edge behavior, and is an analytic function on the rest of the wing surface.

Higher order pressure modes.- In the development of the higher order pressure modes, two circumstances must be accommodated. One is that there is an existing usage of the second subscript m of $B_{nm}(\theta,\eta)$ as even for spanwise symmetry and odd for spanwise antisymmetry. The other is that the subscript r on the spanwise varying Legendre polynomial $P_r\left[\bar{\delta}_c(\bar{y}_{c0} - \bar{\eta})\right]$ introduced into equation (11) can take successive values $r = 0, 1, 2, \ldots$, and so forth. These circumstances are accommodated by the following definition:

$$B_{nm}(\theta,\eta) = \eta^p C_{nr}(\theta,\eta) \qquad (r = 0, 1, 2, \ldots) \tag{30}$$

where $p = 0$ for spanwise symmetry, $p = 1$ for spanwise antisymmetry, and

$$m = 2r + p \tag{31}$$

The higher order functions $C_{nr}(\theta,\eta)$ which appear in the definition of the flap modes of pressure $B_{nm}(\theta,\eta)$ can be obtained by introducing the above-mentioned

modifications in the higher order terms $C_{H_{nr}}(\bar{x},\bar{y},0)$ listed in appendix B. Then, since $B_{00}(\theta,\eta) = C_{00}(\theta,\eta)$,

$$B_{10}(\theta,\eta) = C_{10}(\theta,\eta) = \frac{s}{\mu}\left(y_{c2} - |\eta|\right) \ln \frac{\sqrt{X^2\left(\theta,\theta_c,\eta\right) + \beta^2 s_e{}^2\left(y_{c2} - |\eta|\right)^2} - X\left(\theta,\theta_c,\eta\right)}{\sqrt{X_T{}^2 + \beta^2 s_e{}^2\left(y_{c2} - |\eta|\right)^2} - X_T}$$

$$- \frac{s}{\mu}\left(y_{c1} - |\eta|\right) \ln \frac{\sqrt{X^2\left(\theta,\theta_c,\eta\right) + \beta^2 s_e{}^2\left(y_{c1} - |\eta|\right)^2} - X\left(\theta,\theta_c,\eta\right)}{\sqrt{X_T{}^2 + \beta^2 s_e{}^2\left(y_{c1} - |\eta|\right)^2} - X_T}$$

$$+ \frac{b}{b_0} \frac{\cos\theta - \cos\theta_{c0}}{\mu} C_{00}(\theta,\eta) \tag{32a}$$

where

$$\left.\begin{aligned} \theta_{c0} &= \arccos\left\{\frac{b_0}{b}\left[\xi_m(\eta) - \xi_{c0}(\eta)\right]\right\} \\ \text{and} \\ \xi_{c0}(\eta) &= \frac{\xi_T(\eta) + \xi_c(\eta)}{2} \end{aligned}\right\} \tag{32b}$$

For the swept tapered wing with untapered flap which has been considered, θ_{c0} becomes

$$\theta_{c0} = \pi - \arccos\left\{1 - \frac{\mu}{2\left[1 - |\eta|(1 - \lambda)\right]}\right\} \tag{32c}$$

Similarly,

$$B_{20}(\theta,\eta) = C_{20}(\theta,\eta) = \frac{s}{\mu^2}\left(\frac{b}{b_0}\right)^2 \frac{1 - \cos\left(\theta - \theta_{c0}\right)}{\cos\theta - \cos\theta_{c0}}\left[\left(y_{c2} - |\eta|\right) \ln \frac{\sqrt{X^2\left(\theta,\theta_c,\eta\right) + \beta^2 s_e{}^2\left(y_{c2} - |\eta|\right)^2} - X\left(\theta,\theta_c,\eta\right)}{\sqrt{X_T{}^2 + \beta^2 s_e{}^2\left(y_{c2} - |\eta|\right)^2} - X_T}\right.$$

$$\left. - \left(y_{c1} - |\eta|\right) \ln \frac{\sqrt{X^2\left(\theta,\theta_c,\eta\right) + \beta^2 s_e{}^2\left(y_{c1} - |\eta|\right)^2} - X\left(\theta,\theta_c,\eta\right)}{\sqrt{X_T{}^2 + \beta^2 s_e{}^2\left(y_{c1} - |\eta|\right)^2} - X_T}\right] + \left[\left(\frac{b}{b_0}\right)^2\left(\frac{\cos\theta - \cos\theta_{c0}}{\mu}\right)^2 - \frac{1}{12}\right] C_{00}(\theta,\eta) \tag{33}$$

$$B_{02}(\theta,\eta) = C_{01}(\theta,\eta) = \frac{16\delta_c}{s\beta^2}\left[\sqrt{X^2\left(\theta,\theta_c,\eta\right) + \beta^2 s_e{}^2\left(y_{c2} - |\eta|\right)^2} - \sqrt{X_T{}^2 + \beta^2 s_e{}^2\left(y_{c2} - |\eta|\right)^2}\right.$$

$$\left. - \sqrt{X^2\left(\theta,\theta_c,\eta\right) + \beta^2 s_e{}^2\left(y_{c1} - |\eta|\right)^2} - \sqrt{X_T{}^2 + \beta^2 s_e{}^2\left(y_{c1} - |\eta|\right)^2}\right]$$

$$+ 16\delta_c\left(y_{c0} - |\eta|\right)C_{00}(\theta,\eta) \tag{34a}$$

where

$$\left.\begin{aligned} y_{c0} &= \frac{y_{c2} + y_{c1}}{2} \\ \delta_c &= \frac{2}{y_{c2} - y_{c1}} \end{aligned}\right\} \tag{34b}$$

and

$$B_{04}(\theta,\eta) = C_{02}(\theta,\eta) = \left[100\,\frac{3\delta_c{}^2}{2}\left(y_{c0} - |\eta|\right)^2 + 75\,\frac{3\delta_c{}^2}{4\beta^2 s^2}\,X^2\left(\theta,\theta_c,\eta\right)\right]C_{00}(\theta,\eta) \tag{35}$$

These five modes may be enough to represent the influence of the control surfaces on the pressure distribution in many practical calculations. But if still higher order modes are needed, it would be possible to generate them by calculating the appropriate functions $C_{H_{nr}}(\bar{x},\bar{y},0)$ in the way which has been indicated and applying the mentioned modifications to translate these functions to the lifting pressure distributions $C_{nr}(\theta,\eta)$.

The functions $C_{H_{nr}}(\bar{x},\bar{y},0)$, which come from calculations in which sweepback is not considered, are used to generate the general higher order modes. This way is chosen in order to simplify somewhat the analytical expressions obtained for the higher order functions $C_{nr}(\theta,\eta)$. Anyway, an important influence of the sweepback effect is introduced in all these functions through the first-order mode $C_{00}(\theta,\eta)$.

RESULTS AND DISCUSSION

The results presented in figures 1(a), 1(b), and 1(c) were discussed in the section "Preliminary Investigation Based on Separation of Variables." The rest of the results are now presented and discussed. Figure 2 applies to a square planform wing (aspect ratio of 1.0) with full-span flap hinged at 75 percent of the chord. Chordwise distributions of downwash are plotted for the three span stations indicated. At the top is the downwash $w^{(2)}_{B_{00}}$ originated by the pressure mode $B^{(2)}_{00}(\theta,\eta)$ in equation (21b), and at

the bottom is W_{B00} from pressure mode $B_{00}(\theta,\eta)$ in equation (24) with $E_S = 3/2$. Both distributions display the desired characteristic of nearly a first-order discontinuity (finite jump) chordwise at the hinge line and the magnitude of the jump is nearly uniform spanwise. Of the two distributions, W_{B00} has the slight advantages of lower slope chordwise (away from the hinge) and less variation spanwise.

Figure 3 applies to the same configuration as figure 2 and the effects are shown of decreasing the factor E_S (eqs. (23d) and (24)) to three values successively lower than that at the bottom of figure 2. As E_S is decreased, at first the chordwise slope of the downwash decreases both forward and aft of the hinge, but for the lowest value of E_S (3/20), some irregularity appears just forward of and aft of the hinge. For this range of results, an intermediate value of E_S most nearly gives the desired uniform step-function discontinuity from wing to flap.

Figures 4(a) to 4(e) apply to a spanwise symmetric rectangular planform wing (the half-span is sketched on the figure) with an aspect ratio of 4.0, partial-span controls from 0.3 to 0.7 of wing semispan and hinge at wing 3/4 chord. Chordwise distributions of downwash are shown at each of three semispan stations. In figures 4(a) to 4(e), E_S has the values 3/2, 3/4, 1/2, 3/8, and 1/4, respectively. The figures show how effective the parameter E_S can be; figures 4(b) and 4(c) show that E_S in the neighborhood of 3/4 to 1/2 produces a downwash distribution fairly close to the fundamental (first) flap downwash mode that is desired. Figure 5 shows a three-dimensional view of the downwash distribution for $E_S = 1/2$.

Figure 6 shows for comparison the downwash distributions $W^{(2)}_{B00}(x,y)$ originated by the pressure mode $B^{(2)}_{00}(\theta,\eta)$ of equation (21b) for the same configuration as in figure 4. The positive chordwise slope displayed is associated with the multiplying factor $\sin\theta$ in $B^{(2)}_{00}(\theta,\eta)$.

Figures 7(a) and 7(b) show for the configuration in figure 6 the effect on W_{B00} of increasing the Mach number from 0 to 0.5 and 0.8, respectively. The value of E_S was increased to 3/5 for what is judged a better quality of the downwash distribution than that in figure 6. For $M = 0.8$ the distribution is higher at the outboard station $y = 0.8$ than for $M = 0.5$, and a further variation of E_S might have disclosed a better overall choice than the value 3/5.

Figures 8(a), 8(b), and 8(c) apply to an untapered wing with a flap like that of figures 4 to 7 except that the wing is sweptback to 45^o by shearing (full-span aspect ratio remains 4). Downwash distributions are plotted against local chordwise coordinates for the same three semispan stations. In figure 8(a), the downwash $W^{(3)}_{B00}$ was obtained by applying the pressure distribution B_{00} of equation (24) that contains no provision for

sweep. The value of E_S is 1/2. The need for improvement is apparent. In figure 8(b), the results of using B_{00} of equation (28), that does account for sweep, are shown for $E_S = 1/2$. The effect of increasing E_S further to 3/5 is shown in figure 8(c), where the downwash is more uniform at $y = 0.8$ than in figure 8(a).

Figures 9(a), 9(b), and 9(c) apply to the same parameters as 8(a), 8(b), and 8(c), respectively, except that Mach number has been increased from 0 to 0.8, and in figure 9(c), E_S is 0.556. In comparison with the results for $M = 0$, the downwash distributions for $M = 0.8$ are noticeably worsened but are still fairly good in figure 9(c).

Figure 10 shows downwash distributions $W_{B00}(x,y)$ for a rectangular wing with an aspect ratio of 2, for $M = 0$ and $E_S = 3/5$, that can be compared with the distributions for the wing with a higher aspect ratio in figures 4(b), 4(c), and 5. A strong similarity is apparent.

Figures 11(a) and 11(b) apply to a tapered, swept wing with partial-span constant-chord flaps. The taper ratio λ is 0.6, the quarterchord sweep angle Λ is 35^o, the ratio s is 2, the ratio μ of flap chord to root half-chord is 0.4, and the parameter $E_S = 0.512$. The downwash for $M = 0$ in figure 11(a) is good although improvement for $y = 0.8$ could be desired. In figure 11(b), M is increased to 0.8 and the distribution at $y = 0.8$ is noticeably worsened. Investigation of a range of E_S might reveal a better overall choice.

The discussion now turns from consideration of fundamental or first-order pressure and associated downwash modes to consideration of higher-order pressure and downwash modes. A commonly used method for developing higher order pressure modes has been to multiply the fundamental mode by powers of $(\cos\theta - \cos\theta_c)$, as in equation (7). It was desired to determine what would be the effect of such multiplication. The choice here is to use as the reference not the hinge line $\theta = \theta_c$, but rather $\theta = \theta_{c0}$ for the line on the flap midway between its hinge and trailing edge. The very last terms that contain $C_{00}(\theta,\eta)$ in equations (32a) and (33) are of the type described. With the definitions

$$\left.\begin{aligned} B'_{10}(\theta,\eta) &= \frac{b}{b_0}\left(\frac{\cos\theta - \cos\theta_{c0}}{\mu}\right)C_{00}(\theta,\eta) \\ B'_{20}(\theta,\eta) &= \left[\left(\frac{b}{b_0}\right)^2\left(\frac{\cos\theta - \cos\theta_{c0}}{\mu}\right)^2 - \frac{1}{12}\right]C_{00}(\theta,\eta) \end{aligned}\right\} \tag{36}$$

the downwashes $W'_{B_{10}}$ and $W'_{B_{20}}$ are originated and for the rectangular wing with an aspect ratio of 4 are shown in figures 12(a) and 12(b) for $M = 0$ and $E_S = 1/2$. Inclusion of the quantities μ and 1/12 has only quantitative, not qualitative, effects. The

downwashes W_{B00} of figure 4(c), W'_{B10}, and W'_{B20} are for the same configuration and represent the first three terms of a series that could be combined linearly in an effort to fit a specified distribution. Hence, they are to be examined for the desired orthogonality. The downwash W'_{B10} of figure 12(a) shows a chordwise slope and passes through zero as is appropriate for a chordwise second-order mode. The downwash W'_{B20} of figure 12(b) shows relatively little of the curvature which would be appropriate for a chordwise third-order mode. Furthermore, W'_{B10} displays a noticeable resemblance to both W_{B00} and W'_{B20}. Hence the set is not strongly linearly independent and is rather far from being orthogonal (with respect to a unit weighting function). The resemblance of W'_{B10} to $W^{(2)}_{B00}$ of figure 6 is even stronger. This resemblance would bring a poor conditioning of the downwash matrix $[W]$ of equation (8b). In addition, the capability for rapid convergence of the downwash expansion of equation (8a) (with a small number of modes) to the desired downwash distribution over the whole wing, might also be impaired. Therefore, the higher order pressure terms of the type $B'_{10}(\theta,\eta)$ and $B'_{20}(\theta,\eta)$ are judged to be less than adequate.

In contrast, use of the finally adopted pressure terms $B_{10}(\theta,\eta)$ from equation (32a) and $B_{20}(\theta,\eta)$ from equation (33) produce the downwash distributions W_{B10} and W_{B20} of figures 13(a) and 13(b), respectively, for the same wing parameters as in figure 12. The distributions on the control, featuring the steep slope and passage through zero of W_{B10} and the strong curvature of W_{B20}, are judged to represent a marked improvement toward achieving rapid convergence of the downwash series in a collocation procedure. The set W_{B00} of figure 4(c), W_{B10} (fig. 13(a)), and W_{B20} (fig. 13(b)) are not perfectly orthogonal over the flap surface but are probably close enough for the downwash fitting process.

Figures 14(a) and 14(b) show the results of using the pressure modes $B_{02}(\theta,\eta)$ and $B_{04}(\theta,\eta)$ to produce the downwashes W_{B02} and W_{B04}, respectively. The latter are primarily spanwise varying second- and third-order modes. In figure 14(a), W_{B02} shows a nearly linear spanwise variation on the control and nearly step-function discontinuities at the control ends. In figure 14(b), W_{B04} shows a parabolic curvature on the control and nearly step-function discontinuities at its ends. The variations of W_{B02} and W_{B04} are markedly less on the wing than on the control. These characteristics are in accord with desired goals.

CONCLUDING REMARKS

For partial-span control surfaces of the trailing-edge-flap type with leading-edge hinge and sealed gaps, a series of lifting pressure distributions have been developed for deflected and deformed flaps on thin, swept, tapered wings for use in aerodynamic and

aeroelastic analysis. The development is based on the lifting-surface integral equation that relates lift and downwash. An important advance is made by hypothesizing an analogy with the flow characteristics over a nonlifting wing with symmetric thickness distribution and then applying the determined pressure perturbation characteristics to the lifting pressure on a wing with control.

For lifting wings, the fundamental or first-order pressure term gives a downwash distribution that is a good approximation to the following: a small uniform downwash on the wing and a step-function jump to a large uniform downwash on the control. A chordwise second-order term gives a downwash with strong linear chordwise variation, and a chordwise third-order term gives a downwash with strong chordwise curvature on the control; both downwashes are well behaved on the wing. Two higher order spanwise varying terms are also developed. These feature downwashes which have strong linear spanwise variation and strong spanwise curvature, respectively, on the flap and are well behaved on the wing. This type of lifting-pressure series is expected to lead to rapid convergence of the downwash collocation procedure for deflected and deformed controls and to provide an advanced basis for extension to the oscillating case of flutter.

Langley Research Center,
National Aeronautics and Space Administration,
Langley Station, Hampton, Va., May 29, 1969.

APPENDIX A

EXPRESSIONS FOR THE POLYNOMIALS $Q_{r-1}(\bar{y}-\bar{\eta})$ AND THE FUNCTIONS $\nu_r(\bar{\xi})$

Expressions for the polynomials $Q_{r-1}(\bar{y}-\bar{\eta})$ and the functions $\nu_r(\bar{\xi})$ from equation (17) for r up to 5 are as follows:

$$Q_0(\bar{y}-\bar{\eta}) = \frac{\bar{\delta}_c}{\beta^2}$$

$$Q_1(\bar{y}-\bar{\eta}) = \frac{3\bar{\delta}_c^{\,2}}{\beta^2}\left[\frac{1}{4}(\bar{y}-\bar{\eta}) + (\bar{y}_{c0}-\bar{y})\right]$$

$$Q_2(\bar{y}-\bar{\eta}) = \frac{5\bar{\delta}_c}{2\beta^2}\left\{\frac{\bar{\delta}_c^{\,2}}{3}(\bar{y}-\bar{\eta})^2 + \frac{3\bar{\delta}_c^{\,2}(\bar{y}_{c0}-\bar{y})}{2}(\bar{y}-\bar{\eta}) + \frac{3}{5}\left[5\bar{\delta}_c^{\,2}(\bar{y}_{c0}-\bar{y})^2 - 1\right]\right.$$
$$\left. - \frac{2\bar{\delta}_c^{\,2}}{3\beta^2}\left[(\bar{x}-\bar{\xi})^2 + \beta^2\bar{z}^2\right]\right\}$$

$$Q_3(\bar{y}-\bar{\eta}) = \frac{5\bar{\delta}_c^{\,2}}{2\beta^2}\left(\frac{7\bar{\delta}_c^{\,2}}{16}(\bar{y}-\bar{\eta})^3 + \frac{7\bar{\delta}_c^{\,2}(\bar{y}_{c0}-\bar{y})}{3}(\bar{y}-\bar{\eta})^2 + \frac{3}{4}\left\{7\bar{\delta}_c^{\,2}(\bar{y}_{c0}-\bar{y})^2\right.\right.$$
$$\left. - \frac{7\bar{\delta}_c^{\,2}}{8\beta^2}\left[(\bar{x}-\bar{\xi})^2 + \beta^2\bar{z}^2\right] - 1\right\}(\bar{y}-\bar{\eta}) + (\bar{y}_{c0}-\bar{y})\left\{7\bar{\delta}_c^{\,2}(\bar{y}_{c0}-\bar{y})^2\right.$$
$$\left.\left. - \frac{14\bar{\delta}_c^{\,2}}{3\beta^2}\left[(\bar{x}-\bar{\xi})^2 + \beta^2\bar{z}^2\right] - 3\right\}\right)$$

$$Q_4(\bar{y}-\bar{\eta}) = \frac{7\bar{\delta}_c}{8\beta^2}\left(\frac{9\bar{\delta}_c^{\,4}}{5}(\bar{y}-\bar{\eta})^4 + \frac{45\bar{\delta}_c^{\,3}}{4}(\bar{y}-\bar{\eta})^3 + \frac{2\bar{\delta}_c^{\,2}}{3}\left\{5\left[9\bar{\delta}_c^{\,2}(\bar{y}_{c0}-\bar{y})^2 - 1\right]\right.\right.$$
$$\left. - \frac{18\bar{\delta}_c^{\,2}}{5\beta^2}\left[(\bar{x}-\bar{\xi})^2 + \beta^2\bar{z}^2\right]\right\}(\bar{y}-\bar{\eta})^2 + 15\bar{\delta}_c^{\,2}(\bar{y}_{c0}-\bar{y})\left\{3\bar{\delta}_c^{\,2}(\bar{y}_{c0}-\bar{y})^2\right.$$
$$\left. - \frac{9\bar{\delta}_c^{\,2}}{8\beta^2}\left[(\bar{x}-\bar{\xi})^2 + \beta^2\bar{z}^2\right] - 1\right\}(\bar{y}-\bar{\eta}) + 3\bar{\delta}_c^{\,2}(\bar{y}_{c0}-\bar{y})^2\left[15\bar{\delta}_c^{\,2}(\bar{y}_{c0}-\bar{y})^2 - 10\right]$$
$$\left. - \frac{20\bar{\delta}_c^{\,2}}{\beta^2}\left[3\bar{\delta}_c^{\,2}(\bar{y}_{c0}-\bar{y})^2 - \frac{1}{3}\right]\left[(\bar{x}-\bar{\xi})^2 + \beta^2\bar{z}^2\right] + \frac{24\bar{\delta}_c^{\,4}}{5\beta^4}\left[(\bar{x}-\bar{\xi})^2 + \beta^2\bar{z}^2\right]^2 + \frac{15}{7}\right)$$

APPENDIX A

$$\nu_0(\bar{\xi}) = 1$$

$$\nu_1(\bar{\xi}) = \bar{\delta}_c\left(\bar{y}_{c0} - \bar{y}\right)$$

$$\nu_2(\bar{\xi}) = \frac{1}{2}\left[3\bar{\delta}_c{}^2\left(\bar{y}_{c0} - \bar{y}\right)^2 - 1\right] - \frac{3\bar{\delta}_c{}^2}{4\beta^2}\left[(\bar{x} - \bar{\xi})^2 + \beta^2\bar{z}^2\right]$$

$$\nu_3(\bar{\xi}) = \frac{\bar{\delta}_c\left(\bar{y}_{c0} - \bar{y}\right)}{2}\left[5\bar{\delta}_c{}^2\left(\bar{y}_{c0} - \bar{y}\right)^2 - 3\right] - \frac{15\bar{\delta}_c{}^3\left(\bar{y}_{c0} - \bar{y}\right)}{4\beta^2}\left[(\bar{x} - \bar{\xi})^2 + \beta^2\bar{z}^2\right]$$

$$\nu_4(\bar{\xi}) = \frac{35\bar{\delta}_c{}^4\left(\bar{y}_{c0} - \bar{y}\right)^4}{8} - \frac{3}{8}\left[10\bar{\delta}_c{}^2\left(\bar{y}_{c0} - \bar{y}\right)^2 - 1\right]$$

$$- \frac{15\bar{\delta}_c{}^2}{8\beta^2}\left[7\bar{\delta}_c{}^2\left(\bar{y}_{c0} - \bar{y}\right)^2 - 1\right]\left[(\bar{x} - \bar{\xi})^2 + \beta^2\bar{z}^2\right] + \frac{105\bar{\delta}_c{}^4}{64\beta^4}\left[(\bar{x} - \bar{\xi})^2 + \beta^2\bar{z}^2\right]^2$$

$$\nu_5(\bar{\xi}) = \frac{\bar{\delta}_c\left(\bar{y}_{c0} - \bar{y}\right)}{8}\left[63\bar{\delta}_c{}^4\left(\bar{y}_{c0} - \bar{y}\right)^4 - 70\bar{\delta}_c{}^2\left(\bar{y}_{c0} - \bar{y}\right)^2 + 15\right]$$

$$- \frac{105\bar{\delta}_c{}^3\left(\bar{y}_{c0} - \bar{y}\right)}{8\beta^2}\left[3\bar{\delta}_c{}^2\left(\bar{y}_{c0} - \bar{y}\right)^2 - 1\right]\left[(\bar{x} - \bar{\xi})^2 + \beta^2\bar{z}^2\right]$$

$$+ \frac{845\bar{\delta}_c{}^5\left(\bar{y}_{c0} - \bar{y}\right)}{64\beta^4}\left[(\bar{x} - \bar{\xi})^2 + \beta^2\bar{z}^2\right]^2$$

APPENDIX B

EXPRESSIONS FOR THE FUNCTIONS $C_{H_m}(\bar{x},\bar{y},0)$ FOR THE CONFIGURATION IN SKETCH 5

Expressions for the functions $C_{H00}(\bar{x},\bar{y},0)$, $C_{H10}(\bar{x},\bar{y},0)$, $C_{H20}(\bar{x},\bar{y},0)$, $C_{H01}(\bar{x},\bar{y},0)$, and $C_{H02}(\bar{x},\bar{y},0)$ for the configuration in sketch 5 are as follows:

$$C_{H00}(\bar{x},\bar{y},0) = \frac{1}{\beta} \ln \frac{\sqrt{(\bar{x} - \bar{x}_c)^2 + \beta^2(\bar{y} - \bar{y}_{c1})^2} - \beta(\bar{y} - \bar{y}_{c1})}{\sqrt{(\bar{x} - \bar{x}_c)^2 + \beta^2(\bar{y} - \bar{y}_{c2})^2} - \beta(\bar{y} - \bar{y}_{c2})}$$

$$C_{H10}(\bar{x},\bar{y},0) = \frac{2}{\bar{\mu}}\left[(\bar{y} - \bar{y}_{c1}) \ln \frac{\sqrt{(\bar{x} - \bar{x}_c)^2 + \beta^2(\bar{y} - \bar{y}_{c1})^2} + (\bar{x} - \bar{x}_c)}{\bar{\mu}}\right.$$

$$\left. - (\bar{y} - \bar{y}_{c2}) \ln \frac{\sqrt{(\bar{x} - \bar{x}_c)^2 + \beta^2(\bar{y} - \bar{y}_{c2})^2} + (\bar{x} - \bar{x}_c)}{\bar{\mu}}\right] + \frac{2}{\bar{\mu}}(\bar{x}_{c0} - \bar{x})C_{H00}(\bar{x},\bar{y},0)$$

$$C_{H20}(\bar{x},\bar{y},0) = \frac{6}{\bar{\mu}^2}\left\{(\bar{y} - \bar{y}_{c1})\sqrt{(\bar{x} - \bar{x}_c)^2 + \beta^2(\bar{y} - \bar{y}_{c1})^2} - (\bar{y} - \bar{y}_{c2})\sqrt{(\bar{x} - \bar{x}_c)^2 + \beta^2(\bar{y} - \bar{y}_{c2})^2}\right.$$

$$+ 2(\bar{x}_{c0} - \bar{x})\left[(\bar{y} - \bar{y}_{c1}) \ln \frac{\sqrt{(\bar{x} - \bar{x}_c)^2 + \beta^2(\bar{y} - \bar{y}_{c1})^2} + (\bar{x} - \bar{x}_c)}{\bar{\mu}}\right.$$

$$\left.\left. - (\bar{y} - \bar{y}_{c2})\left[\ln \frac{\sqrt{(\bar{x} - \bar{x}_c)^2 + \beta^2(\bar{y} - \bar{y}_{c2})^2} + (\bar{x} - \bar{x}_c)}{\bar{\mu}}\right]\right\}\right.$$

$$+ \left[\frac{6}{\bar{\mu}^2}(\bar{x}_{c0} - \bar{x})^2 - \frac{1}{2}\right]C_{H00}(\bar{x},\bar{y},0)$$

$$C_{H01}(\bar{x},\bar{y},0) = \frac{\bar{\delta}_c}{\beta^2}\left[\sqrt{(\bar{x} - \bar{x}_c)^2 + \beta^2(\bar{y} - \bar{y}_{c2})^2} - \sqrt{(\bar{x} - \bar{x}_c)^2 + \beta^2(\bar{y} - \bar{y}_{c1})^2}\right]$$

$$+ \bar{\delta}_c(\bar{y}_{c0} - \bar{y})C_{H00}(\bar{x},\bar{y},0)$$

APPENDIX B

$$C_{H02}(\bar{x},\bar{y},0) = \frac{3\bar{\delta}_c^{\,2}}{4\beta^2}\left[(\bar{y}-\bar{y}_{c2})\sqrt{(\bar{x}-\bar{x}_c)^2+\beta^2(\bar{y}-\bar{y}_{c2})^2}-(\bar{y}-\bar{y}_{c1})\sqrt{(\bar{x}-\bar{x}_c)^2+\beta^2(\bar{y}-\bar{y}_{c1})^2}\right]$$

$$+\frac{3\bar{\delta}_c^{\,2}}{\beta^2}(\bar{y}_{c0}-\bar{y})\left[\sqrt{(\bar{x}-\bar{x}_c)^2+\beta^2(\bar{y}-\bar{y}_{c2})^2}-\sqrt{(\bar{x}-\bar{x}_c)^2+\beta^2(\bar{y}-\bar{y}_{c1})^2}\right]$$

$$+\left[\frac{3\bar{\delta}_c^{\,2}}{2}(\bar{y}_{c0}-\bar{y})^2+\frac{3\bar{\delta}_c^{\,2}}{4\beta^2}(\bar{x}-\bar{x}_c)^2-1\right]C_{H00}(\bar{x},\bar{y},0)$$

APPENDIX C

NUMERICAL INTEGRATION

The wing modes of pressure $A_{nm}(\theta,\eta)$ can be integrated by some of the already developed and well-known procedures. (See refs. 1 to 6.) For the present calculations, the method of integration described in reference 1 is used. This method can also be applied to integrate the flap modes of pressure $B_{nm}(\theta,\eta)$ if some modifications are introduced into the chordwise integration.

Each mode $B_{nm}(\theta,\eta)$ is related to its associated flap mode of downwash $W_{B_{nm}}(x,y)$ through the following expression that results from substituting equations (3) and (8a) into equation (1):

$$W_{B_{nm}}(x,y) = \int\!\!\!\!\!\!\diagup_{-1}^{1} \eta^p \frac{\sqrt{1-\eta^2}}{(y-\eta)^2}\, d\eta \int_0^{\pi} C_{nr}(\theta,\eta)\overline{K}\left[M,x-\xi(\theta),s(y-\eta)\right]\sin\theta\, d\theta \qquad (C1)$$

where the relation between p, m, and r is given by equation (31) and that between B_{nm} and C_{nr} by equation (30).

Special care is needed in the numerical evaluation of the chordwise integral

$$F_{nr}(\eta;x,y) = \int_0^{\pi} C_{nr}(\theta,\eta)\overline{K}\sin\theta\, d\theta \qquad (C2)$$

The main difficulty comes from the logarithmic singularity that the function $C_{00}(\theta,\eta)$ has along the control-surface hinge. This singularity also appears, through the influence of the same $C_{00}(\theta,\eta)$, in all higher order functions $C_{nr}(\theta,\eta)$.

In cases of a full-span-flap configuration, the elemental logarithmic singularity $\ln\left(|\theta-\theta_c|\sin\theta_c\right)$ can be extracted from the functions $C_{nr}(\theta,\eta)$ and the more simple integral

$$\int_0^{\pi} \ln\left(|\theta-\theta_c|\sin\theta_c\right)\overline{K}\sin\theta\, d\theta$$

can be evaluated in three steps:

$$\left.\begin{aligned} \int_0^{\pi} &= \int_0^{\theta_x} + \int_{\theta_x}^{\theta_c} + \int_{\theta_c}^{\pi} \qquad (\theta_x < \theta_c) \\ \text{or} \\ \int_0^{\pi} &= \int_0^{\theta_c} + \int_{\theta_c}^{\theta_x} + \int_{\theta_x}^{\pi} \qquad (\theta_x > \theta_c) \end{aligned}\right\} \qquad (C3)$$

where θ_x and θ_c represent the chordwise coordinates of the control point and the control-surface hinge, respectively, at the station η. The integrals from 0 to θ_x and from θ_x to π can be evaluated by a Legendre-Gaussian quadrature, with unity as the weighting function. The rest of these integrals, in which θ_c appears as a limit of integration, can be evaluated by the Berthod-Zaborowski quadrature (see table 9 in ref. 27), which provides highly accurate numerical results.

But this procedure of integration cannot be applied to the more general and common case in which the control-surface spans are smaller than the wing span. Further, it is not feasible to divide the wing span in several regions isolating those where the control surfaces are located because, in spite of the fact that the function $C_{00}(\theta,\eta)$ is not singular at any point outside a control-surface hinge, it has numerical values that increase without limit as the hinge end is approached. This effect introduces an important difficulty in the numerical integration of the spanwise regions which do not have a control surface.

The adopted solution has been to extract (subtract and add) the function $\ln N_0(\theta,\theta_c,\eta)$ where

$$N_0(\theta,\theta_c,\eta) = \frac{\sqrt{(\cos\theta - \cos\theta_c)^2 + \beta^2 s_e^2 (y_{c1} - |\eta|)^2} + \beta s_e (y_{c1} - |\eta|)}{\sqrt{(\cos\theta - \cos\theta_c)^2 + \beta^2 s_e^2 (y_{c2} - |\eta|)^2} + \beta s_e (y_{c2} - |\eta|)} \tag{C4}$$

from the expressions $C_{nr}(\theta,\eta)$ and evaluate its chordwise integration in closed form. Since the function $\ln N_0(\theta,\theta_c,\eta)$ is an elementary representation of the singular part of the functions $C_{nr}(\theta,\eta)$, the expressions which remain as a result of this extraction can each be integrated numerically without difficulty when suitably arranged.

The singular part of each function $C_{nr}(\theta,\eta)$ is defined as $\ln N_{nr}(\theta,\theta_c,\eta)$ where for $C_{00}(\theta,\eta)$,

$$N_{00}(\theta,\theta_c,\eta) \equiv \Pi_0(\eta)\Pi(\theta,\theta_c,\eta) \tag{C5}$$

for $C_{10}(\theta,\eta)$,

$$N_{10}(\theta,\theta_c,\eta) \equiv \left[\Pi_0(\eta)\Pi(\theta,\theta_c,\eta)\right]^{\left(\frac{b}{b_0}\,\frac{\cos\theta-\cos\theta_{c0}}{\mu}\right)} \tag{C6}$$

for $C_{01}(\theta,\eta)$,

$$N_{01}(\theta,\theta_c,\eta) \equiv \left[\Pi_0(\eta)\Pi(\theta,\theta_c,\eta)\right]^{16\delta_c(y_{c0}-|\eta|)} \tag{C7}$$

and so on.

APPENDIX C

For general nr, from equation (C2),

$$F_{nr}(\eta;x,y) \equiv \frac{1}{\sqrt{\beta^2 + m_c^2}} F^*_{nr}(\eta;x,y) \tag{C8}$$

Then, with the definitions in equations (C5) to (C7), the problem is reduced to the numerical integration of the expression

$$F^*_{nr}(\eta;x,y) = \int_0^{\pi} \ln N_{nr}(\theta,\theta_c,\eta)\overline{K} \sin\theta \, d\theta \tag{C9}$$

By introducing the function $\ln N_0(\theta,\theta_c,\eta)$, this expression becomes

$$F^*_{nr}(\eta;x,y) = \int_0^{\pi} H_{nr}(\theta,\eta)d\theta + \int_0^{\pi} \ln N_0(\theta,\theta_c,\eta)\overline{K} \sin\theta \, d\theta \tag{C10}$$

where

$$H_{nr}(\theta,\eta) \equiv \ln \frac{N_{nr}(\theta,\theta_c,\eta)}{N_0(\theta,\theta_c,\eta)} \overline{K} \sin\theta$$

and where $H_{nr}(\theta,\eta)$ is not singular at $\theta = \theta_c$.

With the definition

$$\phi(\theta,\eta) \equiv \left\{ \overline{K}\left[M,x-\xi(\theta),s(y-\eta)\right] - \overline{K}\left[M,x-\xi_c(\theta_c),s(y-\eta)\right] \right\} \ln N_0(\theta,\theta_c,\eta)\sin\theta \tag{C11}$$

which is zero at $\theta = \theta_c$, then

$$F^*_{n,r}(\eta;x,y) = \int_0^{\pi} H_{nr}(\theta,\eta)d\theta + \int_0^{\pi} \phi(\theta,\eta)d\theta + \overline{K}\left[M,x-\xi_c(\theta_c),s(y-\eta)\right]\lambda(\theta_c,\eta) \tag{C12}$$

where

$$\lambda(\theta_c,\eta) \equiv \int_0^{\pi} \ln \frac{\sqrt{(\cos\theta - \cos\theta_c)^2 + \beta^2 s_e^2 (y_{c1} - |\eta|)^2} + \beta s_e(y_{c1} - |\eta|)}{\sqrt{(\cos\theta - \cos\theta_c)^2 + \beta^2 s_e^2 (y_{c2} - |\eta|)^2} + \beta s_e(y_{c2} - |\eta|)} \sin\theta \, d\theta$$

(Equation continued on next page)

$$= (1 + \cos\theta_c) \ln \frac{\sqrt{(1 + \cos\theta_c)^2 + \beta^2 s_e^2 (y_{c1} - |\eta|)^2} + \beta s_e (y_{c1} - |\eta|)}{\sqrt{(1 + \cos\theta_c)^2 + \beta^2 s_e^2 (y_{c2} - |\eta|)^2} + \beta s_e (y_{c2} - |\eta|)}$$

$$+ (1 - \cos\theta_c) \ln \frac{\sqrt{(1 - \cos\theta_c)^2 + \beta^2 s_e^2 (y_{c1} - |\eta|)^2} + \beta s_e (y_{c1} - |\eta|)}{\sqrt{(1 - \cos\theta_c)^2 + \beta^2 s_e^2 (y_{c2} - |\eta|)^2} + \beta s_e (y_{c2} - |\eta|)}$$

$$+ \beta s_e (y_{c1} - |\eta|) \ln \frac{\sqrt{(1 + \cos\theta_c)^2 + \beta^2 s_e^2 (y_{c1} - |\eta|)^2} + (1 + \cos\theta_c)}{\sqrt{(1 - \cos\theta_c)^2 + \beta^2 s_e^2 (y_{c1} - |\eta|)^2} - (1 - \cos\theta_c)}$$

$$- \beta s_e (y_{c2} - |\eta|) \ln \frac{\sqrt{(1 + \cos\theta_c)^2 + \beta^2 s_e^2 (y_{c2} - |\eta|)^2} + (1 + \cos\theta_c)}{\sqrt{(1 - \cos\theta_c)^2 + \beta^2 s_e^2 (y_{c2} - |\eta|)^2} - (1 - \cos\theta_c)} \qquad \text{(C13)}$$

The integrals $\int_0^\pi H_{nr}(\theta,\eta)d\theta$ and $\int_0^\pi \phi(\theta,\eta)d\theta$ are evaluated by Gaussian quadratures, with unity as a weighting function, once they are divided into the three intervals defined in equation (C3).

For the planform considered,

$$\theta_c = \pi - \arccos\left[1 - \frac{\mu}{1 - |\eta|(1 - \lambda)}\right] \qquad \text{(C14)}$$

and

$$\theta_x = \arccos\left\{\frac{y\left[s\tan\Lambda - \frac{1}{2}(1 - \lambda)\right] - x}{1 - y(1 - \lambda)}\right\} \qquad (y > 0) \qquad \text{(C15)}$$

When the function $\lambda(\theta_c,\eta)$ is evaluated at the points $|\eta| = y_{c1}$ or $|\eta| = y_{c2}$, or at any point very close to y_{c1} or y_{c2}, a minor numerical difficulty appears. It comes from the term

$$\beta s_e (y_{c1} - |\eta|) \ln \frac{\sqrt{(1 + \cos\theta_c)^2 + \beta^2 s_e^2 (y_{c1} - |\eta|)^2} + (1 + \cos\theta_c)}{\sqrt{(1 - \cos\theta_c)^2 + \beta^2 s_e^2 (y_{c1} - |\eta|)^2} - (1 - \cos\theta_c)}$$

and the equivalent term for y_{c2} in equation (C13).

APPENDIX C

The logarithmic functions are indeterminate at the points $|\eta| = y_{c1}$ and $|\eta| = y_{c2}$, respectively, and nearby can produce an "overflow" or an "indefinite" number, depending on the computer, that causes computation to stop. The adopted preventive measure is to specify two narrow bands:

$$\left.\begin{aligned} (y_{c1} - |\eta|) &\leqq \epsilon \\ \text{and} \\ (y_{c2} - |\eta|) &\leqq \epsilon \end{aligned}\right\} \tag{C16}$$

and define as zero therein the value of the products $(y_{c1} - |\eta|)$ and $(y_{c2} - |\eta|)$ multiplied by their respective logarithmic functions. The value of ϵ used in the calculations is 10^{-10}.

The same difficulty appears in the nonsingular parts of the functions $C_{n0}(\theta,\eta)$ (the parts that do not include C_{00}) and the same preventive measure is used.

REFERENCES

1. Watkins, Charles E.; Woolston, Donald S.; and Cunningham, Herbert J.: A Systematic Kernel Function Procedure for Determining Aerodynamic Forces on Oscillating or Steady Finite Wings at Subsonic Speeds. NASA TR R-48, 1959.

2. Laschka, Boris: Zur Theorie der harmonisch schwingenden tragenden Fläche bei Unterschallanströmung. Z. Flugwissenschaften, Jahrg. 11, Heft 7, July 1963, pp. 1-292.

3. Davies, D. E.: Calculation of Unsteady Generalized Airforces on a Thin Wing Oscillating Harmonically in Subsonic Flow. R. & M. No. 3409, Brit. A.R.C., 1965.

4. Richardson, J. R.: A Method for Calculating the Lifting Forces on Wings (Unsteady Subsonic and Supersonic Lifting-Surface Theory). R. & M. No. 3157, Brit. A.R.C., 1955.

5. Hsu, Pao-Tan: Some Recent Developments in the Flutter Analysis of Low-Aspect-Ratio Wings. Proc. Nat. Specialists Meeting on Dynamics and Aeroelasticity (Fort Worth, Texas), Inst. Aero. Sci., Nov. 1958, pp. 7-26.

6. Multhopp, H.: Methods for Calculating the Lift Distribution of Wings. (Subsonic Lifting-Surface Theory). R. & M. No. 2884, Brit. A.R.C., Jan. 1950.

7. Flax, A. H.: Reverse-Flow and Variational Theorems for Lifting Surfaces in Nonstationary Compressible Flow. J. Aeronaut. Sci., vol. 20, no. 2, Feb. 1953, pp. 120-126.

8. Stark, Valter J. E.: A Method for Solving the Subsonic Problem of the Oscillating Finite Wing With the Aid of High-Speed Digital Computers. SAAB TN 41, SAAB Aircraft Co. (Linköping, Sweden), Dec. 16, 1958.

9. Destuynder, Roger: Utilisation des Mesures Locales de Pression Instationnaire Pour la Détermination des Coefficients Aérodynamiques. La Rech. Aérospatiale, no. 102, Sept.-Oct. 1964, pp. 35-42.

10. Falkner, V. M.: The Solution of Lifting-Plane Problems by Vortex-Lattice Theory. R. & M. No. 2591, Brit. A.R.C., 1953.

11. Dulmovits, John: A Lifting Surface Method for Calculating Load Distributors and the Aerodynamic Influence Coefficient Matrix for Wings in Subsonic Flow. Rep. No. ADR 01-02-64.1, Grumman Aircraft Eng. Corp., Aug. 1964.

12. Belotserkovskii, S. M.: Calculating the Effect of Gusts on an Arbitrary Thin Wing. Fluid Dyn., vol. 1, no. 1, Jan.-Feb. 1966, pp. 34-40.

13. Belotserkovskii, S. M.: Osobennosti Rascheta Obtekaniia Kryl'ev Slozhnoi Formy v Plane pri Dozvukovykh Skorostiakh (Special Features of the Calculation of Flow Past Wings of Complex Planform at Subsonic Velocities). Izv. Akad. Nauk. SSSR, Mekh. Zhidk., Gaza, Nov.-Dec. 1966, pp. 74-80.

14. Dat, Roland; Leclerc, Jacques; and Akamatsu, Yoshio: Optimisation de L'emploi de la Théorie de la Surface Portante en Aéroélasticité Subsonique. La Rech. Aérospatiale, no. 113, July-Aug. 1966, pp. 37-52.

15. Van de Vooren, A. I.: Some Modifications to Lifting Surface Theory. J. of Eng. Math., vol. 1, no. 2, Apr. 1967, pp. 87-102.

16. Panchenkov, R. N.: Nelineinaia Teoriia Nesushchei Poverkhnosti Proizvol'nogo Udlineniia. (Nonlinear Theory of a Lifting Surface of Arbitrary Aspect Ratio.) Gidrodinamika Bol'shikh Skorostei, I. L. Rozovskii, ed., Izdatel'stvo Naukova Dumka (Kiev), 1967, pp. 21-30.

17. Darovsky, L.; and Dat, Roland: Determination des Forces Aerodynamiques Instationnaires Tridimensionnelles. AGARD Rep. 512, June 1965.

18. Zwaan, R. J.: Some Comparative Calculations With the Lifting Surface Theory of Laschka for Circular and Elliptic Wings Oscillating in Subsonic Flow. NLR-TN F.241, Nat. Aero- Astronaut. Res. Inst. (Amsterdam), Sept. 28, 1964.

19. Yates, E. Carson, Jr.: A Kernel-Function Formulation for Nonplanar Lifting Surfaces Oscillating in Subsonic Flow. AIAA J., vol. 4, no. 8, Aug. 1966, pp. 1486-1488.

20. Landahl, M. T.: Kernel Function for Nonplanar Oscillating Surfaces in a Subsonic Flow. AIAA J., vol. 5, no. 5, May 1967, pp. 1045-1046.

21. Betz, A.; and Petersohn, E.: Zur Theorie der Querruder (Theory of the Rudder). Z. Angew. Math. Mech., vol. 8, no. 4, Aug. 1928, pp. 253-257.

22. Pearson, H. A.: Theoretical Span Loading and Moments of Tapered Wings Produced by Aileron Deflection. NACA TN 589, 1937.

23. Theodorsen, Theodore: General Theory of Aerodynamic Instability and the Mechanism of Flutter. NACA Rep. 496, 1935.

24. Hsu, Pao-Tan; and Weatherill, Warren H.: Pressure Distribution and Flutter Analysis of Low-Aspect-Ratio Wings in Subsonic Flow. ASRL Tech. Rep. 64-3 (Contract No. Noa(s) 55-771-c), Massachusetts Inst. Technol., June 1959.

25. Berman, J. H.; Shyprykevich, P.; Smedfjeld, J. B.; and Kelly, R. F.: Unsteady Aerodynamic Forces for General Wing/Control-Surface Configurations in Subsonic Flow. AFFDL-TR-67-117, Pts. I and II, U.S. Air Force, May 1968.

26. Landahl, M.: Pressure-Loading Functions for Oscillating Wings With Control Surfaces. AIAA J., vol. 6, no. 2, Feb. 1968, pp. 345-348.

27. Stroud, A. H.; and Secrest, Don: Gaussian Quadrature Formulas. Prentice-Hall, Inc., c.1966.

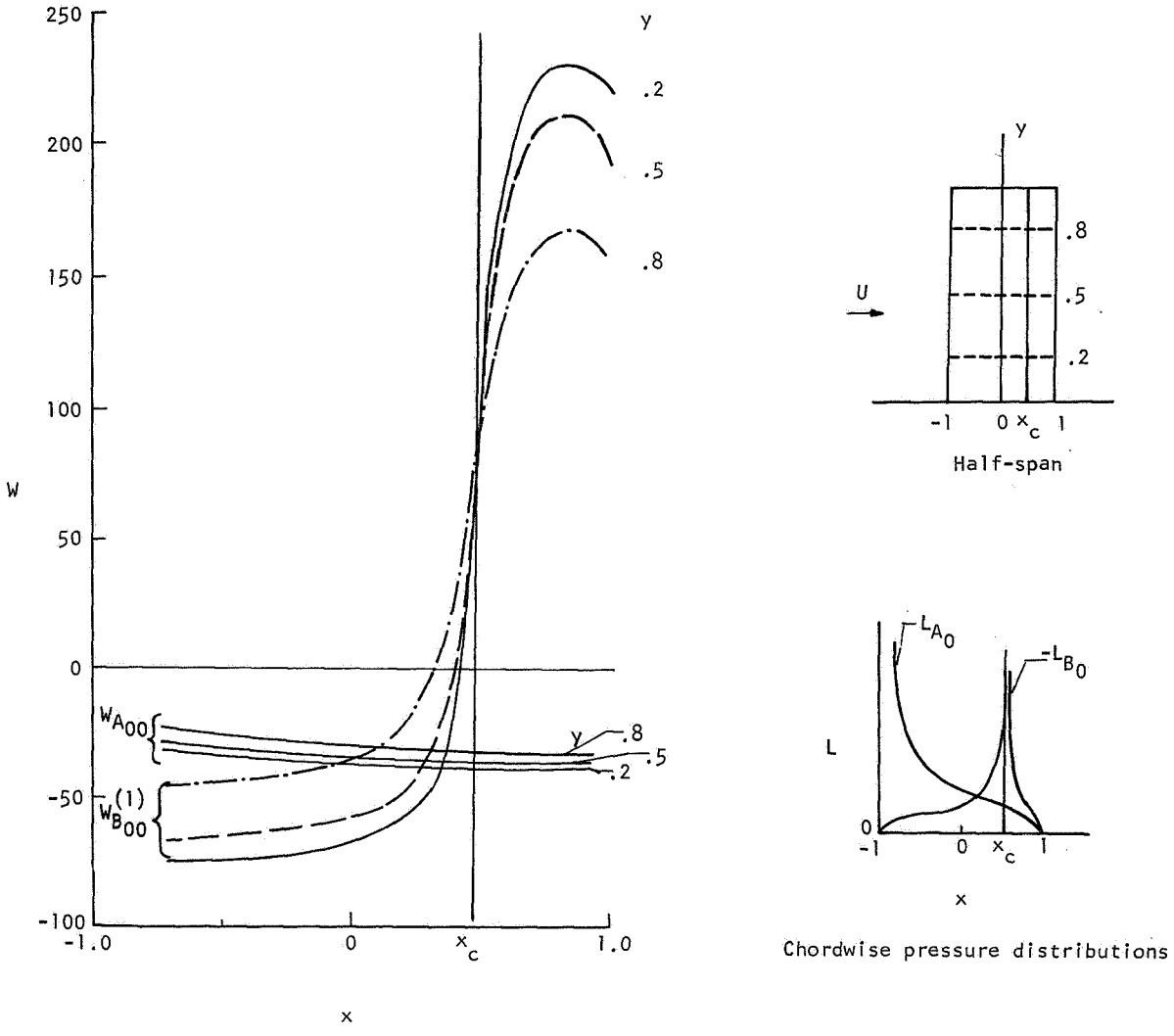

(a) Mode n = 0.

Figure 1.- Chordwise distributions of downwash W_{An0} and $W^{(1)}_{Bn0}$ and the associated lift distributions L_{An} from equation (5) and L_{Bn} from equation (7) for a rectangular wing of aspect ratio 4 with full-span flap and parameters M = 0 and μ = 1/2.

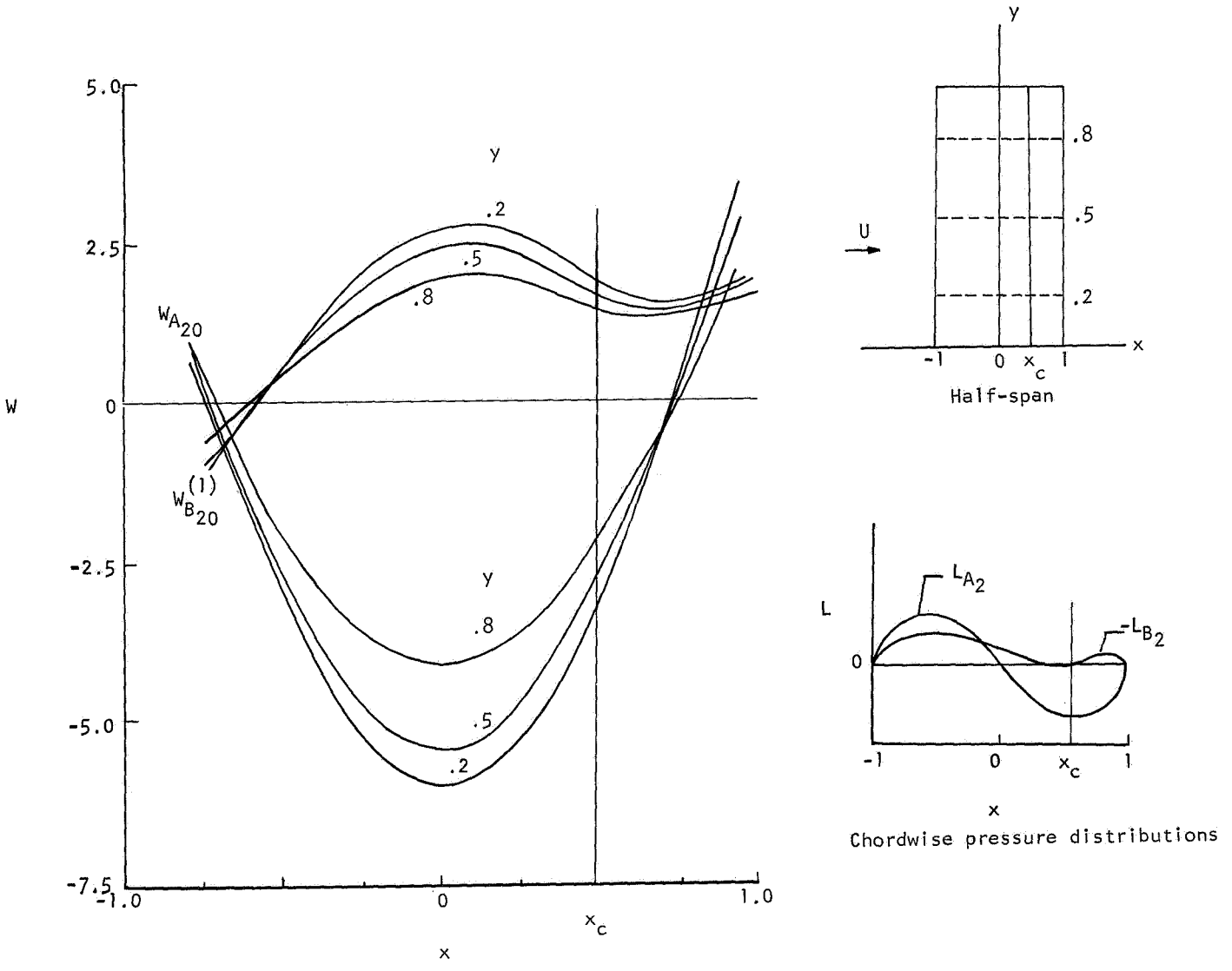

(b) Mode n = 2.

Figure 1.- Continued.

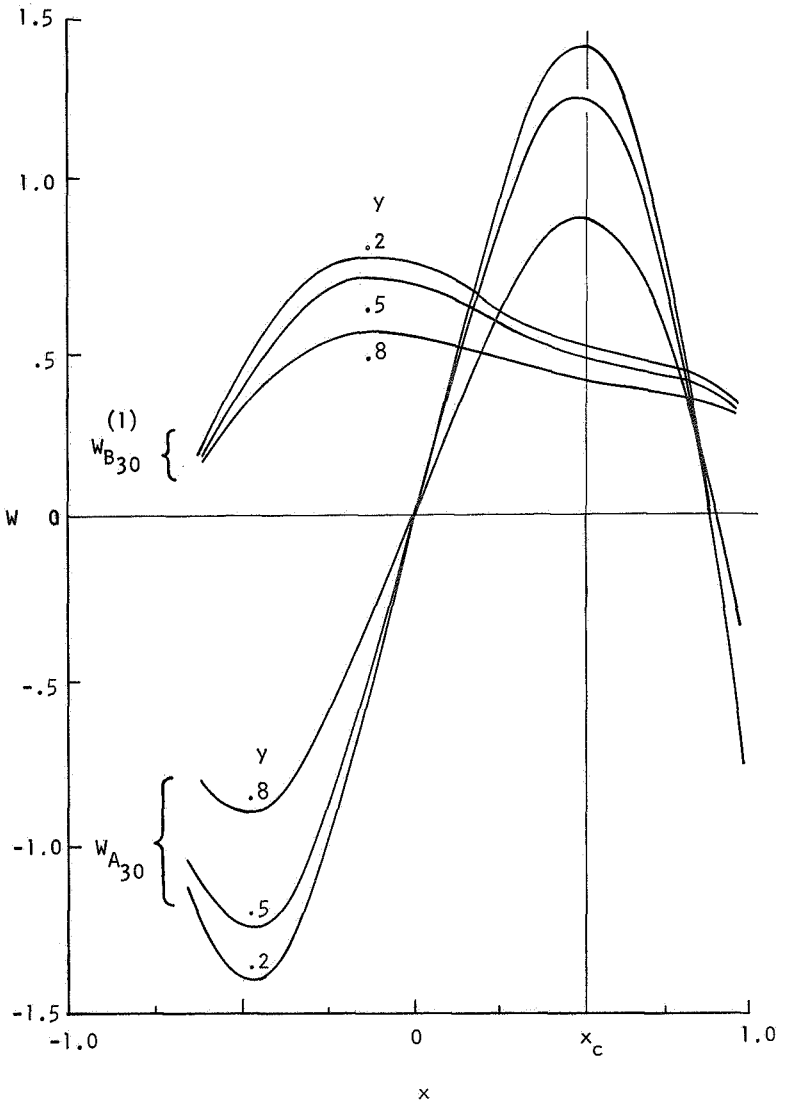

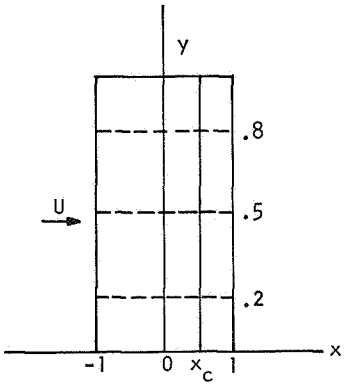

Half-span

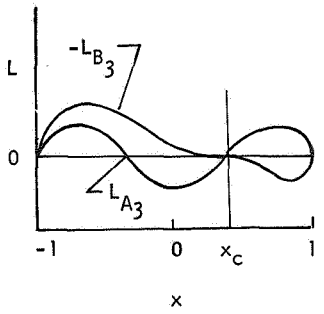

Chordwise pressure distributions

(c) Mode n = 3.

Figure 1.- Concluded.

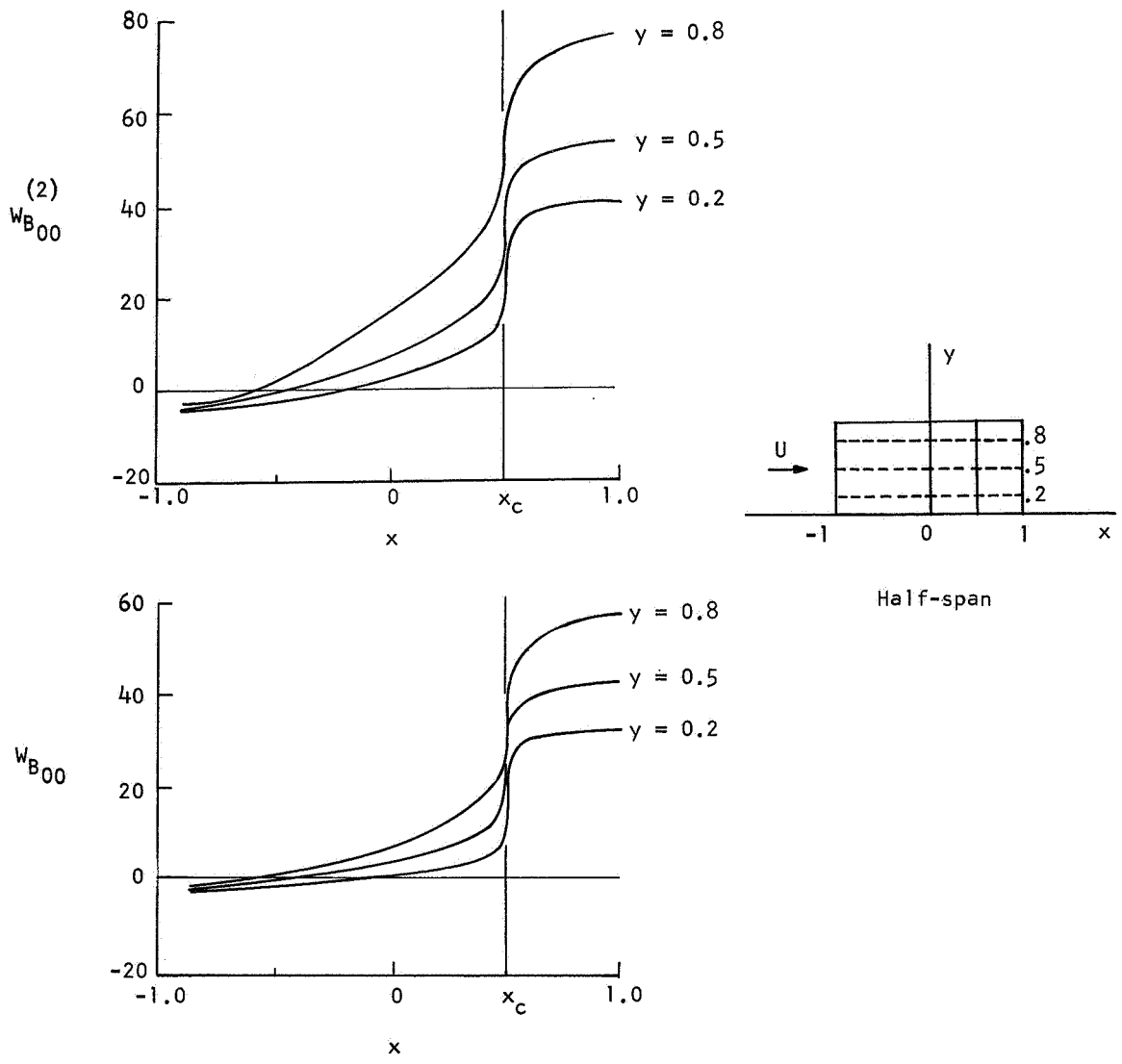

Figure 2.- Chordwise distributions of downwash $W^{(2)}_{B00}$ from pressure mode $B^{(2)}_{00}(\theta,\eta)$ of equation (21b), and W_{B00} from $B_{00}(\theta,\eta)$ of equation (24) (with $E_s = 3/2$) for a square planform wing with full-span flap and parameters $s = 1$, $M = 0$, $\mu = 1/2$, $y_{c1} = -1$, and $y_{c2} = 1$.

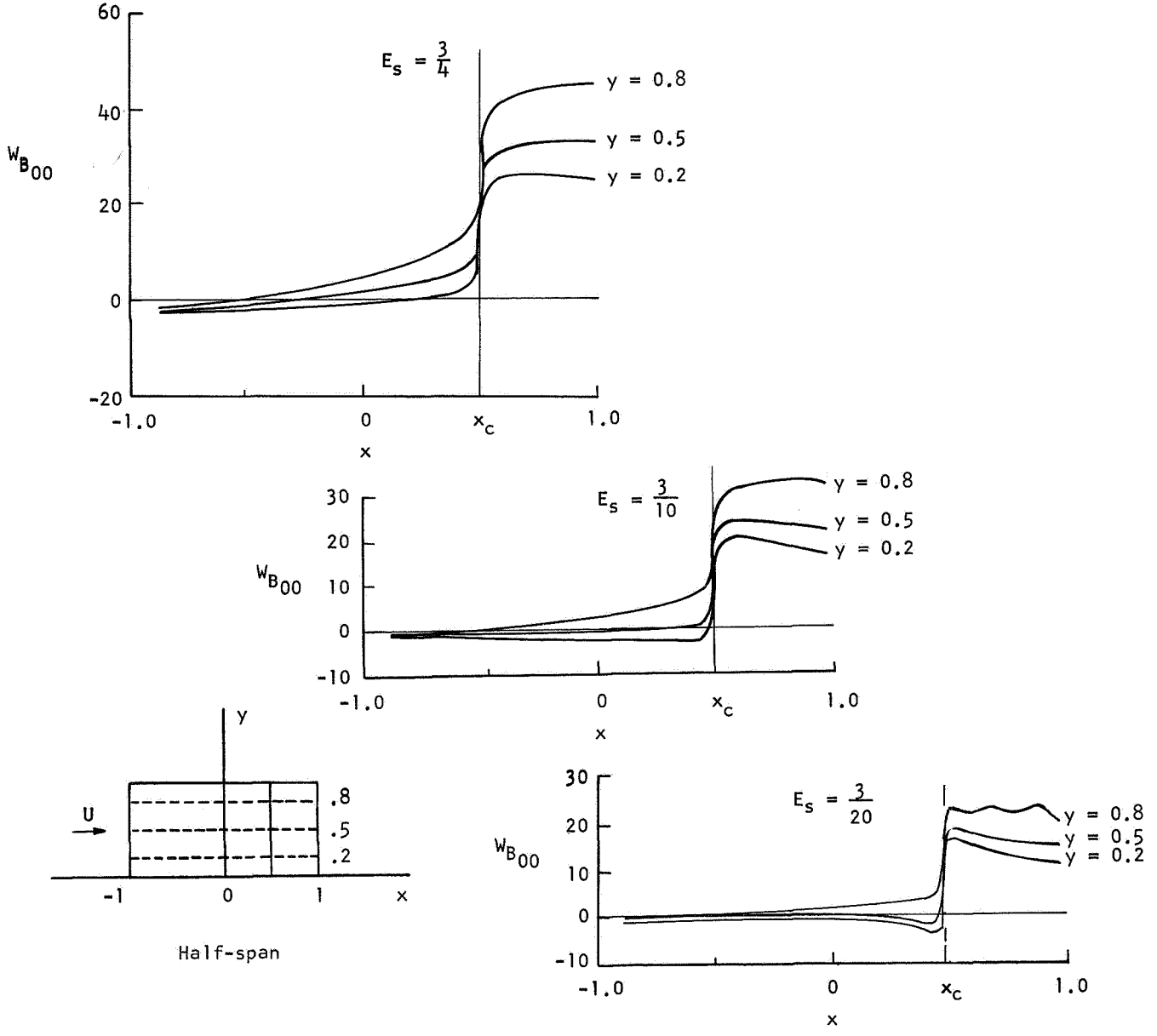

Figure 3.- Downwash distributions $W_{B_{00}}$ from pressure mode $B_{00}(\theta,\eta)$ of equation (24) for the same wing and flap as in figure 2 but with E_S = 3/4, 3/10, and 3/20.

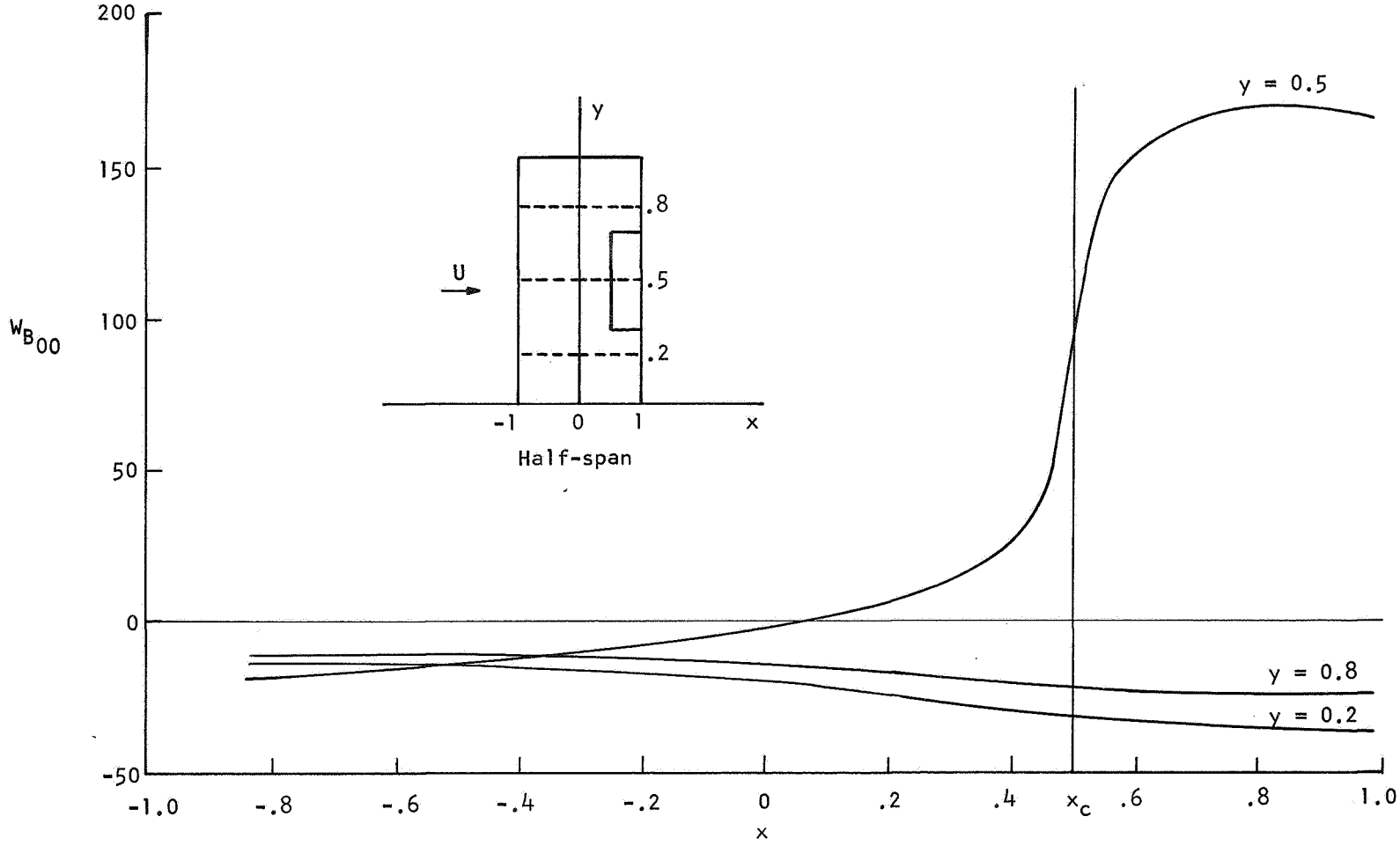

(a) $E_S = 3/2$.

Figure 4.- Downwash distributions $W_{B_{00}}$ from pressure mode $B_{00}(\theta,\eta)$ for a rectangular wing of aspect ratio 4 with partial-span flaps, five different values of E_S, and parameters $\mu = 1/2$, $y_{c1} = 0.3$, $y_{c2} = 0.7$, and $M = 0$.

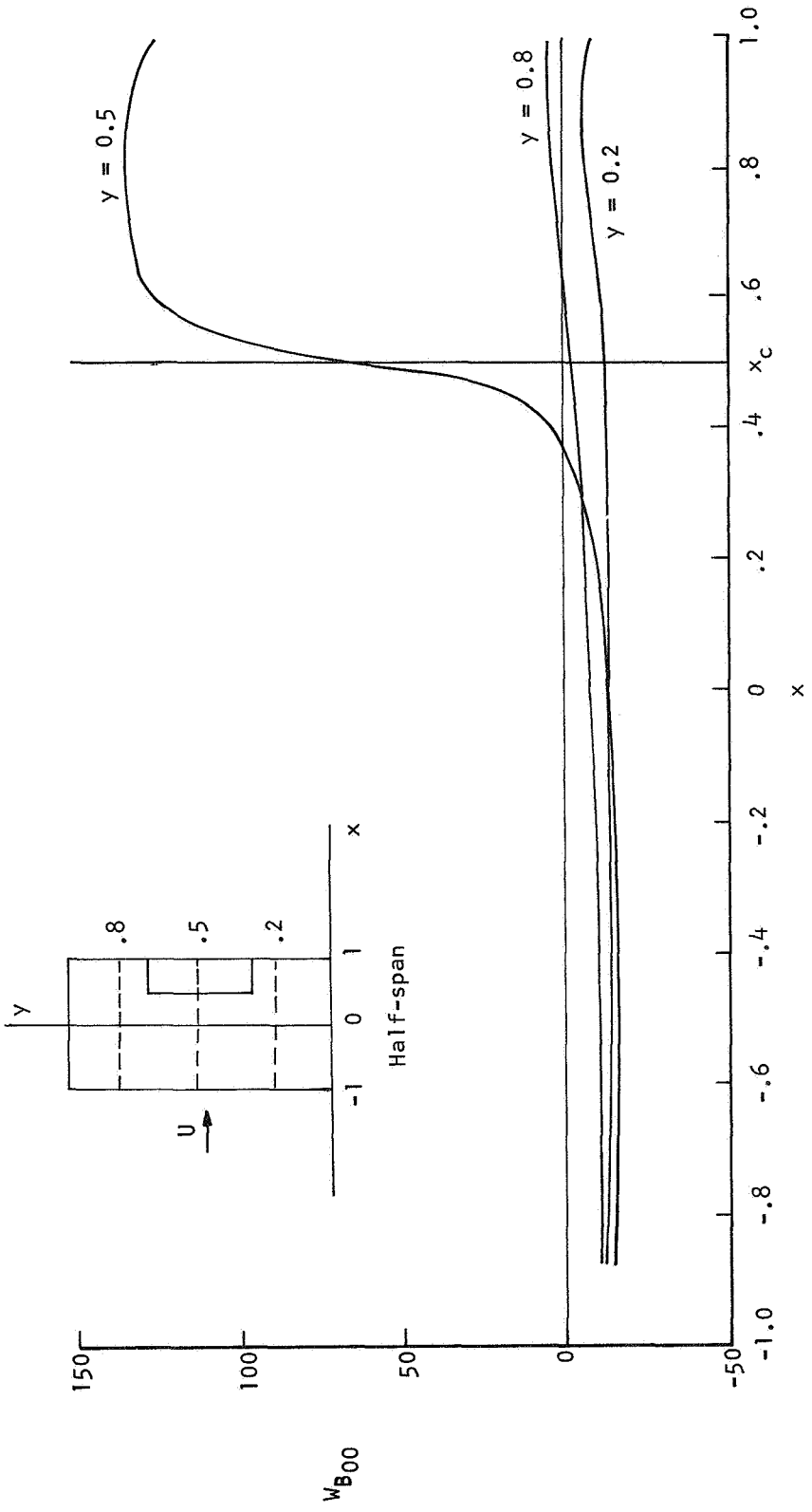

(b) $E_s = 3/4$.

Figure 4.- Continued.

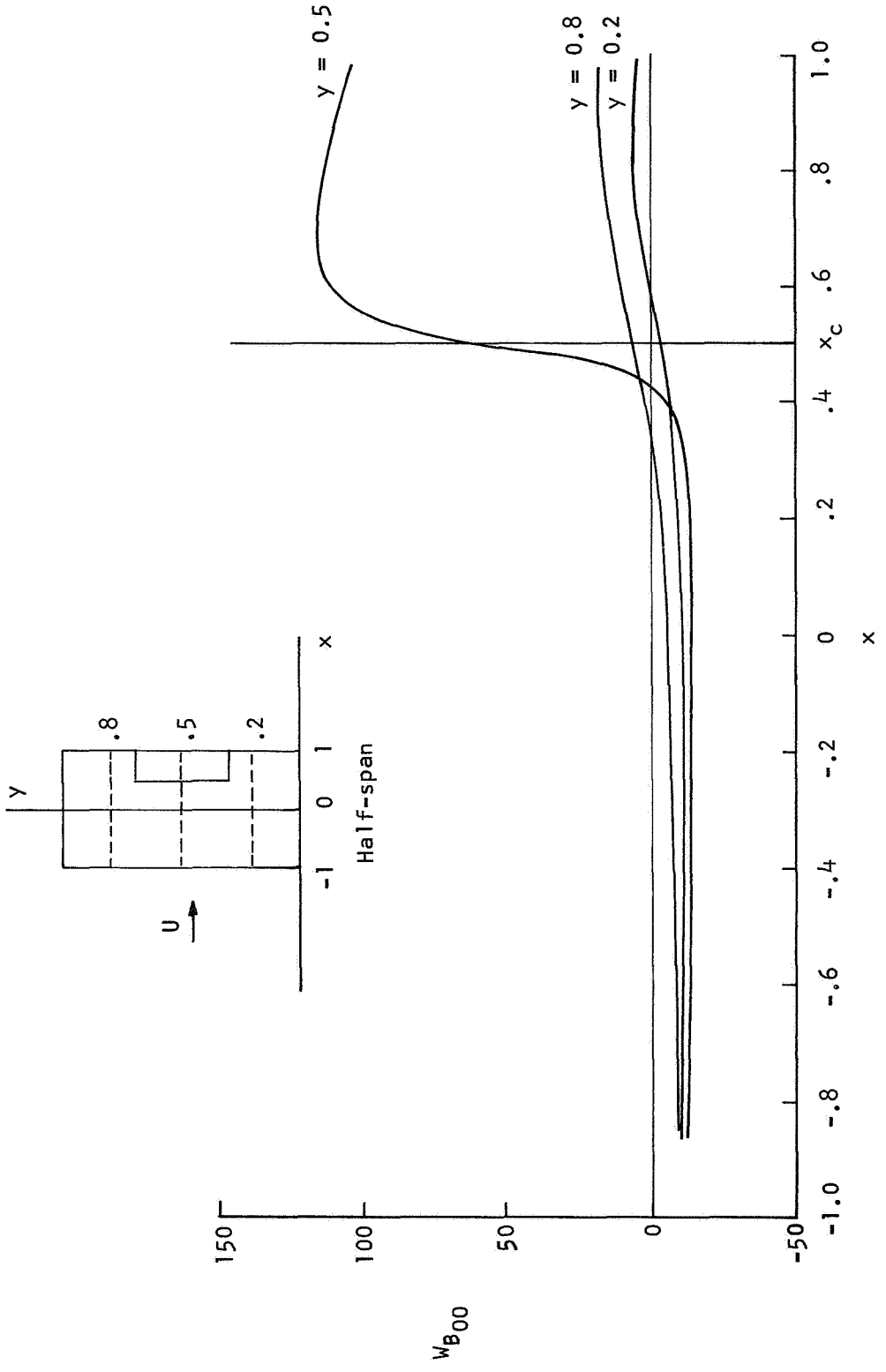

(c) $E_S = 1/2$.

Figure 4.- Continued.

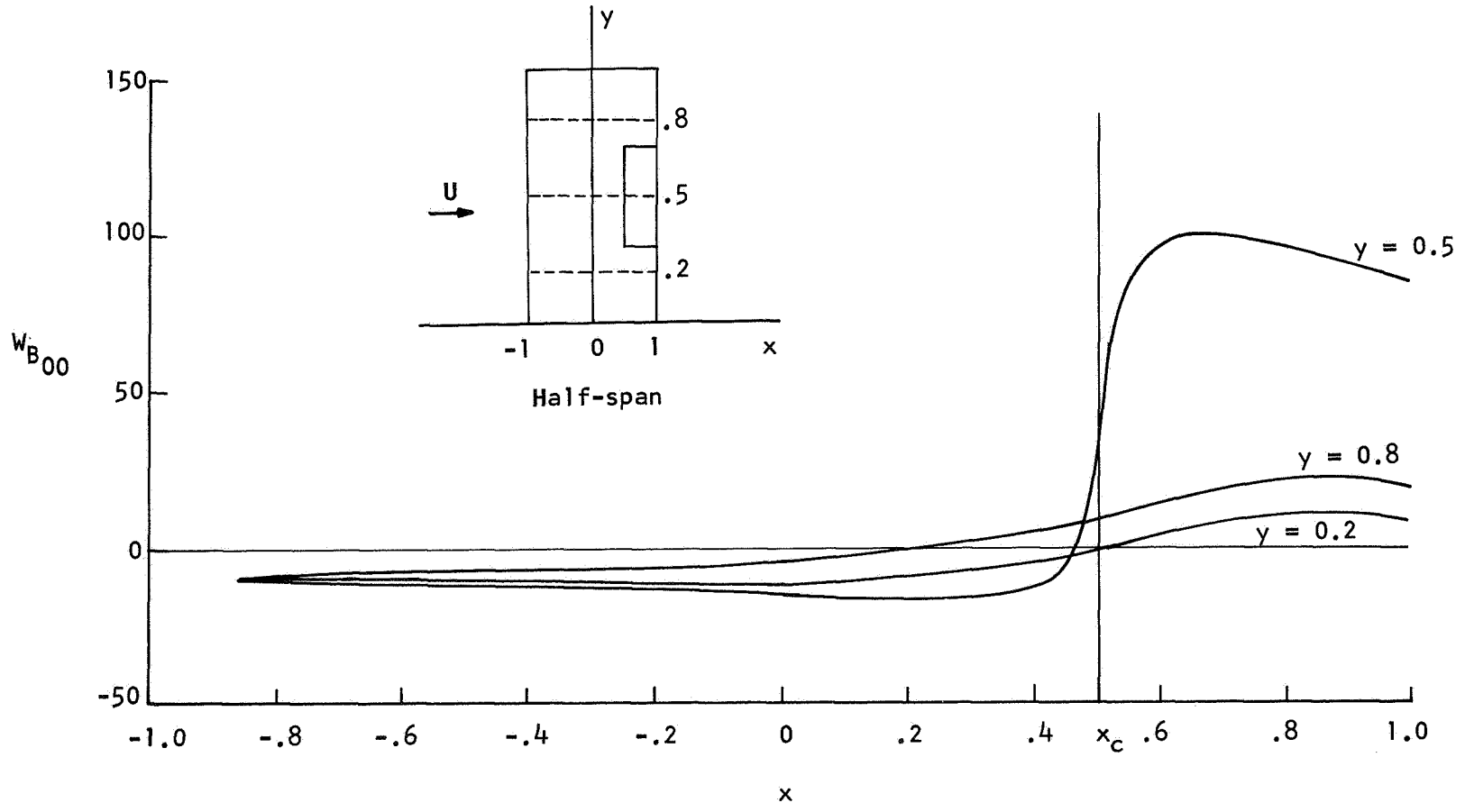

(d) $E_S = 3/8$.

Figure 4.- Continued.

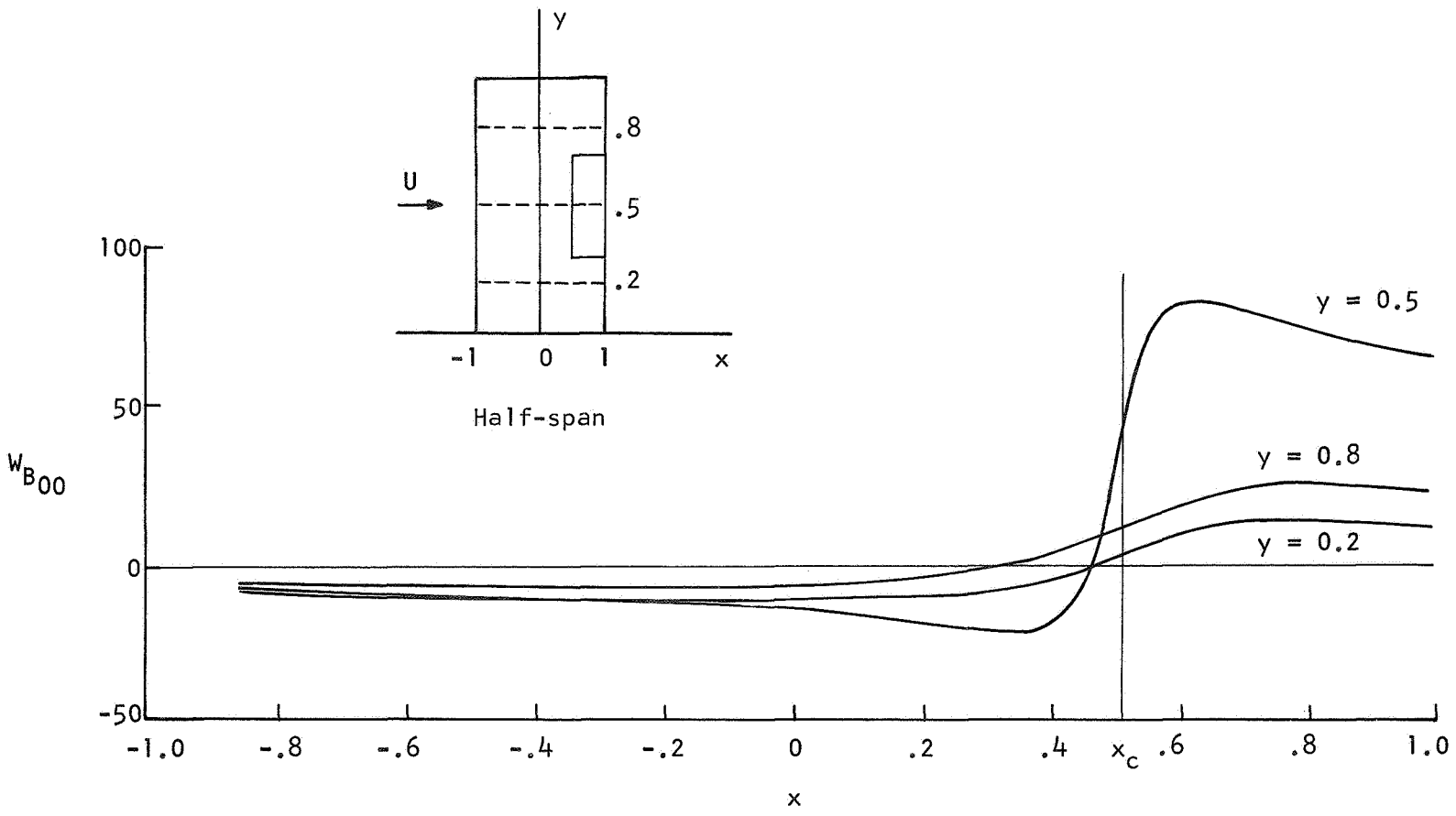

(e) $E_S = 1/4$.

Figure 4.- Concluded.

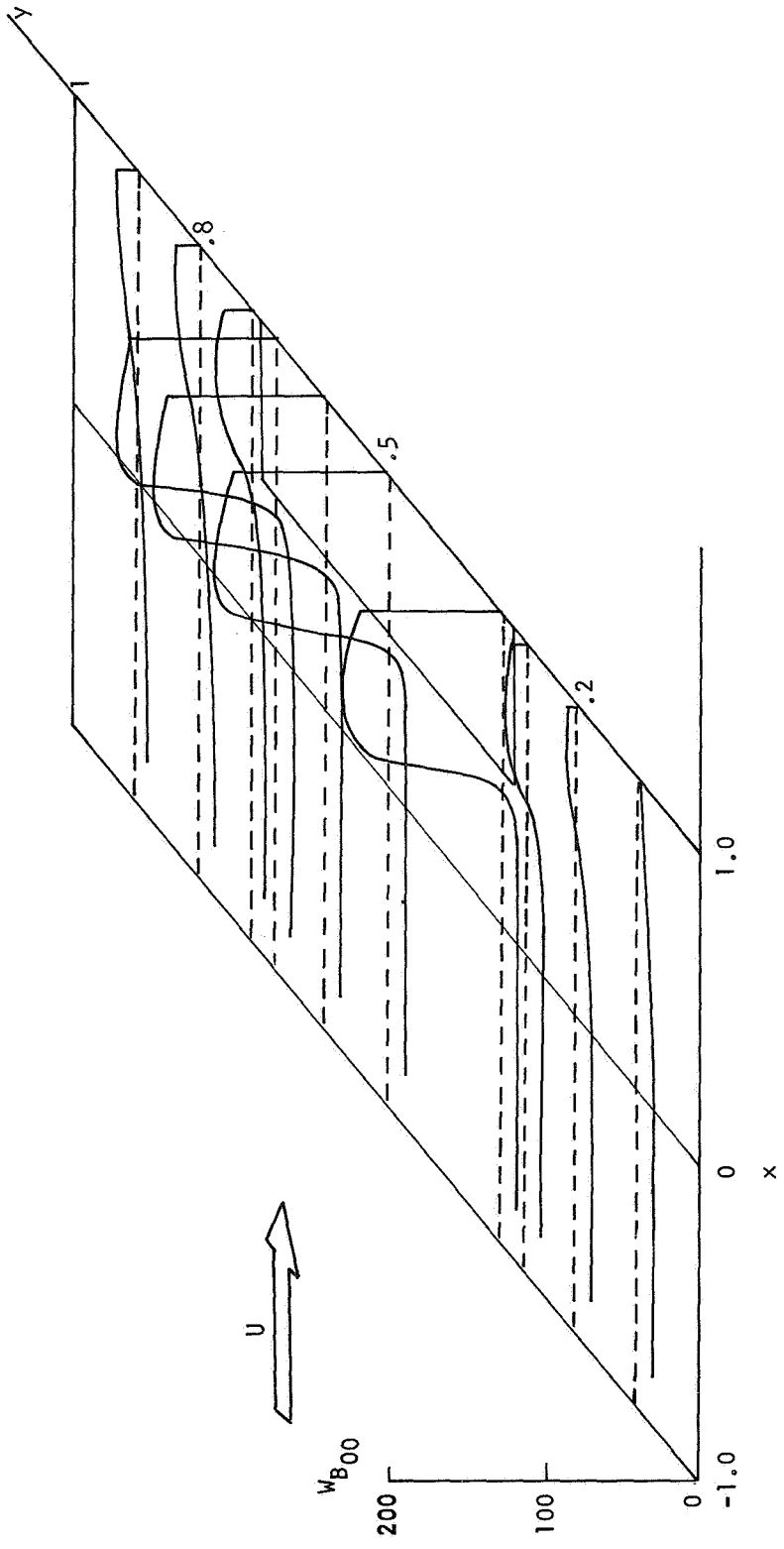

Figure 5.- Three-dimensional half-span view of the downwash distribution w_{B00} over the same rectangular wing as in figure 4 for $E_s = 1/2$ (as in fig. 4(c)).

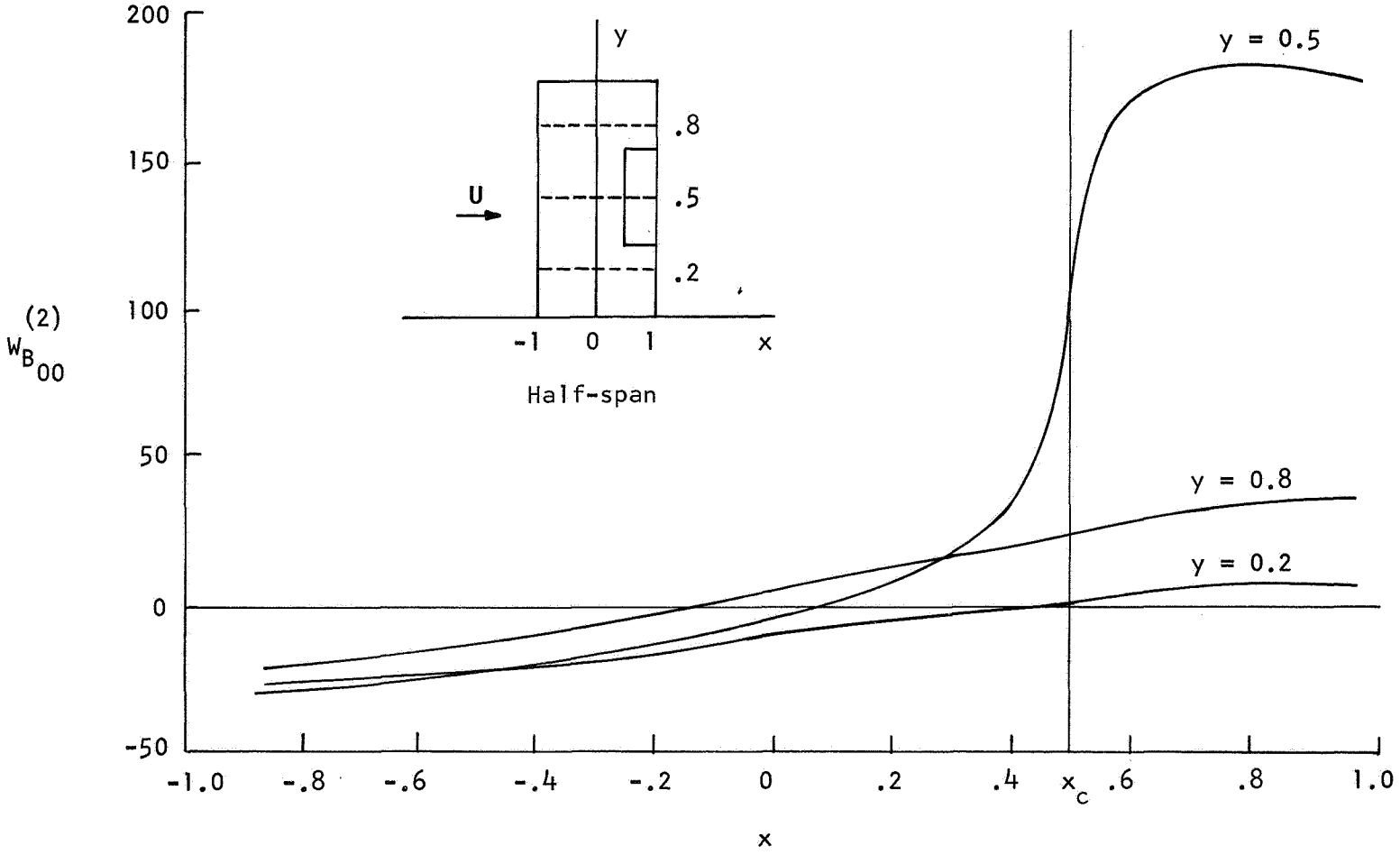

Figure 6.- Downwash distributions $W^{(2)}_{B_{00}}$ from pressure mode $B^{(2)}_{00}(\theta,\eta)$ of equation (21b) for the same rectangular wing and flap as in figures 4 and 5.

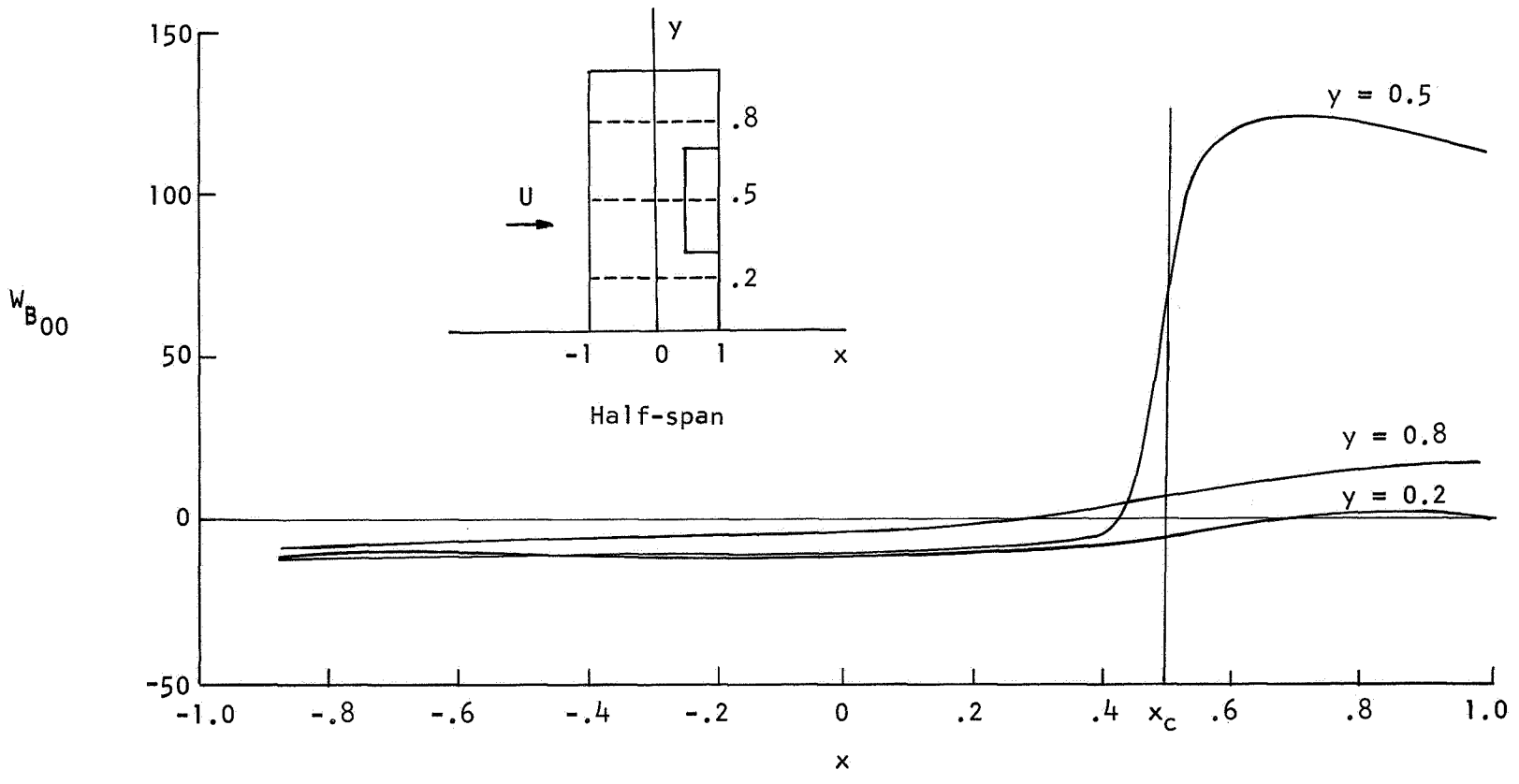

(a) M = 0.5.

Figure 7.- Effect of two nonzero Mach numbers (M = 0.5 and 0.8) on the downwash distributions W_{B00} over the same rectangular wing and flap as in figures 4 to 6 for E_s = 3/5.

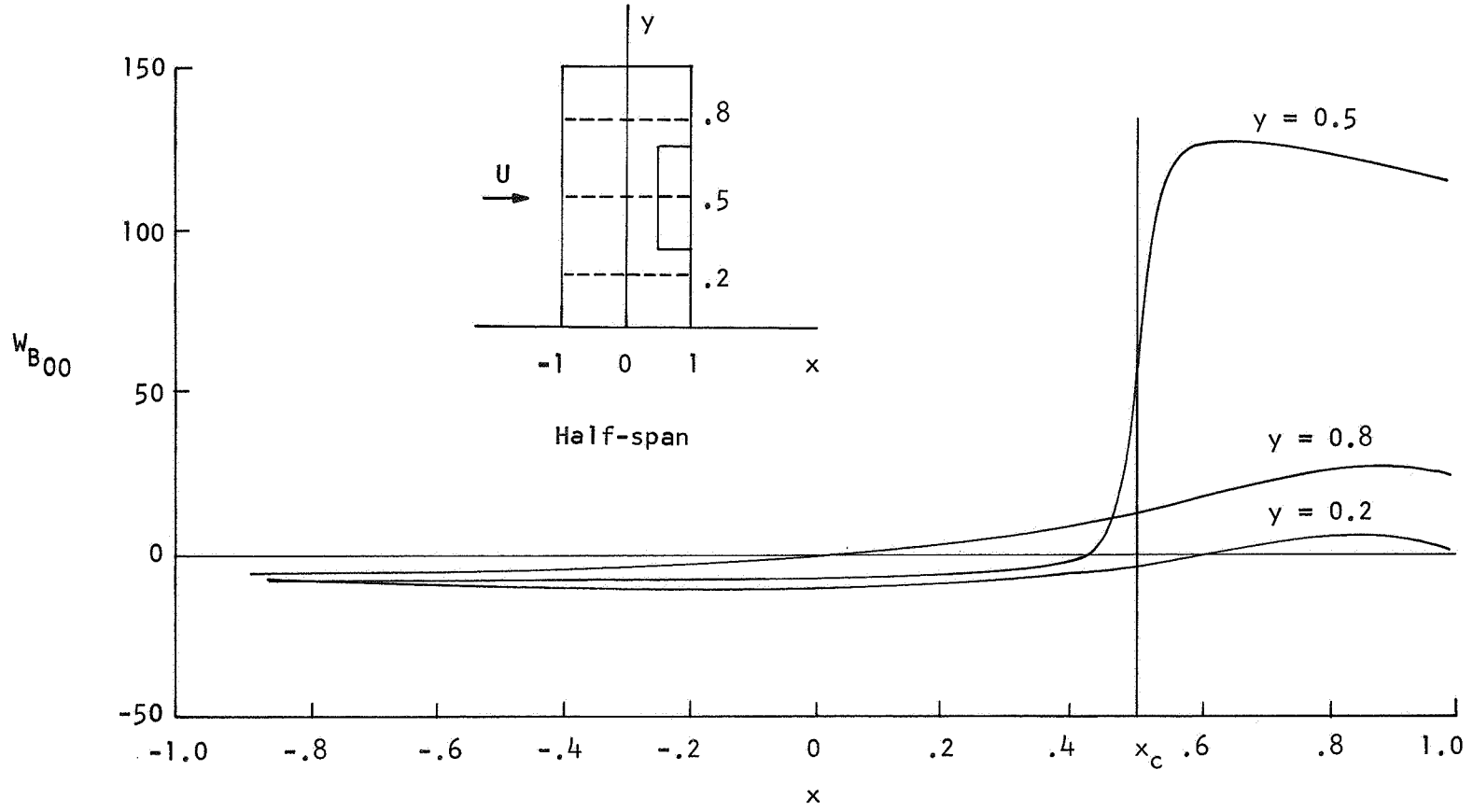

(b) M = 0.8.

Figure 7.- Concluded.

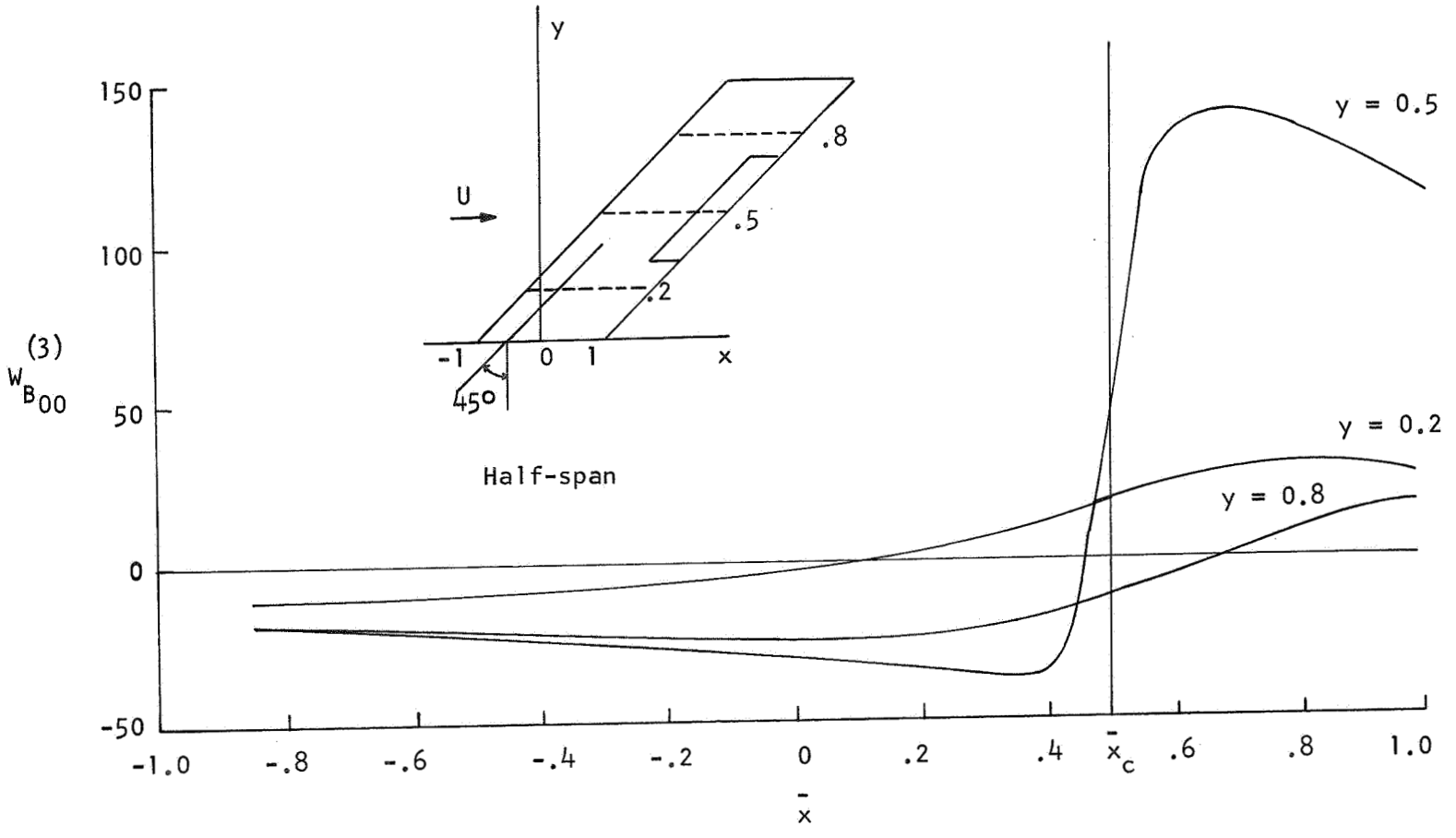

(a) $W^{(3)}_{B00}$ with $E_S = 1/2$.

Figure 8.- Downwash distributions $W^{(3)}_{B00}$ from pressure mode $B_{00}(\theta,\eta)$ of equation (24), and W_{B00} from $B_{00}(\theta,\eta)$ of equations (28) on a swept untapered wing with parameters $s = 4$, $\Lambda = 45^o$, $\mu = 1/2$, $y_{c1} = 0.3$, $y_{c2} = 0.7$, and $M = 0$.

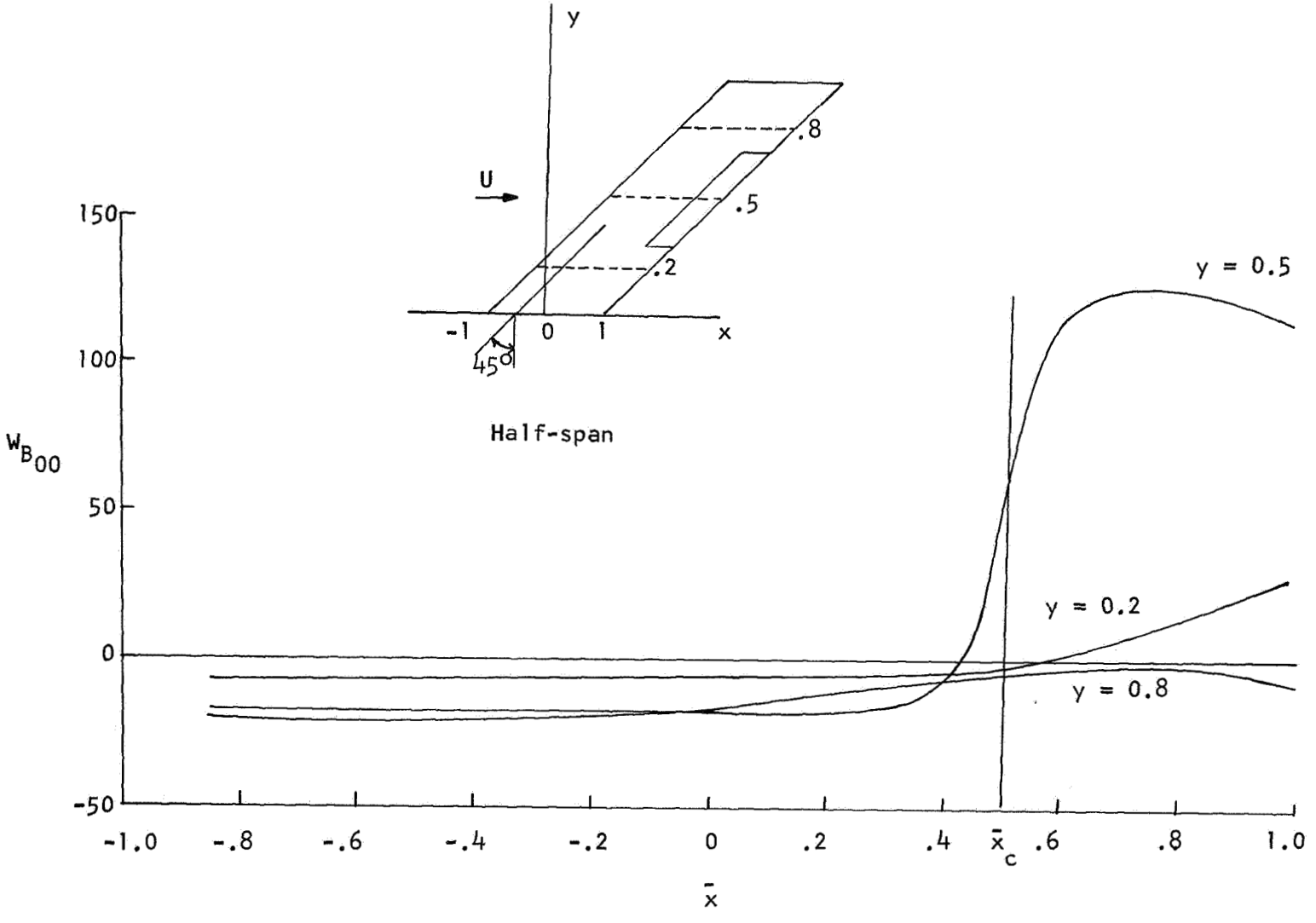

(b) $W_{B_{00}}$ with $E_S = 1/2$.

Figure 8.- Continued.

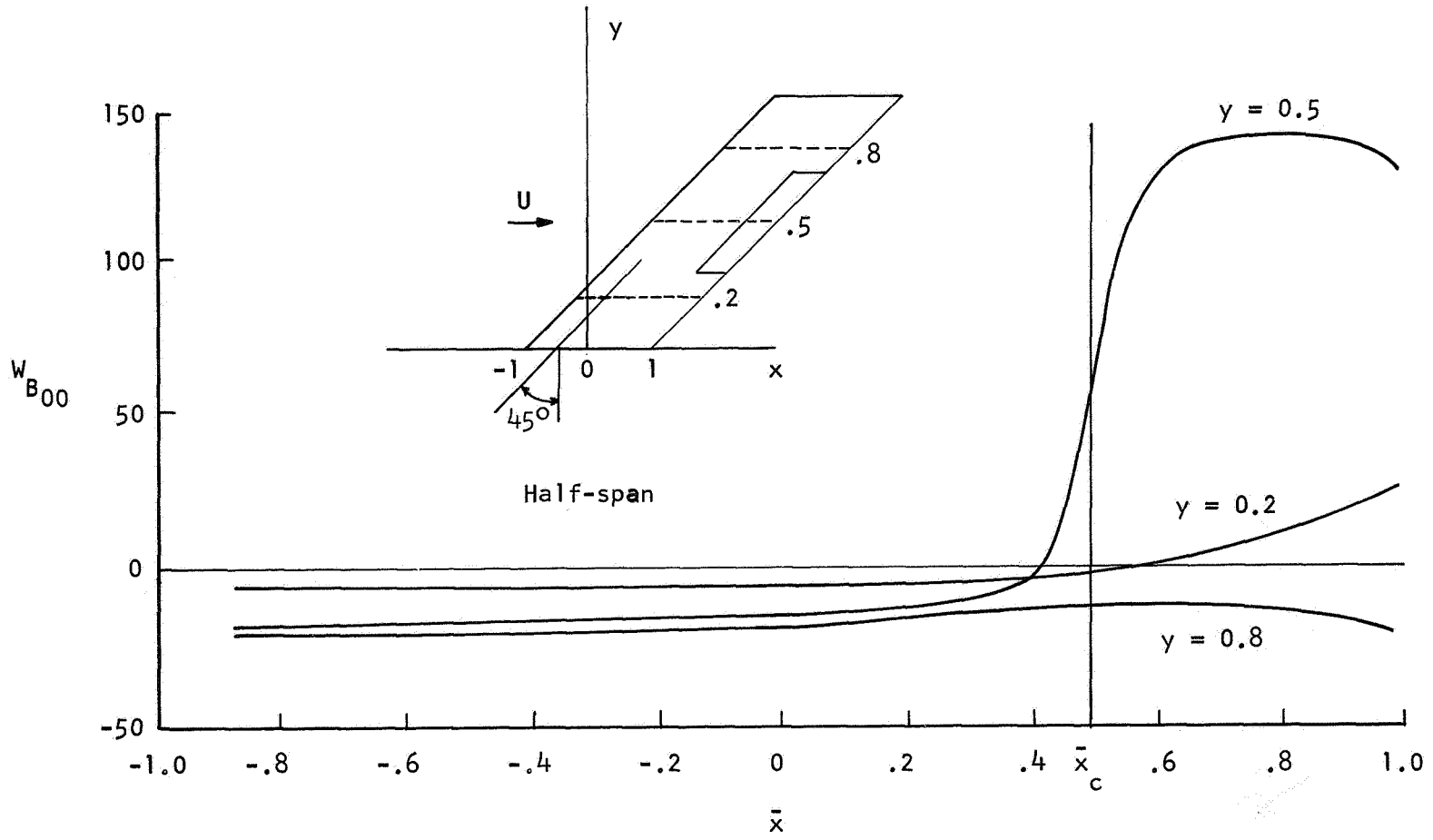

(c) W_{B00} with $E_S = 3/5$.

Figure 8.- Concluded.

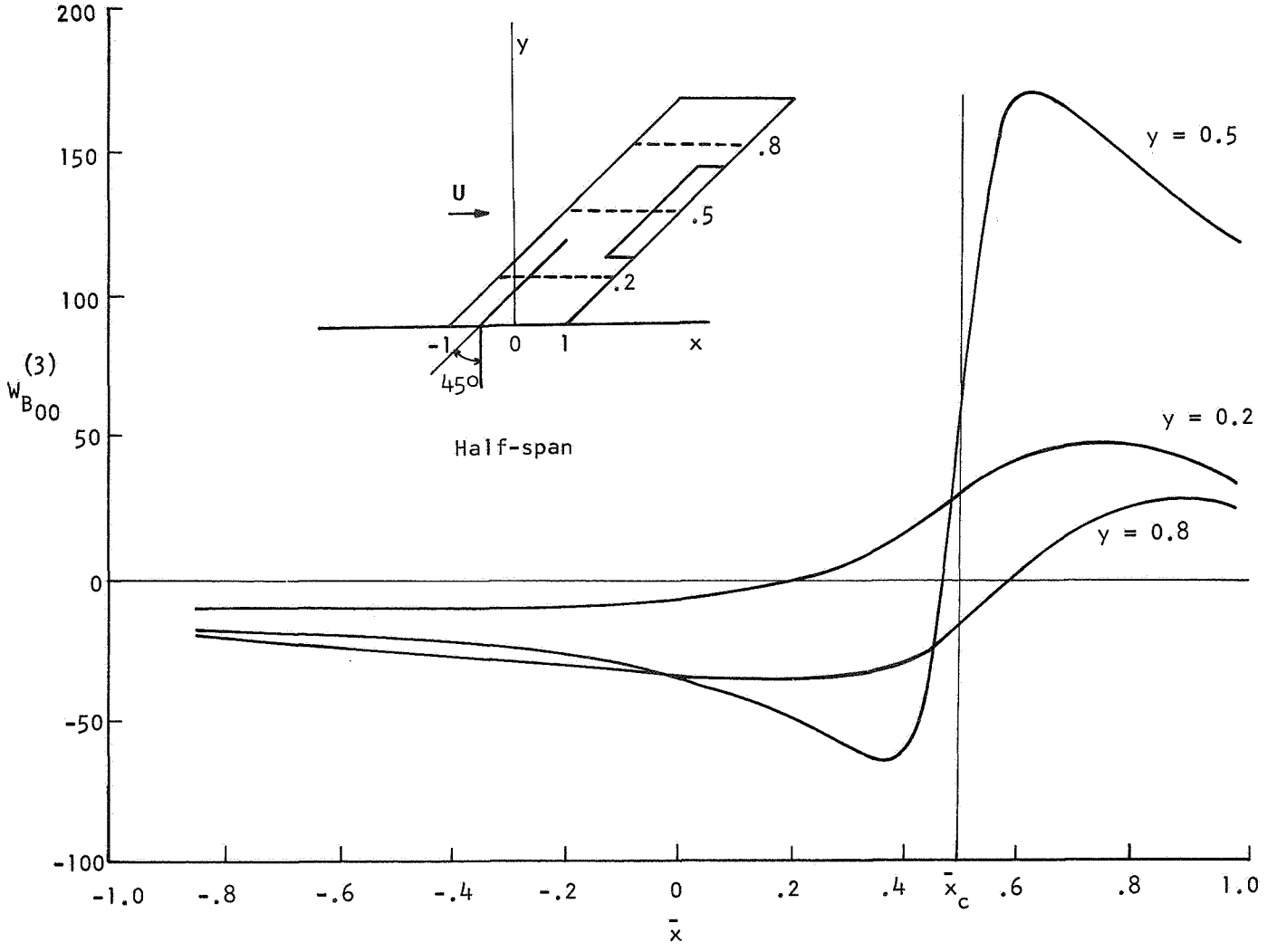

(a) $W^{(3)}_{B00}$ with $E_s = 1/2$.

Figure 9.- Downwash distributions $W^{(3)}_{B00}$ and W_{B00} for $M = 0.8$ on the same swept wing as in figure 8.

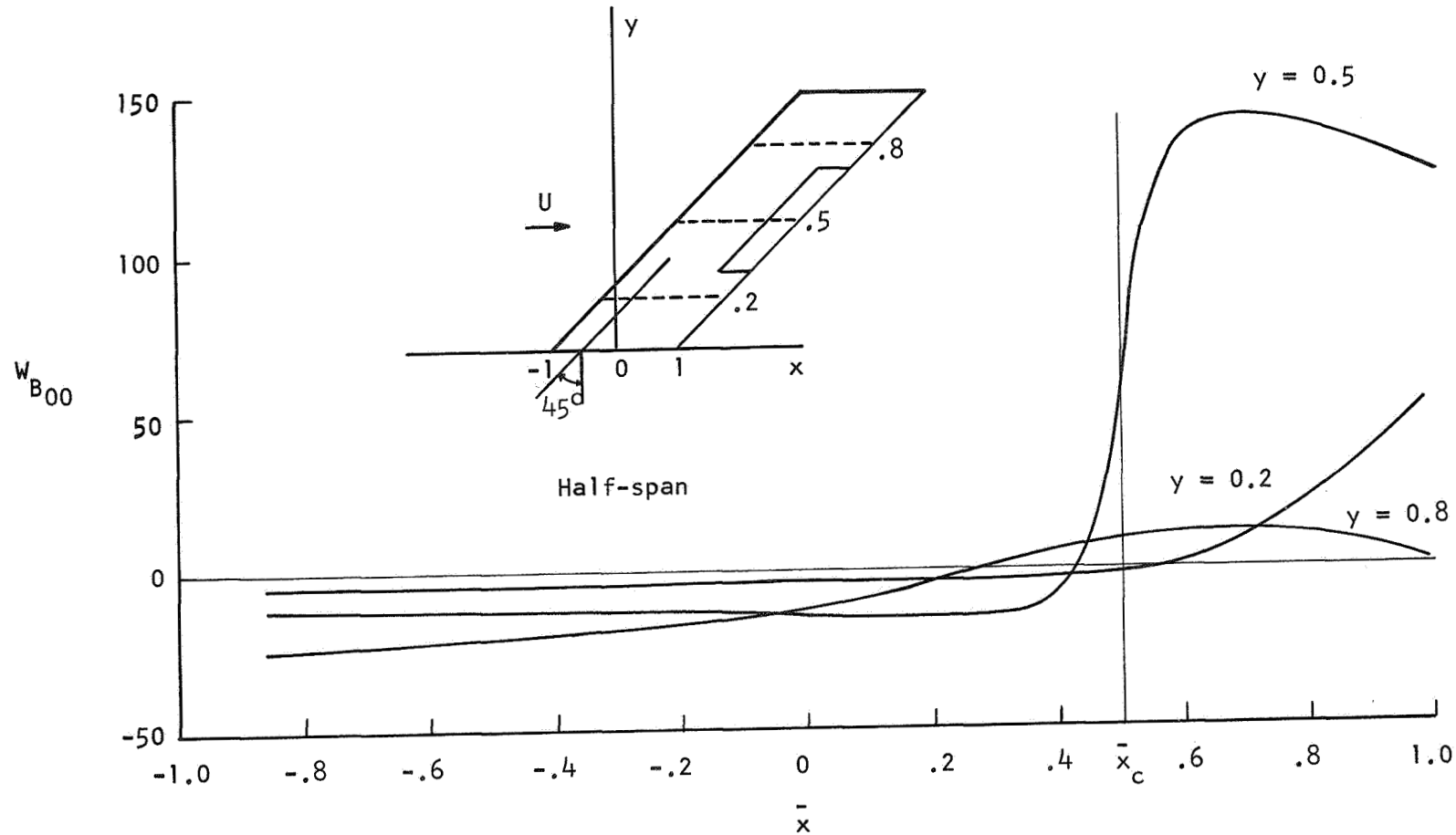

(b) W_{B00} with $E_S = 1/2$.

Figure 9.- Continued.

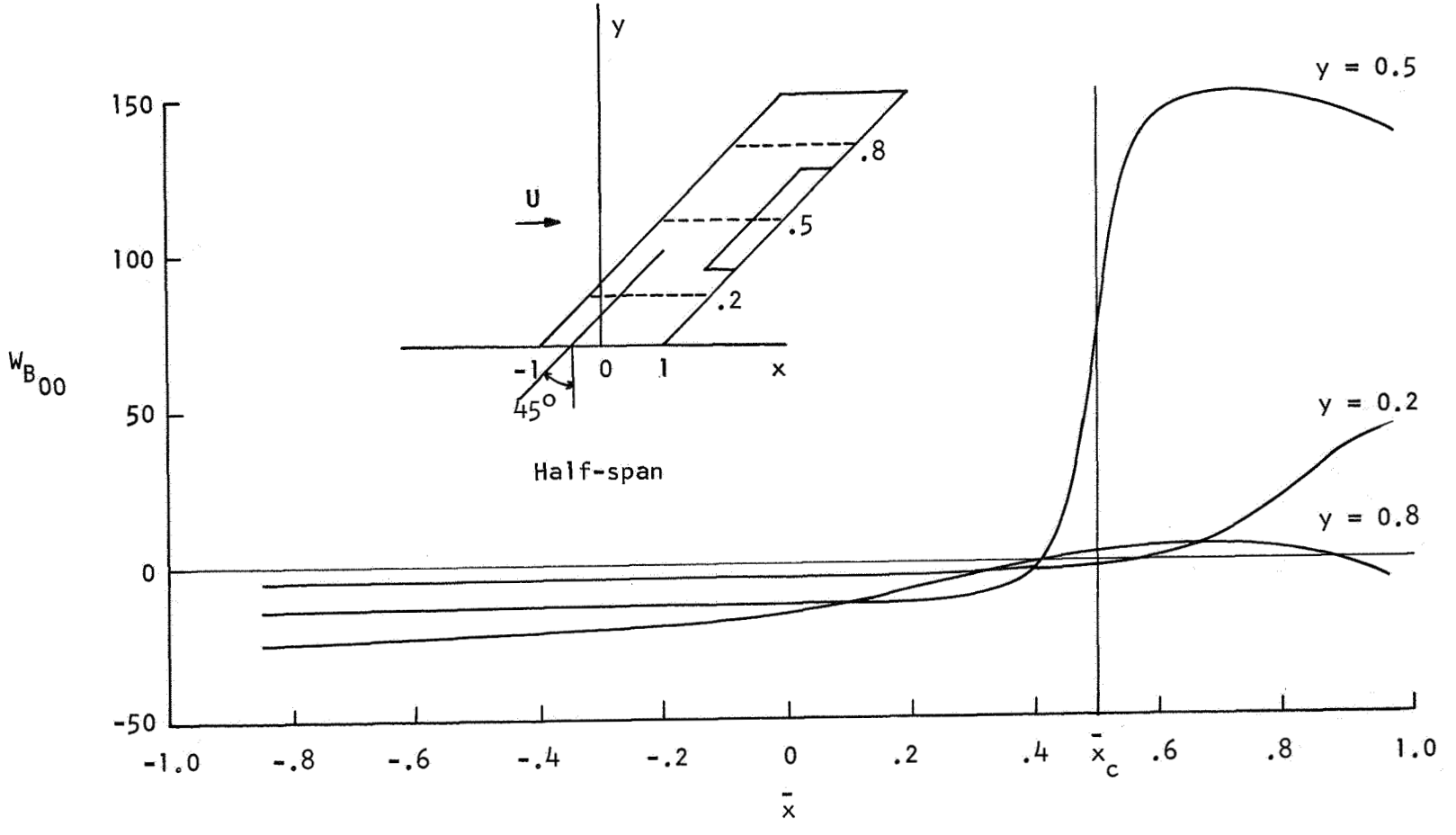

(c) $W_{B_{00}}$ with $E_S = 0.556$.

Figure 9.- Concluded.

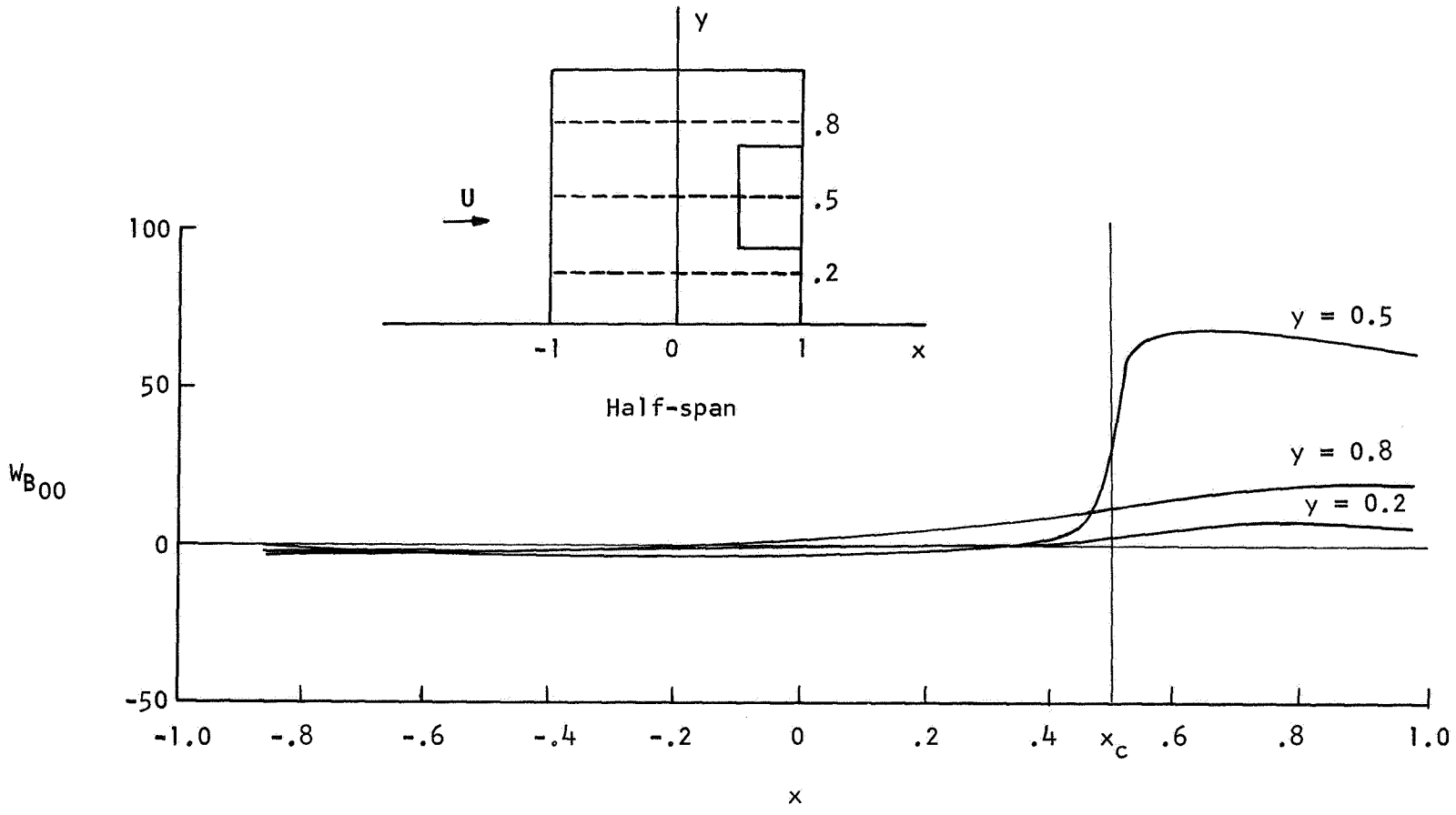

Figure 10.- Downwash distributions $W_{B_{00}}$ from pressure mode $B_{00}(\theta,\eta)$ of equation (28a) for a rectangular wing of aspect ratio 2 with partial-span flaps and parameters $s = 2$, $\mu = 1/2$, $y_{c1} = 0.3$, $y_{c2} = 0.7$, $M = 0$, and $E_s = 3/5$.

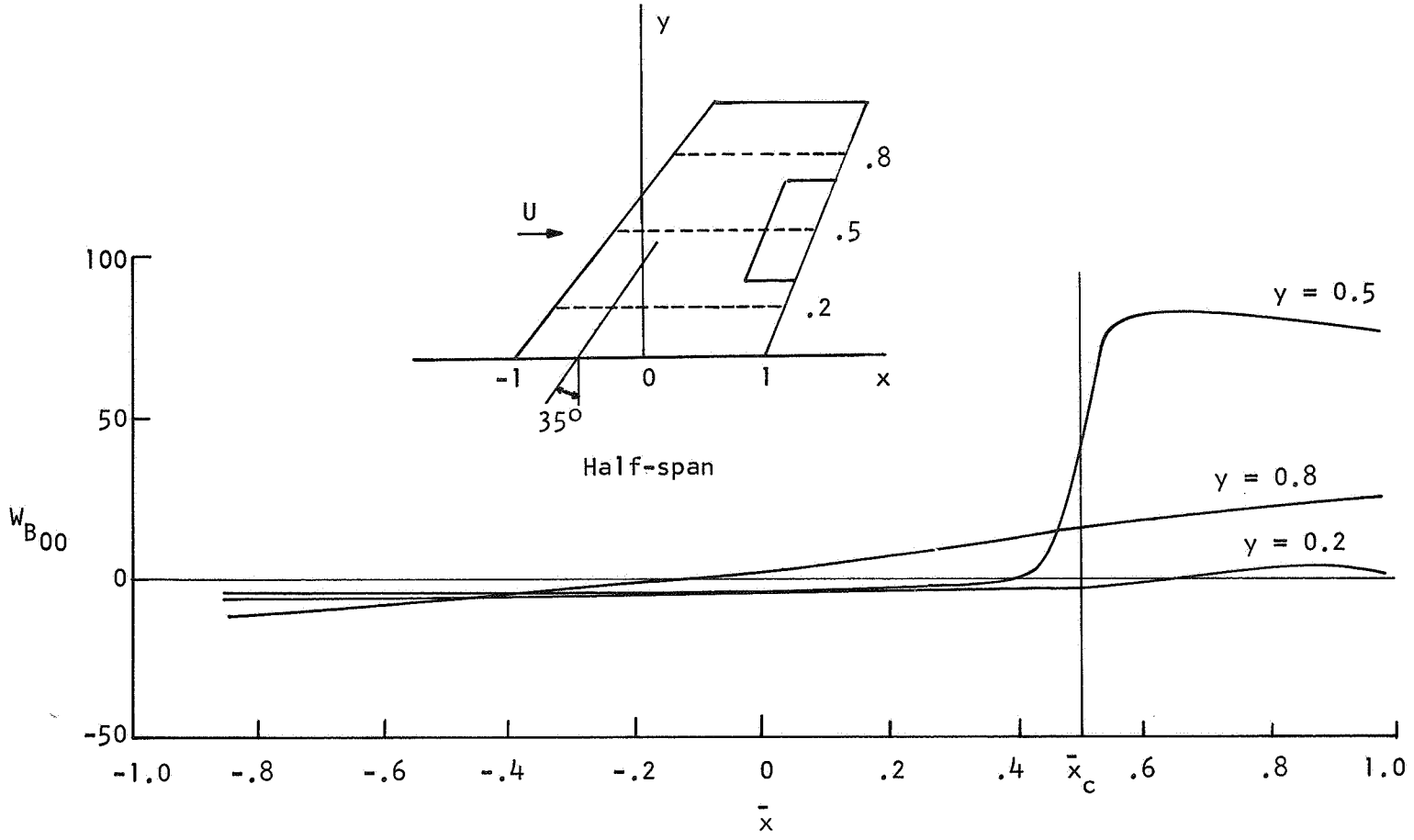

(a) M = 0.

Figure 11.- Downwash distributions W_{B00} from pressure mode $B_{00}(\theta,\eta)$ of equation (28a) for a swept, tapered wing with partial-span flaps for two Mach numbers and parameters $s = 2$, $\lambda = 0.6$, $\Lambda = 35^0$, $\mu = 0.4$, $y_{c1} = 0.3$, $y_{c2} = 0.7$, and $E_s = 0.512$.

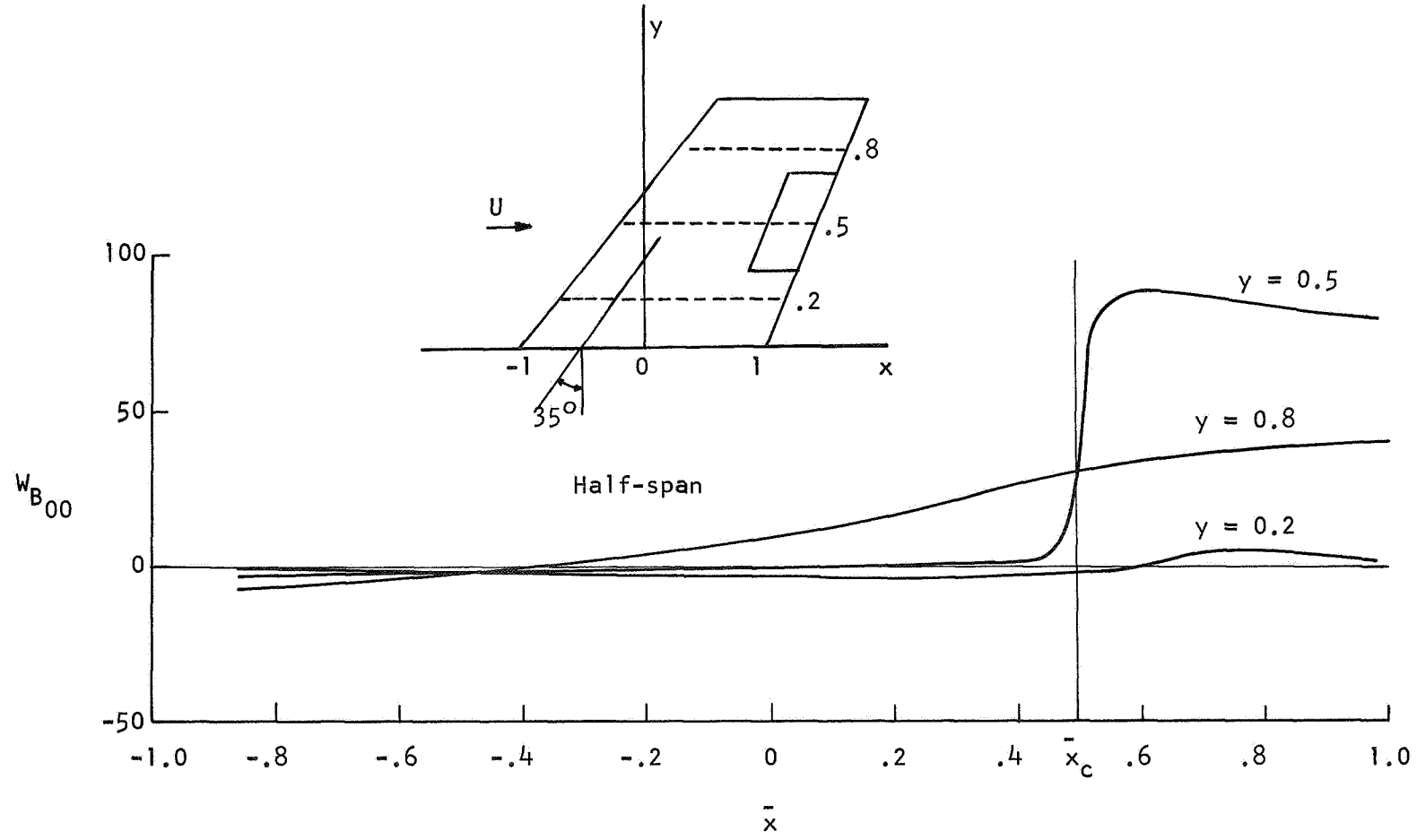

(b) M = 0.8.

Figure 11.- Concluded.

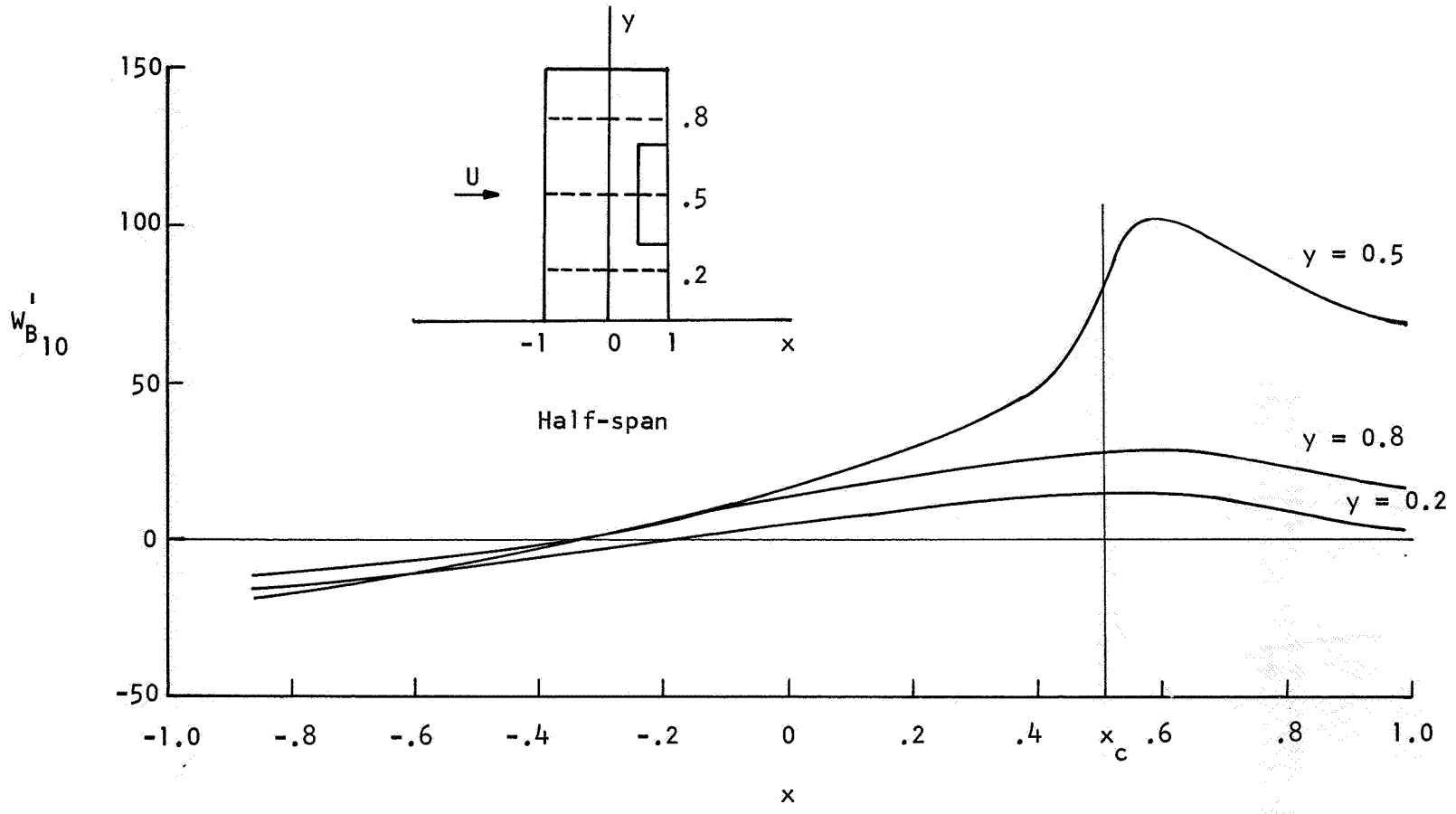

(a) $W_{B'_{10}}$.

Figure 12.- Second- and third-order chordwise varying downwash distributions $W_{B'_{10}}$ and $W_{B'_{20}}$ from the partial pressure modes $B'_{10}(\theta,\eta)$ and $B'_{20}(\theta,\eta)$ (eq. (36)) for the same rectangular wing as in figures 4 to 7, and with $E_S = 1/2$.

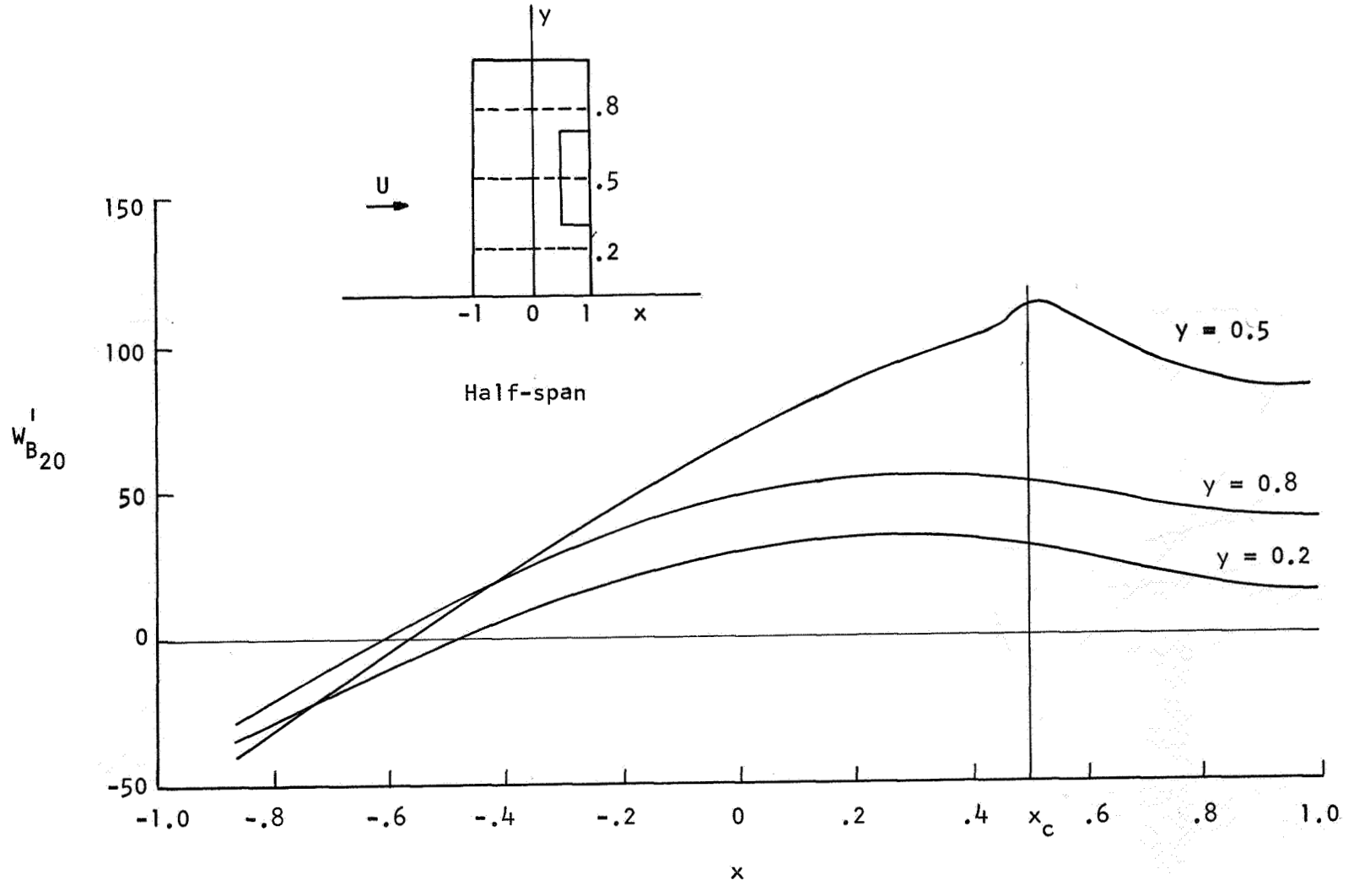

(b) $W_{B'_{20}}$.

Figure 12.- Concluded.

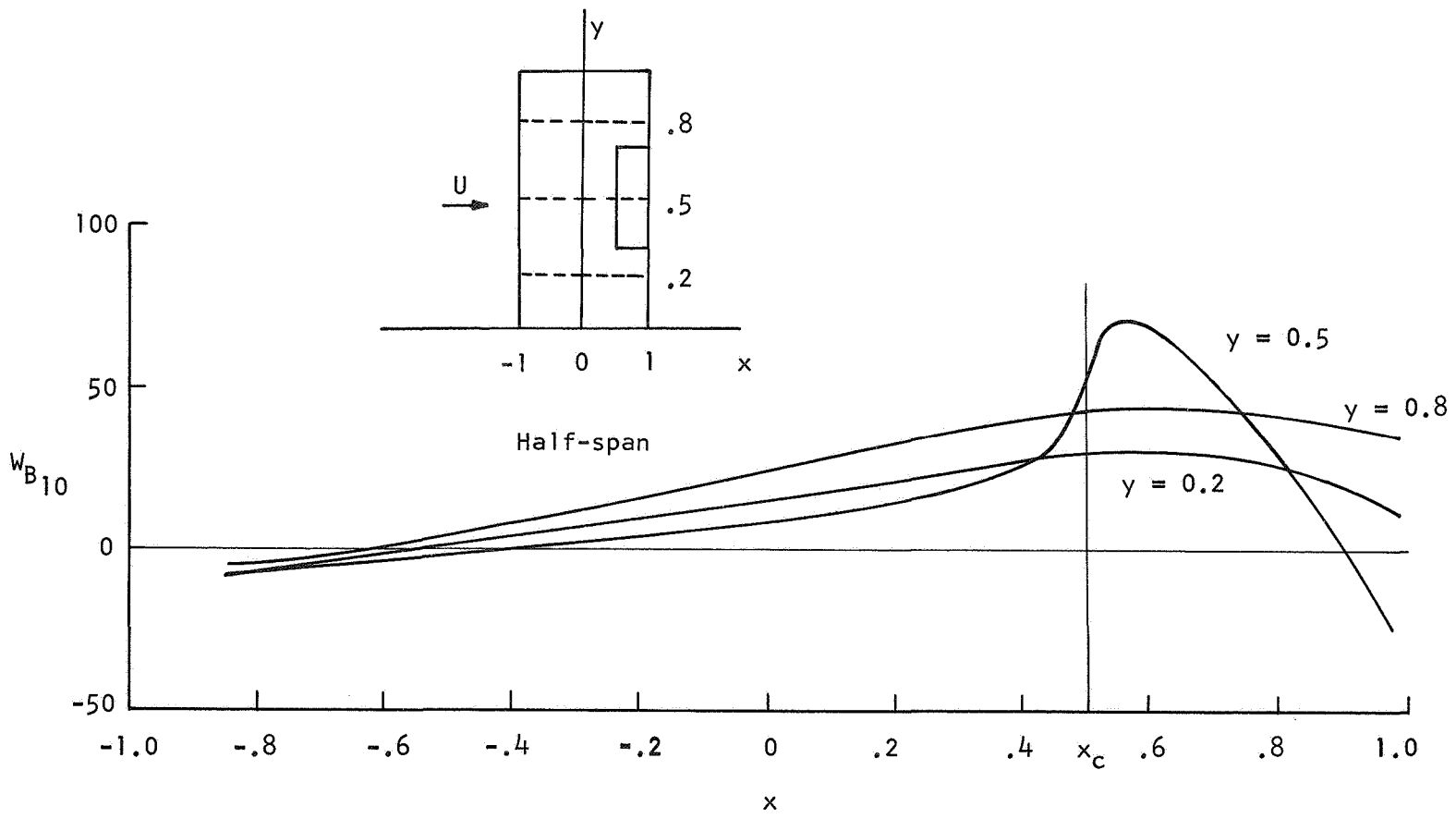

(a) $W_{B_{10}}$.

Figure 13.- Second- and third-order chordwise varying downwash distributions $W_{B_{10}}$ and $W_{B_{20}}$ from the pressure modes $C_{10}(\theta,\eta)$ (eq. (32a)) and $C_{20}(\theta,\eta)$ (eq. (33)) for the same rectangular wing as in figures 4 to 7 and 12, and with $E_S = 1/2$.

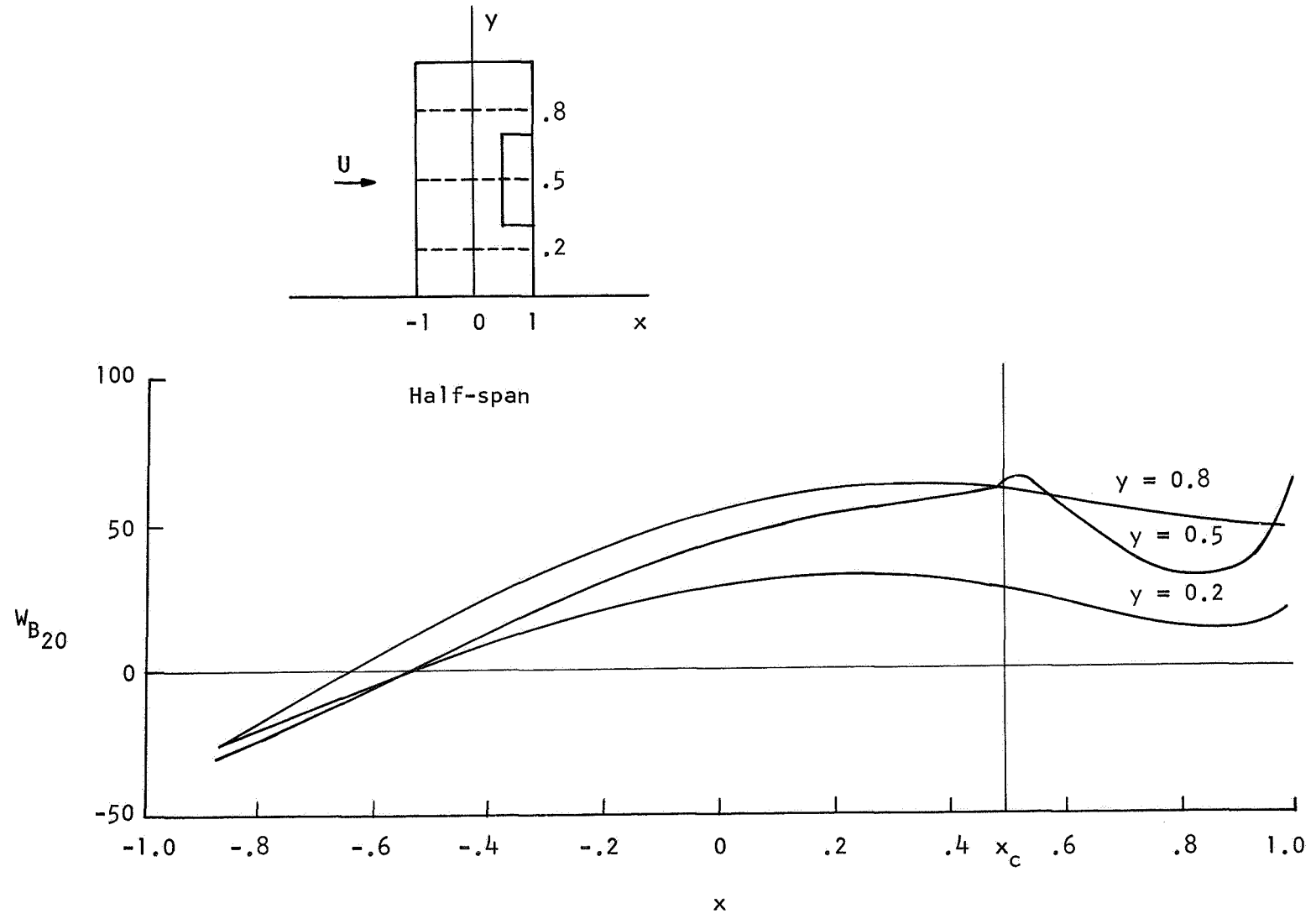

(b) $W_{B_{20}}$.

Figure 13.- Concluded.

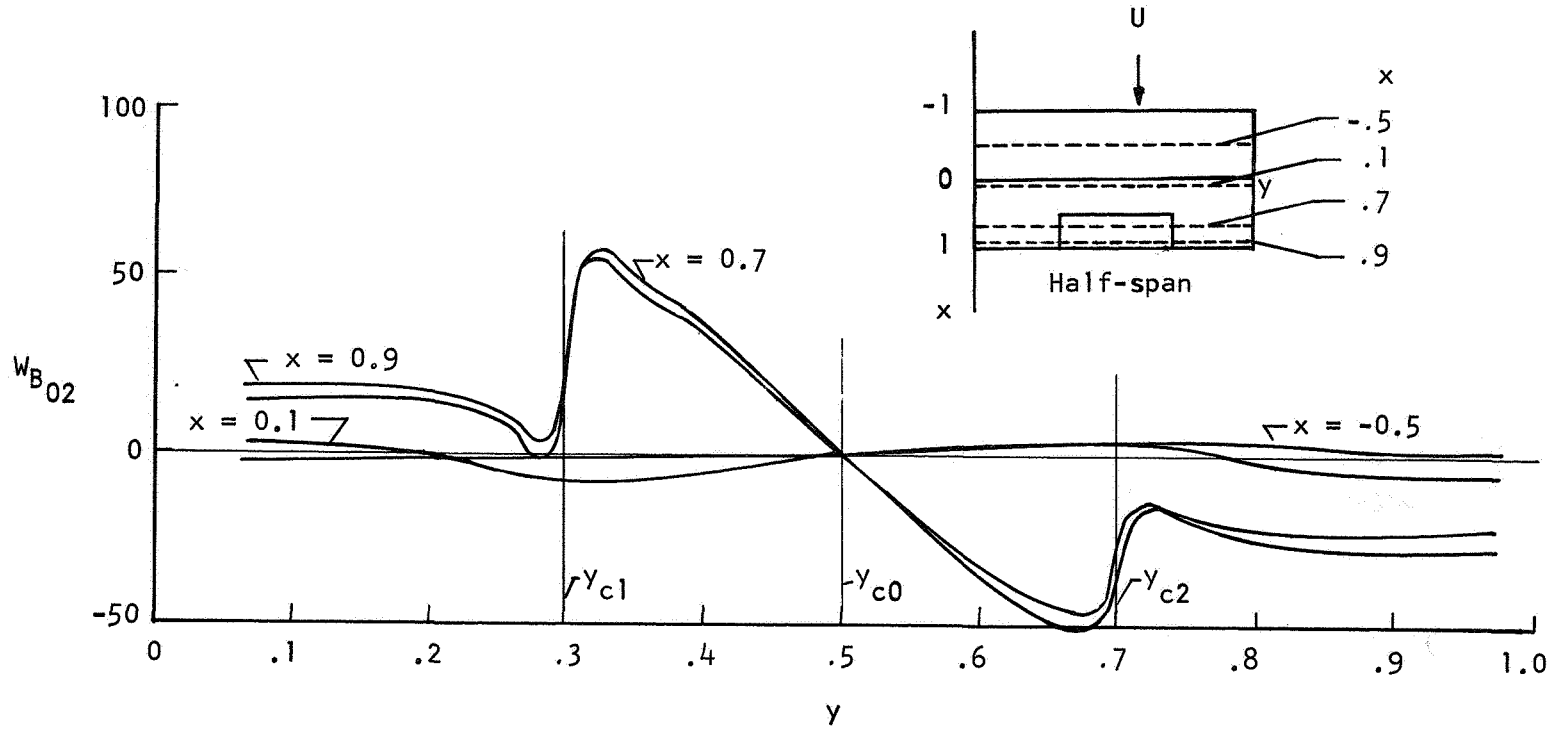

(a) $W_{B_{02}}$.

Figure 14.- Second- and third-order spanwise varying downwash distributions $W_{B_{02}}$ and $W_{B_{04}}$ from the pressure modes $C_{01}(\theta,\eta)$ (eq. (34a)) and $C_{02}(\theta,\eta)$ (eq. (35)) for the same rectangular wing as in figures 4 to 7, 12, and 13, and with $E_s = 1/2$.

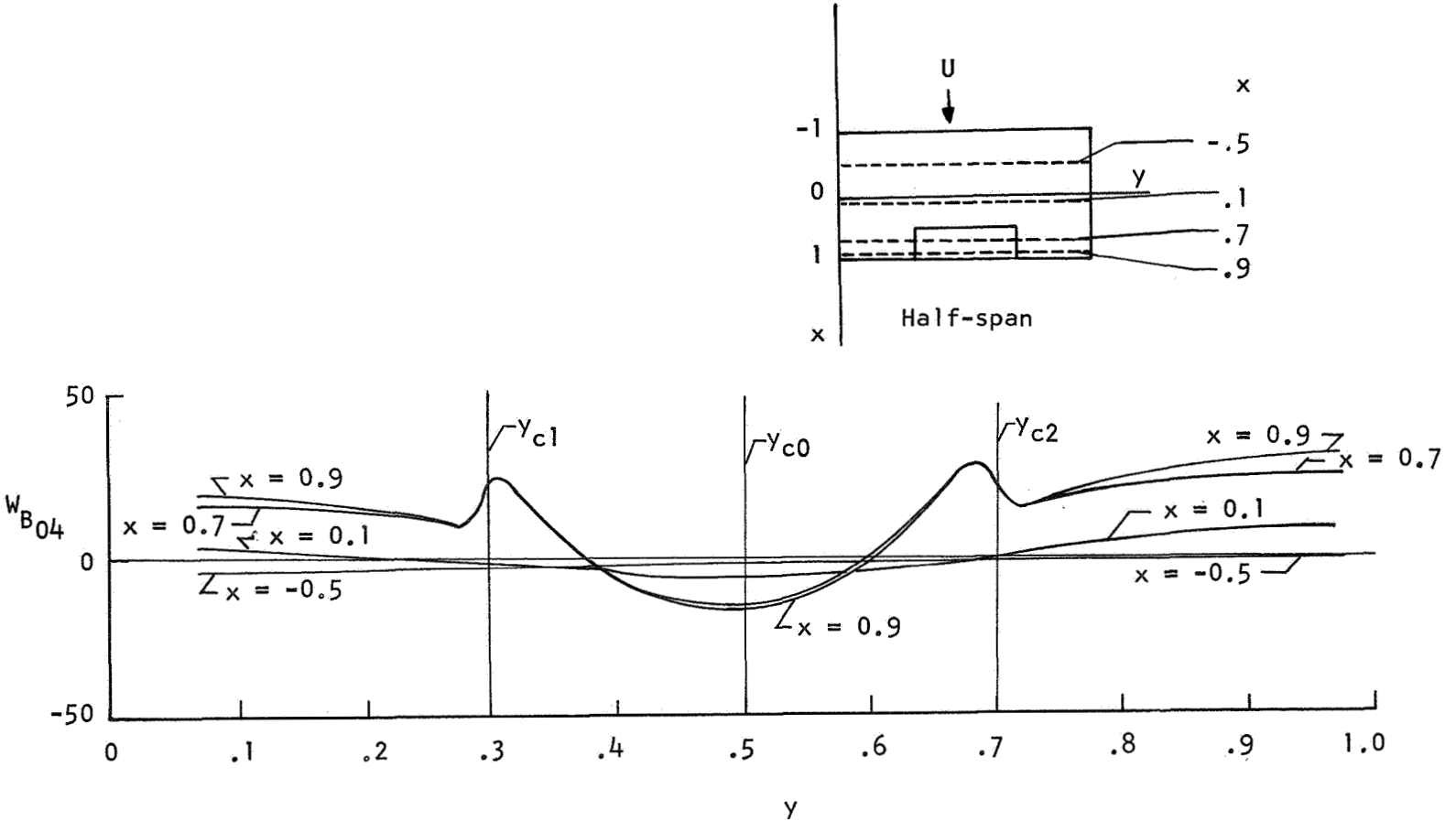

(b) W_{B04}.

Figure 14.- Concluded.

"The aeronautical and space activities of the United States shall be conducted so as to contribute . . . to the expansion of human knowledge of phenomena in the atmosphere and space. The Administration shall provide for the widest practicable and appropriate dissemination of information concerning its activities and the results thereof."

—NATIONAL AERONAUTICS AND SPACE ACT OF 1958

NASA SCIENTIFIC AND TECHNICAL PUBLICATIONS

TECHNICAL REPORTS: Scientific and technical information considered important, complete, and a lasting contribution to existing knowledge.

TECHNICAL NOTES: Information less broad in scope but nevertheless of importance as a contribution to existing knowledge.

TECHNICAL MEMORANDUMS: Information receiving limited distribution because of preliminary data, security classification, or other reasons.

CONTRACTOR REPORTS: Scientific and technical information generated under a NASA contract or grant and considered an important contribution to existing knowledge.

TECHNICAL TRANSLATIONS: Information published in a foreign language considered to merit NASA distribution in English.

SPECIAL PUBLICATIONS: Information derived from or of value to NASA activities. Publications include conference proceedings, monographs, data compilations, handbooks, sourcebooks, and special bibliographies.

TECHNOLOGY UTILIZATION PUBLICATIONS: Information on technology used by NASA that may be of particular interest in commercial and other non-aerospace applications. Publications include Tech Briefs, Technology Utilization Reports and Notes, and Technology Surveys.

Details on the availability of these publications may be obtained from:

SCIENTIFIC AND TECHNICAL INFORMATION DIVISION

NATIONAL AERONAUTICS AND SPACE ADMINISTRATION

Washington, D.C. 20546